University of Oklahoma

Graduate College

A Radio & X-ray Search For Intermediate-Age Supernovae: Tuning Into the Oldies

A Dissertation Submitted to the Graduate Faculty

In Partial Fulfillment of the Requirements for the Degree of

Doctor of Philosophy

Christopher J. Stockdale

Norman, Oklahoma

2001

UMI Number: 3014513

Bell & Howell Information and Learning Company
300 North Zeeb Road
P.O. Box 1346
Ann Arbor, MI 48106-1346

A Radio & X-ray Search For Intermediate-Age Supernovae:

Tuning Into the Oldies

A Dissertation Approved for the
Department of Physics and Astronomy

BY

J. J. Cowan (Chair)

E. Baron

K. M. Leighly

S. Postawko

W. R. Romanshin

M. Santos

Acknowledgments

Being a student for as long as I have, there are so many people who I should thank for their friendship and assistance. I know that many of those individuals may go unmentioned here, but that in no way diminishes my gratitude to them.

My former teachers, especially Michael Friedlander, Loretta "Ole Lady" Hargroder, George Hummer, Rose Lacasse, and Jack Looper: You made learning exciting.

Michael P. Rupen, Steven Jones, You-Hua Chu, W. Miller Goss, R. A. Sramek, Christina Lacey, Andrea Prestwich, and my other collaborators: Thank you for assistance and contributions to this work.

Ed Baron, Karen Leighly, Susan Postawko, Bill Romanishin, and Mike Santos: Your support and guidance as members of my doctoral committee has been outstanding and is deeply appreciated.

Kim Milton, David Branch, Dick Henry, Tibor Herczeg, Ron Kantowski, Jack Cohn, Bruce Mason, Sheena Murphy, Matt Johnson, Kieran Mullen, Stu Ryan, Ryan Doezema, Andy Feldt, Danette Loyd, and the entire Physics & Astronomy faculty and staff: Having been at OU long enough to acquire "tenure", I thank you for support and encouragement.

John J. Cowan: I can't imagine a better mentor and friend. Without your tutelage, I seriously doubt that I would be where I am today. I hope that I will be able to do as much for my students in the future as you have done for me.

My sisters, Angelia and Josephine: You are my oldest and dearest friends. May I be able to be of as much help to you as you have been to me.

My parents and grandparents: You have made me the person who I am today. I love you all and am grateful for all that you have done.

My fellow graduate students along the way, especially Jackie Milingo, Chris Eck, Heidi Morris, Larry Maddox, Pam Jenkins, Scott McCartney, Steve Richichi, Joe Howard, Debra Burris, Giti Khodaparast, Sharon Kennedy, Dean Richardson, Ted Mansell, Terry Caldwell, Lauren Cohen, Whitley Cooke, Doug Canfield, Russ Goodman, Kory Goldammer, Francesca Boffi, Brett McKinney, and Blake Laing: Thanks for your friendship.

My dear friends, especially Drew Berke, Jim Mummert, John Dindot, Christy Wells, George & Carla Kober, John, Jeff, & Jason Ottenad, Michael Bell, Adrian & Lucianna Simmons, Stephen Sandifer, Cochanna Rush, Sandra Mah, and Jenn Churchill: Thanks for being there when I needed you.

And a special thanks to my friend and "copy editor", Grettie Bondy.

Contents

List of Tables

List of Figures

Abstract

Type II supernovae (SNe) are the cataclysmic and very luminous last stage in the evolutionary track of very high mass stars, resulting in the destruction of the star and the ejection of large amounts of material into their surroundings, with initial velocities in excess of 10,000 km s^{-1} . SNe II are the primary sources responsible for the production and distribution of elements with atomic masses larger than iron throughout their host galaxies. There also are significant contributors of elements lighter than iron, in particular oxygen and calcium. The creation of these elements has a large impact on the chemical evolution of the host spiral galaxies. Not much is known about the later development of the progenitor stars of SNe II, as they are an extremely small subset of the stars in our Universe and are difficult to distinguish from other stars prior to the SN events. One of the best methods to study the properties of the progenitor star is to study the interaction of the SN ejecta with the circumstellar material around the SN, presumably lost in the years proceeding the SN event. This interaction produces radio and X-ray emission, which among other things is influenced by the speed of the outward shock and the density of the circumstellar material. By observing this emission over the course of decades, I garner insight into the late evolution of the very

massive stars. Only a few SNe II have been detected and monitored in the radio (22) and X-ray (12) wavelengths. In this study, I have detected radio emission from five historical, decades-old SNe II (nearly doubling the radio sampling size of such events) and established X-ray upper limits for two.

Using the Very Large Array (VLA), we have detected radio emission from the site of SN 1961V in the Sc galaxy NGC 1058. With a peak flux density of 0.063 ± 0.008 mJy/beam at 6 cm and 0.147 ± 0.026 mJy/beam at 18 cm, the source is non-thermal, with a spectral index of -0.79 ± 0.23. Within errors, this spectral index is the same value reported for previous VLA observations taken in 1984 and 1986. The radio emission at both wavelengths has decayed since the mid 1980's observations with power-law indices of $\beta_{20cm} = -0.69 \pm 0.23$ and $\beta_{6cm} = -1.75 \pm 0.16$. We discuss the radio properties of this source and compare them with those of Type II radio SNe and luminous blue variables.

Using the VLA, we have detected radio emission from the site of SN 1970G in the Sc galaxy M101. These observations are 31 years after the SN event, making SN 1970G the longest monitored radio SN. With flux densities of 0.12 ± 0.020 mJy at 6 cm and 0.16 ± 0.015 mJy at 20 cm, the spectral index of -0.24 ± 0.20 appears to have flattened somewhat when compared with the previously reported value of -0.56 ± 0.11, taken in 1990. The radio emission at 20 cm has decayed since the 1990 observations with a power-law index of $\beta_{20cm} = -0.28 \pm 0.13$.

We have also detected radio emission from the sites of SNe 1923A, 1950B, and 1957D in the SABc galaxy M83. These observations are 75 years after the first detection of SN 1923A, making it the oldest monitored radio supernova. With flux densities of 0.20 ± 0.03 mJy at 20 cm and 0.15 ± 0.03 mJy at 6 cm, the spectral index of -0.24 ± 0.26 appears to have flattened considerably when compared with the previously reported value of -1.00 ± 0.24, taken in 1990. The radio emission from SN 1923A at 20 cm has decayed since the 1990 observations with a power-law index of $\beta_{20cm} = -4.54 \pm 0.22$ and increased at 6 cm with a decay index of $\beta_{6cm} = +4.24 \pm 0.38$. The flux densities of SN 1950B at 20 cm and 6 cm are 0.52 ± 0.03 mJy and 0.42 ± 0.03 mJy, respectively, resulting in a spectral index of -0.18 ± 0.12. The radio emission from SN 1950B has evolved since 1990 and 1992, with decay indices of $\beta_{20cm} = -2.27 \pm 0.08$ and $\beta_{6cm} = +0.70 \pm 0.11$. The flux densities of SN 1957D at 20 cm and 6 cm are 0.82 ± 0.03 mJy and 0.34 ± 0.03 mJy, respectively, resulting in a spectral index of -0.73 ± 0.12. The radio emission from SN 1957D has evolved since 1990 and 1992, with decay indices of $\beta_{20cm} = -2.29 \pm 0.07$ and $\beta_{6cm} = -6.42 \pm 0.09$. I also report that emission was not detected from the Type II supernovae, SNe 1945B and 1968L, nor from the Type Ib supernova, SN 1983N. We discuss the radio properties of these sources and compare them to those of other Type II radio SNe.

Using the High Resolution Imager (HRI) on the Roentgen Satellite (ROSAT)

I have made the first deep X-ray observations of NGC 7331, discovering a nuclear X-ray source coincident with the previously determined radio and optical nuclear centers. Positions, luminosities, and fluxes of X-ray sources in the field are compared to previously identified radio and optical sources. The nucleus of NGC 7331 has been analyzed to discern any new evidence supporting the presence of a massive black hole (MBH), and comparisons are made with other Low-Ionization Nuclear Emission-line Region (LINER) galaxies. The flux ratio of core radio to soft X-ray emission in NGC 7331 is lower than in other LINERs included in our sample.

Using the HRI on ROSAT I have made the first deep X-ray observations of NGC 1058, discovering a nuclear X-ray source coincident with the previously determined optical nuclear center. We report an upper limit on the X-ray luminosity of SN 1961V, in NGC 1058, of 1×10^{38} erg s^{-1}, but this limit cannot differentiate between the two possible explanations for the nature of this unusual object. We also report the X-ray detection of a source, which might be a previously unreported galaxy cluster in the field near NGC 1058. Positions and fluxes of other X-ray sources in the field are also presented.

Chapter 1

Introduction

Supernovae (SNe) are arguably the most popular and most studied astrophysical phenomena. The first historical SN was observed by Chinese astronomers in 386 A.D. and recovered as a pulsar, G 11.2-0.3, with a rotation period of 0.54s (Trimble 2001; Kothes & Reich 2001). There are nine confirmed historical SNe, over the course of $\sim$ 1,500 years, whose discoveries pre-date the first modern optically recovered SN, SN 1885A in the galaxy M31 (Trimble 2001). Since then, the number of objects identified as SNe through 1998 is well over 1,400 (although a small fraction of these sources were later proven to not be actual SNe) with 134 identifications in 1998 alone (Barbon *et al.* 1998).

The first modern recovery of a radio supernova (RSN) was SN 1970G (Gottesman *et al.* 1972; Allen *et al.* 1976). This was made with the National Radio Astronomy Observatory (NRAO) three-element interferometer, resulting in poorer resolution and higher noise than the best current interferometer (the Very Large Array[1] [VLA]) allows. The first SN to be detected and observed with the VLA was SN 1979C (Weiler *et al.* 1986; Weiler *et al.* 1991; Montes *et al.* 1998). There have been 30 RSNe, with low radio upper limits established for over 100 others. As one can see, the radio sampling is quite small compared to the optical detections. The total number of observed X-ray SNe is currently 12. The reason for the low number of X-ray detections has primarily been due to instrumentational limits in spatial resolution and photon sensitivity. With the recent launch of the *Chandra X-Ray Observatory*, this will change dramatically, as this instrument is far more sensitive than any previous X-ray mission and has a spatial resolution comparable to that of the VLA.

1.1 Types of Supernovae

There are two distinct optical classifications of SNe, Type I and Type II (Minkowski 1941). The key difference between them is that Type I SNe have no conspicuous hydrogen absorption lines in their optical spectra, unlike Type II SNe. The Type I SNe are also divided into three further classifications. The first, Type Ia SNe, are the result of the thermo-nuclear detonation of a white dwarf. These

[1]The National Radio Astronomy Observatory is a facility of the National Science Foundation operated under cooperative agreement by Associated Universities, Inc.

SNe are characterized by blue shifted Si II ($\lambda\lambda$ 6347, 6371) absorption lines. The other two groups, SNe Ib and Ic, are the result of core collapse of a very massive star with initial Main Sequence masses in excess of $\sim$ 10 $M_\odot$. SNe Ib, Ic, and II are usually detected near H II regions and are indicators of recent star formation, given that their progenitor stars have Main Sequence lifetimes on the order of 1—10 million years (Filippenko *et al.* 1995). What distinguishes SNe Ib and Ic from SNe II, is that both SNe Ib and Ic lost their hydrogen envelopes prior to the core collapse (Filippenko 1997). This is usually due to either interaction with a companion star which strips the SN progenitor star of its outer envelope, as the progenitor exceeds its Roche lobe, or in the case of a single star, extreme mass loss preceding the explosion. SNe Ic also have no strong helium lines in their spectra, evidence of even greater pre-detonation mass loss. Also, SNe Ia have practically no circumstellar material (CSM) when they explode (Branch *et al.* 1995; Cumming *et al.* 1996), while SNe Ib and Ic, have some CSM due to the progenitor's stellar wind and the fact that not all of their envelopes accrete onto their companion stars (Filippenko 1997).

The subjects of this dissertation, SNe II, are the result of the core collapse of massive stars with more CSM present than for SNe I. SNe II can be broken down into three main subclasses based on their optical decay rates (Barbon *et al.* 1979; Doggett & Branch 1985). Type II-L SNe decay linearly for the first

100 days following maximum optical light, similar to SNe Ia. Type II-P SNe decay very slowly, maintaining a plateau within ~ 1 mag of maximum brightness in the same intervening period. The key difference between these two types is that the progenitors of SNe II-L have either a more extended or lower mass hydrogen envelope than SNe II-P, which is the cause of the plateau (Filippenko 1997). A third classification has recently been added, Type II-n SNe (Schlegel 1990; Filippenko 1991a; Filippenko 1991b; Leibundgut 1994), whose ejecta is interacting with a dense CSM. They are characterized by a narrow Hα line, resulting from the slow-moving CSM, superimposed upon a broader component (typical velocities of 200 km s^{-1} and 2,000 km s^{-1}, respectively; Filippenko 1997).

1.2 Radio Properties of Supernovae

Of the RSNe detected, there are no Ia's, only three SNe Ib, five SNe Ic, and 22 SNe II. The radio emission from SNe Ib and Ic is quite luminous and homogeneous with steep spectral indices ($\alpha < -1$; S $\propto \nu^{+\alpha}$, with S standing for the radio flux density and ν standing for frequency) and a fast radio turn-on/turn-off time, on a timescale equivalent with the optical emission (Weiler *et al.* 2001). On the other hand, SNe II are rather heterogeneous. They have a range of radio luminosities with flatter spectral indices ($\alpha > -1$) and slow turn-on/turn-offs, sometimes lagging the optical light curves by 1—10 years (Weiler *et al.* 2001).

Regardless of these differences, all RSNe share the following common properties (Weiler *et al.* 1996; Weiler *et al.* 1990):

1. non-thermal synchrotron emission with a high brightness temperature;

2. a decrease in absorption with time, resulting in a smooth rapid turn-on at low wavelengths and later at lower wavelengths;

3. a power-law decline of the flux density with time, after radio maximum light is reached at each wavelength (optical depth ~ 1); and

4. a final asymptotic approach of the spectral index to an "optically thin", non-thermal, constant value.

At the end of the last century, only 12 SNe had been positively detected at X-ray wavelengths. Of this group, SN 1994I (Immler *et al.* 1998b) is a Type Ic SN and the others [SNe 1978K (Ryder *et al.* 1993; Schlegel *et al.* 1998), 1979C (Immler, Pietsch, & Aschenbach 1998a), 1980K (Canizares, Kriss, & Feigelson 1982), 1986J (Houck *et al.* 1998), 1987A (Hasinger, Aschenbach, & Trümper 1996; Burrows *et al.* 2000), 1988Z (Fabian & Terlevich 1996), 1993J (Zimmerman *et al.* 1994), 1994W (Schlegel 1999), 1995N (Lewin, Zimmerman, & Aschenbach 1996) 1998S, and 1999em (Pooley *et al.* 2001)] are Type II SNe. Only four of these SNe have been bright enough to obtain an X-ray spectra (SNe 1978K, 1986J, 1987A, and 1993J). The fact that X-ray emission from all four sources is quite luminous, is the result of a sampling bias due to the poor photon sensitivity of past X-ray missions. Only three of these sources (SNe 1978K, 1979C, and 1987A) have been followed in the X-ray for more than 10 years. SNe 1978K and SN 1979C are exceptionally bright and SN 1987A is in our backyard (located in the Large Magellanic Cloud).

1.2.1 Theory of Radio Emission

Chevalier (1982b, 1982c) proposes that the source of emission from RSNe is synchrotron emission from relativistic electrons interacting with enhanced magnetic fields. These fields arise from the SN shock interacting with either the expanding photosphere (in the case of SNe Ib & Ic and young SNe II) or a relatively dense CSM (in the case of older SNe II). The interacting media has been heated and ionized by the initial UV/X-ray flash associated with the core collapse. The Main Sequence mass of the progenitors for RSNe is likely to exceed 15 $M_\odot$, in order to produce sufficient CSM for radio emission to be detected (Chevalier 1990). The ionized CSM (free-free absorption) is the primary source of all the initial absorption in young SNe II, with synchrotron self-absorption (SSA) playing a role in some specific cases (Chevalier 1998). Under the simplest of models, the CSM is presumed to have been established by a constant, spherical mass-loss rate ($\dot{M}$), constant velocity wind (w) from a massive progenitor or companion star resulting in a uniformly declining density (assuming free-free absorption), *i.e.*, $\rho \propto r^{-2}$ (Chevalier 1982a, 1982b). Many observed SNe demonstrate $\rho \propto r^{-1.5} \sim r^{-1.7}$ which can either be attributed to non-spherical and irregular mass loss or to SSA being the dominant absorption mechanism which yields the simple decay model of $\rho_{CSM} \propto r^{-2}$ (Montes *et al.* 2000; Fransson *et al.* 1996; Chevalier 1998; Fransson & Björnsson 1998). Chevalier (1998) identifies two cases where SSA plays an important role in SNe II, SN 1993J and 1987A, while most RSNe (*e.g.* SN 1979C and 1980K) are better explained by free-free absorption. In both absorption processes, a rapid initial rise in the observed radio flux density results from a decrease in the absorption processes as the radio emitting region expands with the outward moving shock front, however the turn-on is later and steeper the more free-free absorption dominates.

Weiler *et al.* (1990) propose that this CSM could be "clumpy" or "filamentary", contributing to slower turn-on times, as is evident with some SNe II. Montes *et al.* (1997) further propose that the possible presence of a disassociated ionized medium (*i.e.*, an HII region) along the line-of-sight, which is time-independent, can cause a spectral turn-over at longer wavelengths. Cowan, Roberts, & Branch (1994) observed this phenomena with SN 1957D in M83. Further, the CSM may also be structured, with rings, disks, shells, or gradients, which have yet to be properly incorporated into the current mathematical models.

Following Weiler *et al.* (1986,1990,2001) and Montes *et al.* (1997), the parameterized model, shown below, is commonly used to describe the emission from RSNe:

$$\mathrm{S(mJy)} = K_1 \left(\frac{\nu}{5\ \mathrm{GHz}}\right)^{\alpha} \left(\frac{t - t_o}{1\ \mathrm{day}}\right)^{\beta} e^{-\tau_{\mathrm{external}}} \left(\frac{1\ -\ e^{-\tau_{\mathrm{CSM_{clumps}}}}}{\tau_{\mathrm{CSM_{clumps}}}}\right) \left(\frac{1 -\ e^{-\tau_{\mathrm{internal}}}}{\tau_{\mathrm{internal}}}\right) \tag{1.1}$$

$$\tau_{\mathrm{external}} = \tau_{\mathrm{CSM_{uniform}}} + \tau_{\mathrm{distant}} \tag{1.2}$$

$$\tau_{\mathrm{CSM_{uniform}}} = K_2 \left(\frac{\nu}{5\ \mathrm{GHz}}\right)^{-2.1} \left(\frac{t - t_o}{1\ \mathrm{day}}\right)^{\delta} \tag{1.3}$$

$$\tau_{\mathrm{distant}} = K_4 \left(\frac{\nu}{5\ \mathrm{GHz}}\right)^{-2.1} \tag{1.4}$$

$$\tau_{\mathrm{CSM_{clumps}}} = K_3 \left(\frac{\nu}{5\ \mathrm{GHz}}\right)^{-2.1} \left(\frac{t - t_o}{1\ \mathrm{day}}\right)^{\delta'} \tag{1.5}$$

with the parameters K_1, K_2, K_3, and K_4 corresponding, formally, to the flux density (K_1) and uniform (K_2 and K_4) and clumpy (K_3) absorption, at 5 GHz one day after the supernova explosion (t_o). The terms $\tau_{\mathrm{CSM_{uniform}}}$ and $\tau_{\mathrm{CSM_{clumps}}}$ describe the attenuation of the local, uniform CSM and clumpy CSM that are near enough to the SN progenitor that they are altered by the outward shockwave. $\tau_{\mathrm{CSM_{uniform}}}$ is produced by an ionizing medium which uniformly covers the emitting region, and the $(1 - e^{-\tau_{\mathrm{CSM_{clumps}}}})\ \tau^{-1}_{\mathrm{CSM_{clumps}}}$ term describes the attenuation produced by an inhomogeneous medium with optical depths evenly distributed from 0 to $\tau_{\mathrm{CSM_{clumps}}}$ (*i.e.*, smooth to clumpy absorption). The τ_{distant} term describes the attenuation produced by a homogeneous medium which uniformly covers the emitting region, but is constant with time and is a sufficient distance from the SN progenitor so as not to be affected by the expanding shockwave. All absorbing media are assumed to be purely thermal, singly ionized gas (*e.g.*, H II) which absorbs via free-free transitions with frequency dependence ($\nu^{-2.1}$). The parameters δ and δ' describe the time dependence of the uniform and clumpy "optical" depths for the local, uniform and clumpy CSM, respectively.

To account for processes which would affect early observations of RSNe at high frequencies [although outside the scope of this dissertation, but included for completeness], it becomes necessary to include a term in Eq. 1.1 for internal absorption (τ_{internal}):

$$\tau_{\mathrm{internal}} = \tau_{\mathrm{internal_{SSA}}} + \tau_{\mathrm{internal_{ff}}} \tag{1.6}$$

$$\tau_{\mathrm{internal_{SSA}}} = K_5 \left(\frac{\nu}{5\ \mathrm{GHz}}\right)^{-2.5} \left(\frac{t - t_o}{1\ \mathrm{day}}\right)^{\delta''} \tag{1.7}$$

$$\tau_{\mathrm{internal}_{\mathrm{ff}}} = K_6 \left(\frac{\nu}{5\ \mathrm{GHz}}\right)^{-2.1} \left(\frac{t - t_o}{1\ \mathrm{day}}\right)^{\delta'''} \tag{1.8}$$

with the parameters K_5 and K_6 corresponding, formally, to the internal, non-thermal ($\nu^{-2.5}$) SSA (K_5) and the internal, mixed with non-thermal, thermal ($\nu^{-2.1}$) free-free absorption (K_6) respectively, at 5 GHz one day after the supernova explosion (t_o). The parameters δ'' and δ''' describe the time dependence of the SSA and free-free absorption components, respectively. Free-free absorption is the dominant process in most SNe II, while SSA is the dominant process in SNe Ib and Ic. It should be noted that radio emission from SN 1993J appears to be influenced by both both processes, while the radio SN 1987A appears to be primarily influenced by SSA.

A cartoon of the structure of the emission mechanism for RSNe is shown in Figure 1.1 (Weiler *et al.* 2001). The radio emission is believed to originate at the blastwave, as indicated in the figure (Chevalier & Fransson 1994).

1.2.2 Theory of X-ray Emission

The two mechanisms by which X-rays have been detected from SNe are Compton-scattered γ-rays from the radioactive decay of ^{56}Co and by the interaction of the SN shock with CSM, which is also the source of radio emission in SNe (Chevalier & Fransson 1994). The former has only been observed for SN 1987A, due to

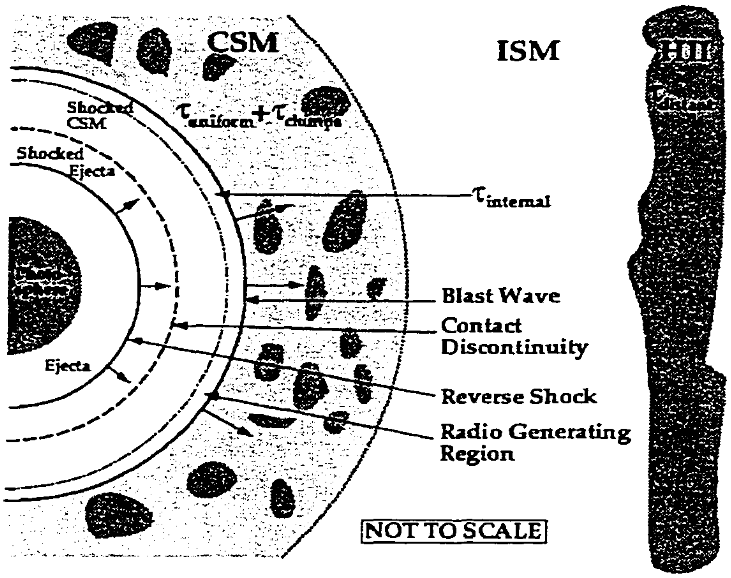

Figure 1.1: Cartoon drawing (not to scale) of a SN and its shocks along with the stellar-wind created CSM and more distant ionized material. The regions of absorption mentioned in Eqs. 1-8 are indicated above. Figure from Weiler *et al.* (2001).

the early monitoring of this object (Hasinger, Aschenbach, & Trümper 1996). But as SN 1987A evolves, the X-ray contribution from Compton-scattered γ-rays continues to diminish, and the shock-CSM interaction is expected to become the dominant process within 2 years (Burrows *et al.* 2000).

Radioactive Decay of ^{56}Co

SN explosions produce large amounts of ^{56}Ni (Colgate & McKee 1969). ^{56}Ni decays with a half-life of 6.5 days into ^{56}Co which decays with a half-life of 78.5 days into ^{56}Fe. Each of these decay processes produces a γ-ray which Compton-scatters and is converted into an X-ray. These hard (*i.e.*, high energy) X-rays are the dominant source of X-ray emission in the early stages of the SN explosion, prior to the CSM-shock interaction turning on. The first X-rays from this process should become visible within $\sim$400 days following the explosion, as the radioactive nuclei are predominately deeper within the star, and this is the time for the typical SN II envelope to become optically thin to X-rays (Sutherland 1990). This time may be shortened to 100+ days with the mixing of these radio-active elements into the hydrogen envelope, as was the case for SN 1987A (Dotani *et al.* 1987).

SN Shock-CSM Interaction

Pursuant to the discussion in the previous section regarding the radio emission resulting from the interaction of the outward moving SN shock and the CSM, a reverse shock is also produced. This is due to the pressure of the swept-up material on the outgoing shock, and it propagates back into the shocked SN gas (Chevalier 1982b,1982c,1998; Fransson 1994; Chevalier & Fransson 1994; Schlegel 1995). The reverse shock is produced sometime shortly after the explosion in SN with extremely dense envelopes, and usually after one year or so, as the shock catches up with the progenitor wind. So, as the radio emission probes the CSM, the X-ray emission can tell us about the progenitor's atmosphere. Models by Chevalier & Fransson (1994) and Fransson (1994) with a uniformly-produced CSM, predict the velocities and temperatures of the forward and reverse shocks to be:

$$V_{\text{For. Shock}} = V_{\text{Max. Ejecta}} \left(\frac{n-3}{n-2}\right) \tag{1.9}$$

$$V_{\text{Rev. Shock}} = \frac{V_{\text{Max. Ejecta}}}{n-2} \tag{1.10}$$

$$T_{\text{For. Shock}} = 1.36 \times 10^9 \left(\frac{n-3}{n-2}\right)^2 \left(\frac{V_{\text{Max. Ejecta}}}{10^9 \text{ km s}^{-1}}\right)^2 \tag{1.11}$$

$$T_{\text{Rev. Shock}} = \frac{T_{\text{For. Shock}}}{(n-3)^2} \tag{1.12}$$

where $n \sim$7—12, is a parameter determined from the hydrodynamic models and the power law exponent relating $\rho_{ejecta} \sim (V_{\text{ejecta}}(t-t_o)/r_{obs.})^n$ (Chevalier & Soker 1989). Typically the reverse and outward shock velocities are 500-1,000 km s^{-1} and 10,000-20,000 km s^{-1}, respectively, and the reverse and outward shock temperatures about $\sim10^7$K and $\sim10^9$K, respectively (Chevalier 1982a;Chevalier & Fransson 1994). The forward shock is too diffuse to produce any noticeable X-rays, so the cooler shocked CSM behind the blastwave is the dominant source of the soft (i.e. low energy photons) X-rays produced by the SN shock-CSM interaction. With the exception of SN 1987A, this is the dominant mechanism of X-ray production in detected X-ray SNe. Perhaps associated with this mechanism is the possibility of a prompt thermal burst producing hard (100 keV) X-ray emission with a black body continuum of ~0.02 keV, which are produced ~1,000 s following the initial explosion (Chevalier 1990). This X-ray burst would be produced by the shock interacting with the progenitor's dense hydrogen envelope and should have a luminosity in excess of 10^{45} erg s^{-1}. Due to the briefness of this event, no X-ray emission has been detected as a result of a prompt thermal blast (Schlegel 1995).

1.2.3 Measurable Results

The current models for radio & X-ray emission from SNe has been very successful in the cases where there are sufficient radio observations to accurately determine the many independent parameters included in Eqs. 1-8. This has been possible for RSNe in each of the 3 subtypes which radio emission is expected, *e.g.*, the Type Ib SN 1983N (Sramek *et al.* 1984), the Type Ic SN 1990B (van Dyk *et al.* 1993a), and the Type II SNe 1979C (Montes *et al.* 2000) and 1980K (Montes *et al.* 1998). The agreement for the more slowly evolving Type II SNe, however, departs from the theoretical model discussed in the previous subsection ~ 4,000 days ($t < 10$ yrs) following the supernova event. The implications of this deviation will be addressed in subsequent chapters. With such a small sample of X-ray events and the fact that only four have observed spectra needed to derive an accurate energy flux, the X-ray study of SNe has been a difficult one. However, X-ray detections of SNe are now entering a Renaissance with the first *Chandra* X-ray results being published. The vast improvement in instrumentation has drastically increased the energy sensitivity and spatial resolution of X-ray astronomy.

Mass-Loss Rate

For younger SNe ($t < 10$ yrs), the Chevalier (1982b,1982c) model provides a way to determine the ratio of the mass-loss rate and the progenitor wind velocity ($\dot{M}/w$). For the case with external absorption being entirely dependent on a uniform medium, Weiler *et al.* (1986) was able to the derive the following expression:

$$\left(\frac{\dot{M}\ /\ \mathrm{M}_\odot\ \mathrm{yr}^{-1}}{w\ /\ 10\ \mathrm{km\ s}^{-1}}\right) = 3\ \times 10^{-6}\ \tau_{\mathrm{CSM_{uniform}}}^{0.5}\ m^{-1.5}\left(\frac{v_i}{10^4\ \mathrm{km\ s}^{-1}}\right)^{1.5} \times \left(\frac{t_i}{45\ \mathrm{days}}\right)^{1.5}\left(\frac{t}{t_i}\right)^{1.5m}\left(\frac{T}{10^4\ \mathrm{K}}\right)^{0.68} \quad (1.13)$$

Because it is often many days before the appearance of optical lines from which the ejecta velocities (v_i) are measured, t_i is arbitrarily measured in units of 45 days. With observational evidence that further constrains $0.8 \leq m \leq 1.0$ ($m = -\delta/3$) and, from Eq. 1.9, $\dot{M} \propto t_i^{1.5(1-m)}$, the dependence of the mass-loss rate on the date, upon which the ejecta velocity is measured, is very weak ($\dot{M} \propto t_i^{<0.3}$) (Weiler *et al.* 1996). Typical mass-loss rates assume a temperature of

20,000 K, CSM ejecta velocities of 10 km/s (standard for red super giant winds), and fitted data from RSNe studies, including $t = t_{6cmpeak} - t_o$ days, $\tau_{CMS_{uniform}}$ from Eq. 1.3, and m = $-\delta/3$ also from Eq. 1.3.

The Chevalier (1982b,1982c) model is incomplete because it assumes a smooth CSM and does not account for the relatively slow turn-on for some SNe II, as compared to SNe Ib and Ic. Weiler *et al.* (1990) have incorporated the "clumpiness or filamentation" phenomena by the inclusion of $\tau_{\mathrm{CSM_{clumps}}}$ in Eqs. 1.1 and 1.5. This improvement was essential in modeling the early radio light curves of SNe 1988Z (van Dyk *et al.* 1993b) and 1993J (van Dyk *et al.* 1994). From these predictions, the typical pre-SN mass-loss rates for the SNe Ib and Ic and the first 10 years of SNe II are typically $\sim 10^{-6}$ $M_{\odot}yr^{-1}$ and $\sim 10^{-4}$ $M_{\odot}yr^{-1}$, respectively (Weiler *et al.* 2001). van Dyk *et al.* (1994), employing very early light curve data, found the mass-loss rate of SN 1993J was initially $\sim 10^{-4}$ $M_{\odot}yr^{-1}$ 1,000 yrs before explosion and then declined to $\sim 10^{-5}$ $M_{\odot}yr^{-1}$ just prior to explosion. Further complicating the situation, this result may not account for the correct contribution of SSA in the evolution of the radio light curve (Fransson & Björnsson 1998).

A careful analysis of the light curve for SN 1979C has indicated quasi-periodic fluctuations in its radio luminosity of order 15%, with a period of 1,575 days (Weiler *et al.* 1991,1992). Weiler *et al.* (1991,1992) attribute this phenomenon to minor (8%) density modulations in the CSM with a period of 4,000 yrs. This is much too long a time to be attributed to any sort of stellar pulsations and is now considered to have been caused by interaction with an eccentric binary and the SN progenitor's stellar wind. Further theoretical work by Schwarz & Pringle (1996) and Boffi & Panagia (2001), and observations of SNe 1993J (Podsiadlowski *et al.* 1993) and 1994I (Nomoto *et al.* 1994) indicate that binaries may be common in pre-SN systems.

X-ray emission from SNe provides additional information to the radio observations about the SN event and its environment. The earliest period in which detectable X-ray emission are produced is the early interaction with a very dense CSM close to the SN progenitor. This was the case for SN 1993J, which was detected in the X-ray 6 days following maximum optical light (Zimmerman *et al.* 1993a, 1983b, 1983c, 1983d). SN 1980K was also detected in the X-ray within 2 months of maximum optical light (Canizares *et al.* 1982), while SN 1987A did produce detectable X-ray emission for more than five months after explosion (Makino *et al.* 1987a,1987b). This early emission could indicate a denser stellar wind for SNe or more likely (as mentioned in the previous section) the possible presence of a binary companion. Further, X-ray studies of SN 1993J, in conjunction with radio observations, have indicated the need for steeper density profiles in the CSM in order to explain the rapid turn-on of the early X-ray SNe (Fransson *et al.* 1996).

Intervening HII Regions

SN 1978K follows the characteristic radio light curve for a Type II SN (Ryder *et al.* 1993; Schlegel *et al.* 1998), but there appears to be a constant absorption term which may indicate either the presence of an intervening HII region or a distant CSM shell associated with the SN progenitor (Montes *et al.* 1997). Ryder *et al.* (1993) note the lack of optical emission lines broader than $\sim$1,000 km s^{-1}, suggesting the presence of slow moving CSM. Chu *et al.* (1999) measure the [N II] 6583/Hα ratio of this absorbing region in a high dispersion spectrum to be 0.8 — 1.3. Their observations support the Ryder *et al.* (1993) contention that the absorbing region is a stellar ejecta nebula.

Shape of Supernova Blast

It has been suggested by many that SN explosions are non-spherical, with the possibilities of jets, lobes, and conical ejecta among the many competing theories for directed mass loss (Weiler *et al.* 2001; Schlegel *et al.* 2001). Radio astronomy offers a unique insight into this topic, with the highest resolution imaging available at any wavelength using the Very Long Baseline Interferometer (VLBI). Marcaide *et al.* (1997) demonstrate this most clearly, with a series of time lapse images of the expanding SN shock of SN 1993J. Their images, over 2 years, shows a ring-shaped emission region indicative of a spherical blast, while optical polarimetry studies indicate a non-spherical structure (Hoeflich *et al.* 1996). This dichotomy remains a mystery to be solved. The Fransson *et al.* (1996) X-ray observations of SN 1993J also appear to indicate that the density of the CSM is $\propto r^{-1.5}$ and not r^{-2}. This could be an indication that the CSM is not distributed spherically, but rather in a more toroidal shape. This interpretation has been questioned by the fact that increasing the SSA contribution into the modeling of the light curve yields a fit which supports a spherical distribution (Fransson & Björnsson 1998).

Pre-Supernova Stellar Evolution

Radio emission from SNe with constant spectral index, but deviation in flux density from the standard decay curve, is an indication of variation in the density of CSM from the canonical r^{-2} law expected with a pre-SN wind with constant velocity of mass-loss rate. Chevalier (1982b) demonstrates that the luminosity of RSNe is proportional to the logarithm of ρ_{CSM}. Since the SN blast wave travels with a speed ~10,000 km s^{-1} and the CSM was ejected with a speed ~10 km s^{-1}, every one year of monitoring a RSNe monitors ~1,000 years of stellar wind evolution (Weiler *et al.* 2001).

Deceleration of Shock Wave

Radio astronomy currently offers the only method to directly measure the deceleration of the SN shock over long periods of time. By fitting a model to radio light curves of SN 1987A, Manchester *et al.* (2001) were able to measure a drop in the velocity of ~32,000 km s^{-1} in the time between the explosion and the shock reaching the prominent optical ring, to a current speed of 3,000 km s^{-1}. As mentioned above, Marcaide *et al.* (1997) were able to directly detect a deceleration from SN 1993J, but not as significant as that for SN 1987A. SN 1993J is currently expanding with a velocity of ~15,000 km s^{-1}, as measured in 1996 (Marcaide *et al.* 1997).

Peak Radio Luminosities as Distance Indicators

Weiler *et al.* (1998,2001) have demonstrated that the radio emission from SNe evolves in a systematic fashion with a distinct flux density at each frequency and a well defined time between the explosion and the optical and radio peak luminosities. In particular, they have found a relationship between the peak spectral luminosity at 6 cm ($L_{6\text{ cm peak}}$) and the time after explosion to reach the 6 cm peak ($t_o - t_{6\text{ cm peak}}$). With 5 SNe Ib and Ic sampled so far, there appears to be very good agreement on a standard 6 cm peak luminosity:

$$L_{6\text{ cm peak}} = 1.3 \times 10^{27}\text{ erg s}^{-1}\text{ Hz}^{-1}. \tag{1.14}$$

With 17 SNe II in their sample, Weiler *et al.* (1998,2001) have found a relationship for

$$L_{6\ \mathrm{cm\ peak}} = 6.0 \times 10^{23} \left(\frac{t_o - t_{6\ \mathrm{cm\ peak}}}{1\ \mathrm{day}} \right)^{1.5} \mathrm{erg\ s^{-1}\ Hz^{-1}}. \tag{1.15}$$

These are still preliminary results, but they could prove invaluable in conjunction with future observations, especially in galaxies with Cepheid-derived distances, in establishing SNe Ib, Ic, and II as standard candles.

Chapter 2

The Fading Radio Emission From SN 1961V: Evidence for a Type II Peculiar Supernova?

2.1 Introduction

SN 1961V, the prototype of Zwicky's Type V SNe (now classified as either a Type II Peculiar SN or a luminous blue variable (LBV)), was unique in several respects (Branch & Greenstein 1971). Its progenitor was visible as an 18th magnitude star from 1937 to 1960. It is the first SN, prior to SN 1987A, whose parent star was identified before it exploded (assuming a SN interpretation is correct for this event). The bolometric correction, the exact distance, and the extinction are all uncertain, but its pre-outburst luminosity apparently exceeded

10^{41} ergs s^{-1}, which is the Eddington limit for a 240 $M_{\odot}$ star. After the explosion in late 1961, the initial peak of the optical light curve was more complex and much broader than for any supernova ever observed. Subsequently, the optical light curve decayed more slowly, by about 5 magnitudes in 8 years. Few SNe have been followed optically for more than 2 years. Optical spectra taken during this extended bright phase showed that the characteristic expansion velocity of SN 1961V was 2,000 km s^{-1}, which differs from the typical value of 10,000 km s^{-1} for most SNe. This velocity is similar to novae expansion velocities. However, no novae are this strong and none have persisted for this long in the radio. This velocity is in fact consistent with the measurements of SN 1986J (another Type II Peculiar SN), which had an expansion velocity (taken well after maximum optical brightness) of 1,000 km s^{-1} (van Gorkom *et al.* 1986; Rupen *et al.* 1987; Weiler & Sramek 1988).

Using the VLA, observations of SN 1961V were made in the mid 1980s, with the most definitive search in 1986 (Cowan, Henry, & Branch 1994; hereafter referred to as CHB). CHB detected a non-thermal radio source at the precise position of SN 1961V. Fesen (1985) also reported recovering SN 1961V in the optical. CHB later detected an optical counterpart to SN 1961V, which was identified as an H II region using filter photometry. [CHB also detected another slightly fainter radio source to the west of SN 1961V with a similar non-thermal spectral index.

This source was identified as a SNR not previously identified. This SNR also has an associated optical counterpart (i.e., an H II region).] At the distance of NGC 1058 (9.3 Mpc; Tully 1980; Silbermann *et al.* 1996), SN 1961V is as radio luminous as the bright Galactic SNR Cas A. SN 1961V's luminosity is also comparable to several historical decades-old (also known as intermediate-age) radio supernovae (RSNe) including SNe 1923A, 1950B, 1957D, 1968D, 1970G and 1986J (Cowan *et al.* 1991; Cowan *et al.* 1994; Eck *et al.* 1998; Eck *et al.* 2001; Hyman *et al.* 1995; Weiler & Sramek 1988).

Recently, however, there has been some question about whether the event identified as SN 1961V was actually a supernova. Goodrich *et al.* (1989) suggest instead that this event was an LBV similar to η Carinae, and that the supposed supernova was an outburst of the variable star. Subsequently, Filippenko *et al.* (1995) observed SN 1961V using the Hubble Space Telescope (HST), although at that time the HST had not been refurbished. Those observations seemed to suggest a (very faint) star is still present at the site, which might or might not argue against a supernova origin. Among the brightest LBVs (e.g. η Car, P Cygni, and V 12 in NGC 2403), η Car is reported to have been the most luminous, reaching $M_{Bol} \simeq -14$. In comparison, SN 1961V was reported to have peaked at $M_{Bol} \simeq -17$ (Humphreys & Davidson 1994). This peak estimate for SN 1961V is likely underestimated by 1.2 magnitudes if one accounts for the more recently derived Cepheid distance (Silbermann *et al.* 1996). This would make SN 1961V nearly 50$\times$ brighter in the optical than η Car at maximum brightness (Humphreys & Davidson 1994).

To assess the exact nature of this event I have performed a series of observations at various wavelengths, employing the phased-VLA with the Very Large Baseline Array (VLBA) and the ROSAT X-ray satellite. In this Chapter I report on our recent VLA radio observations of SN 1961V and what they indicate about the nature of this event. The Very Long Baseline Interferometer (VLBI) [VLA and VLBA] and ROSAT results are reported in Stockdale (2001).

2.2 VLA Observations and Results

The new VLA data on SN 1961V are taken from three observing runs. In the first, SN 1961V was observed for 12 hours on 14 September 1999 at 18cm (1.67 GHz) using the VLA's most extended (A) configuration, with a maximum baseline of 34 km. These data were taken while the VLA was being used in phased-array mode for a VLBA run, and the total bandwidth was 50 MHz in each of the two orthogonal circular polarizations. The phase calibrator was J0253+3835, and both 3C286 and 3C48 were used to set the flux density scale. The total time on-source was 4.7 hours.

During the second pair of observing runs, on 21 and 25 January 2000, the

VLA was in its B configuration (maximum baseline of 10km), and observed at 6cm (4.89 GHz) for a total of 12 hours. Here I used the standard VLA continuum mode, obtaining a total of 100 MHz bandwidth in each of the two orthogonal circular polarizations. The phase calibrator was J0251+4032, and 3C48 was used to set the flux density scale. In all observations the pointing center was CHB's radio position for SN 1961V, and flux densities for 3C48 and 3C286 were taken from Perley, Butler, & Zijlstra (2000).

Data were Fourier transformed and deconvolved using the CLEAN algorithm as implemented in the AIPS routine IMAGR. The data were weighted using Brigg's robustness parameter of -1, which yields a reasonably small point-spread function at the cost of a few percent loss in sensitivity. We have also re-analyzed the CHB observations of the region, using the same data reduction procedures and inputs as were used on the current data. The results of our analyses are presented in Table 2.5 and Figures 2.1 & 2.2. To derive the flux density and position for SN 1961V, a JMFIT two source Gaussian fit yielded the best results for all 4 observations, while a single source Gaussian model yielded the best results for the other sources in the field of view. The positions reported in Table 2.5 are weighted averages of the radio positions for these sources at the various wavelengths and epochs. Uncertainties in the peak intensities are reported as the rms noise from the observations. To check that changes in measured flux densities are real, I also measured the flux density of a resolved background source present at all epochs. The background source's integrated flux densities for each wavelength band are relatively unchanged at both epochs. Our re-measurements of the CHB data are consistent, within the error bars, with those of Cowan *et al.* (1991).

2.3 VLBI Observations and Results

SN 1961V was observed at 18 cm with the VLBA in conjunction with the 18 cm VLA observations described in the previous Section. 3C286 and 3C48 were used to set the flux density scale and J0253+3835 was used as a phase calibrator. We expected SN 1961V to be an extremely faint source, so J0230+4032 was used in embedded scans of the calibrators to serve as a check for the accuracy of the calibrations that were also applied to SN 1961V. The pointing center was CHB's radio position for SN 1961V, and flux densities for 3C48 and 3C286 were taken from Perley *et al.* (2000).

The data reduction was performed at the Array Operations Center in Socorro, NM, over the course of 5 weeks, beginning in October 1999 and continuing through July 2000 with the assistance of Michael Rupen. The reduction process included applying the a priori amplitude and phase calibration, basic spectral flagging based on the auto-correlation (total power) data, and running a preliminary fringe-fit on the whole run with the AIPS routine KRING. Further flagging of the calibrator, J0253+3835, was required for the the bad gain solutions and then the AIPS routine CLCAL was used to interpolate the solutions. Due to the overwhelming amount of data that was taken ~8 Gigabytes, the AIPS routine SPLAT was used to average down in frequency, to get 1 channel per IF (an IF consists of a set of one or more equally spaced frequency channels; a total of 8 IF's were used in this stage of the analysis) for the calibrated data. The calibrated data was then further flagged using the AIPS routine EDITR, examining each baseline pair for amplitude and phase discrepancies. The phase calibrator was then mapped for one IF using only the VLBA antennae with numerous self-calibrations cycles to produce a common amplitude scale. The model for this map was then applied to the other IF's, resulting in a final VLBA only map. This model was used to calibrate the VLA data for the VLBI run. (The 27 VLA antennae were sampled every 10 seconds, and this sampling was used for the VLBI data set.) All of the data for J0253+3835 from 10 VLBA antennae and the VLA were combined and then calibrated further to achieve the best possible phase solutions. The result of this calibration effort for J0253+3835 is shown in Figure 2.4 (see Figure 2.4). (A brief discussion of this fascinating source can be found in Chapter 6.) Finally, these solutions were applied to SN 1961V, and the resulting image is shown in Figure 2.5.

As is evident in Figure 2.5, the source was not clearly detected. There are two potential interpretations for this result. The first is that the emission from

SN 1961V is resolved by the VLBA. This would imply that the source is extended beyond the minimum beam size of 7.56 milli-arcseconds. Accounting for the age of SN 1961V and the Silbermann *et al.* (1996) distance, this would establish a lower limit for the expansion velocity of SN 1961V to be 18,000 km s^{-1}. This velocity is very high, given the age of the source and the deceleration one would expect as the shock propagates out through a relatively dense CSM. The second interpretation is that the source is unresolved and indistinguishable with the noise limits of the VLBI image. There are at least five unresolved sources with flux densities above the 3 sigma limit of 90 μJy within $0\farcs1$ of the VLA position for SN 1961V.

2.4 Discussion

We have recovered a radio source at the position of SN 1961V at 18 cm and 6 cm, coincident, within the error limits, with the CHB position. Our measured flux densities at both wavelengths indicate a clear decline in the radio emissions from SN 1961V from the previous CHB observations, as indicated in Figures 2.1 & 2.2. The recently measured 18 cm flux, when scaled to 20 cm using the newly determined spectral index, indicates a reduction in the 20 cm peak flux intensity by 36% from 1984 to 1999 (see Table 2.5). The 6 cm peak flux intensity has also dropped by 54% in the interval from 1986 to 2000. (The western source shows no change in peak intensity for either the 6 cm or the 20 cm measurements within noise limits.) The radio emission from the vicinity of SN 1961V appears to be much more complicated than originally thought. Our new observations and re-analysis of the CHB data indicate there is at least one previously undetected radio source within $0\rlap{.}''9$ of SN 1961V. The radio emission from this source is non-thermal at both epochs and has decayed by 50% at 20 cm and by 33% at 6 cm. The region where SN 1961V is located in NGC 1058 is clearly one of recent star formation. The peak flux density of this new source near SN 1961V is 0.040 ± 0.008 mJy/beam (at 6 cm) and 0.082 ± 0.026 mJy/beam (at 20 cm). These values are comparable to that of the distinct western source reported by CHB, so this new source may likely be a previously undetected SNR.

The decline in the radio flux density of SN 1961V is consistent with models for radio emission from SNe (Chevalier 1984). Synchrotron radiation is produced in the region of interaction between the ejected supernova shell and the circumstellar shell that originated from the prior mass loss of the progenitor star. In such models the radio emission drops as the expanding shock wave propagates outward through the surrounding and decreasingly dense circumstellar material. The decline in the flux density of SN 1961V is also consistent with Gull's (1973) model for radio emission from SNRs. This predicts an initial decline in the emission of RSNe for the first 100 years as the shock overcomes the circumstellar material (CSM) and a later turn-on as the build up of material from the ISM results in an increase of synchrotron emission, as the object enters the SNR phase. Thus, the radio emission from these intermediate-age SNe, sources with ages comparable to SN 1961V, probes the transition region between fading SNe and the very youngest SNRs. In Figure 2.3, I illustrate the radio light curves of several intermediate-aged SNe along with a few SNRs, plotting the time since supernova explosion versus the luminosity at 20cm. It is clear that the radio emission of SN 1961V at an age of $\simeq$ 38 years is very similar to known radio SNe at comparable ages, and particularly that the radio luminosities of SN 1961V, in NGC 1058, and the Type II SN 1950B, in M83, are virtually identical at similar ages.

As shown in Table 2.5, our new observations indicate that SN 1961V remains a non-thermal radio source. The spectral index, α, is relatively unchanged although the error bars are rather large. The spectral index was derived using the peak intensities, in order to limit the contribution from the surrounding H II region. We might expect a possible flattening of the radio spectrum as the emission from SN 1961V continues to fade. This would be an indication of the increasing contribution from the thermal emission of the associated H II region. Such was the case for the radio (Cowan *et al.* 1994a) and optical (Long *et al.* 1992) emissions of SN 1957D, in M83, which has now faded below the level of an associated H II region. The current and previous values of α for SN 1961V are still consistent with spectral indices of intermediate-age RSNe at similar wavelengths, as shown in Table 2.5. The non-thermal nature of these sources is well-documented, as are those for young radio SNRs, with Cas A, the youngest, whose spectral index ranges from -0.92 to -0.64 (Anderson *et al.* 1991).

We can also compare the rate of decline of radio emission for SN 1961V, as measured by a power-law index ($S \propto t^{\beta}$), with decline rates of known Type II RSNe (see Figure 3). The power-law indices for SN 1961V were determined from the peak intensities to be $\beta_{20cm} = -0.69 \pm 0.23$ and $\beta_{6cm} = -1.75 \pm 0.16$. The decay indices for SN 1961V fall within a range of previously measured indices for some intermediate-age RSNe (see Table 2.5). In particular, SN 1957D and SN 1970G both have fairly rapid decline rates, while the younger Type II RSNe (SN 1979C and SN 1980K) indicate a slower rate of decline. I also note that while the radio emission from SN 1980K has abruptly dropped after approximately ten years (Weiler *et al.* 1992; Montes *et al.* 1998), SN 1979C (at a greater distance than SN 1980K) is still emitting at detectable levels (Weiler *et al.* 1991). Recently the radio emission of SN 1979C appears to have flattened, as indicated in Figure 2.3. This may be a result of the shock wave hitting a denser region of CSM (Montes *et al.* 2000). The implications of these comparisons with SN 1961V are that its shock may be traveling through considerably more circumstellar material (CSM) than similarly-aged RSNe, e.g., SN 1957D. As a result, its radio flux continues to drop at a slower rate more akin to the younger RSNe, i.e. SNe

1979C, 1980K, and 1986J (the only other identified Type II_{pec} SN). Consistent with this interpretation is the very rapid decline in the radio emissions of Type Ib RSNe, e.g. SN 1983N and and SN 1984L, which presumably have less circumstellar material (see Table 2.5). Based on these comparisons the radio observations of SN 1961V are consistent with Type II RSNe.

Radio comparisons between η Car, the super-luminous LBV, and SN 1961V are more problematic since the first radio observations of η Car were made 100 years after its eruption. η Car, with a 20 cm flux density of 0.9 ± 0.3 Jy (Retallack 1983), is in fact not a strong radio source when compared to SN 1961V. In order to determine η Car's 20 cm flux at the current age of SN 1961V, we have naively assumed a range of potential β values for η Car from -1, our measured index for the decline of the flux at 20 cm of SN 1961V, to -3, the index for the decline of SN 1957D. Applying these constant decay rates to η Car, its 20 cm flux (40 years after outburst) would range from 5 to 65 times the Retallack (1983) measurement. This would result in η Car being at least 1,000 times weaker than the radio source at the position of SN 1961V reported in this Chapter. η Car's 3 cm flux was measured over a period of 5 years by Duncan, White, & Lim (1997) and found to vary between 0.5 Jy and 2.8 Jy, well below the levels of 6 cm & 20 cm emissions of SN 1961V. They further report that η Car's spectral index between 3 cm and 6 cm appears to peak at $+1.8$ at the position of η Car and then drops radially toward an index of 0. The source of the radio emission is believed to be thermal radiation from H II regions associated with η Car (Retallack 1983). The spectral index derived from radio observations at 2 cm and 6 cm of Skinner *et al.* (1998) of P Cyg, another LBV, is 0.47 ± 0.12. (P Cyg's last reported outburst was in the 17th century.) The positive values of the LBV spectral indices are obviously very different from the negative (i.e. non-thermal) indices for such events as SN 1961V, SN 1923A [the oldest RSN], and Cas A [the youngest radio SNR] (Anderson *et al.* 1991; Cowan *et al.* 1991; Eck *et al.* 1998). The non-thermal spectral indices for SNe and SNRs result from a shock front interacting with the CSM and ISM. It is possible that P Cyg and η Car may have been non-thermal radio sources immediately following their initial outbursts. Unfortunately, there is no observational evidence to support or refute this possibility. Further, it is uncertain whether the radiation from an LBV event would remain non-thermal this long after the outburst. One of the most recent LBV events in the Small Magellanic Cloud, HD 5980, was observed in the radio by Ye, Turtle, & Kennicutt (1991) prior to LBV outbursts in 1993 and 1994. It was later observed in 1996 using the Australian Telescope Compact Array at 3 cm and 6 cm for $\sim$ 1 hour. No compact radio emission was detected from the vicinity of the star, with an upper limit threshold of a few mJys (S. M. White 2001, private communication).

2.5 Conclusions

Our radio measurements have detected a source at the position of SN 1961V. The source's radio luminosity, its spectral index, and its decay index are all consistent with values reported for Type II RSNe and thus appear to support a supernova interpretation. However, the lack of radio observations of similarly-aged bright LBVs prevents a definitive identification of the true nature of SN 1961V. Additional multiwavelength observations of SN 1961V, as it evolves, will clearly be needed to make a final judgment about the nature of this enigmatic event. These should include further monitoring with the VLA and using the Space Telescope Imaging Spectrograph (STIS) to analyze nebular emission lines from the region near SN 1961V to discriminate LBV ejecta nebulae ([N II]-bright), decades old SNe ([O III] and [O I]-bright), and mature SNRs ([S II]-bright). The latter observations could be very useful in ruling out one of the two scenarios for SN 1961V.

Table 2.1: Radio Observations of the Region Near SN 1961V.

Parameters	SN 1961V	Western Source
Right Ascension (J2000)	$02^h43^m36\overset{s}{.}46 \pm 0\overset{s}{.}02$	$02^h43^m36\overset{s}{.}24 \pm 0\overset{s}{.}01$
Declination (J2000)	$+37°20'43\overset{''}{.}2 \pm 0\overset{''}{.}2$	$+37°20'43\overset{''}{.}8 \pm 0\overset{''}{.}4$
18 cm[a] (14 Sept. 1999)	0.147 ± 0.026	0.117 ± 0.026
6 cm[a] (21 & 25 Jan. 2000)	0.063 ± 0.008	0.056 ± 0.008
Spectral Index[b] α_{6cm}^{18cm}	-0.79 ± 0.23	-0.64 ± 0.28
20 cm[a] (15 Nov. 1984)	0.229 ± 0.020	0.160 ± 0.020
6 cm[a] (13 Aug. 1986)	0.135 ± 0.013	0.070 ± 0.013
Spectral Index[b] α_{6cm}^{20cm}	-0.44 ± 0.15	-0.98 ± 0.22

[a] peak flux density (mJy beam^{-1})
[b] Obtained by $S \propto \nu^{\alpha}$

Table 2.2: Comparison of SN 1961V with Other Radio Supernovae.

Name	SN Type	Spectral Index (α)[a]	Decay Index (β)[b]
SN 1923A	II_P	-1.00 ± 0.24	-7.90 ± 0.42 (6 cm)
SN 1950B	II?	-0.57 ± 0.08	$+0.12 \pm 0.13$ (20 cm)
			$+0.22 \pm 0.04$ (6 cm)
SN 1957D	II?	-0.30 ± 0.02	-2.66 ± 0.07 (20 cm)
			-2.44 ± 0.04 (6 cm)
SN 1961V	II_{pec}	-0.79 ± 0.23	-0.69 ± 0.23 (20 cm)
			-1.75 ± 0.16 (6 cm)
SN 1970G	II	-0.55 ± 0.13	-1.95 ± 0.17 (20 cm)
SN 1979C	II_L	-0.72 ± 0.05	-0.71 ± 0.08 (20 cm & 6 cm)
SN 1980K	II_L	-0.50 ± 0.06	-0.65 ± 0.10 (20 cm & 6 cm)
SN 1986J	II_{pec}	-0.30 ± 0.06	$-1.18^{+.02}_{-.04}$ (20 cm & 6 cm)
SN 1983N	I_{SL}	-1.0 ± 0.2	-1.5 ± 0.3 (20 cm & 6 cm)
SN 1984L	I_{SL}	-1.03 ± 0.06	-1.59 ± 0.08 (20 cm & 6 cm)

[a] Obtained by $S \propto t^{\beta}$
[b] Obtained by $S \propto \nu^{\alpha}$
References — (Cowan *et al.* 1991; Cowan *et al.* 1994a; Eck *et al.* 1998; Panagia *et al.* 1986; Rupen *et al.* 1987; Weiler *et al.* 1986; Weiler *et al.* 1992; Weiler *et al.* 1991)

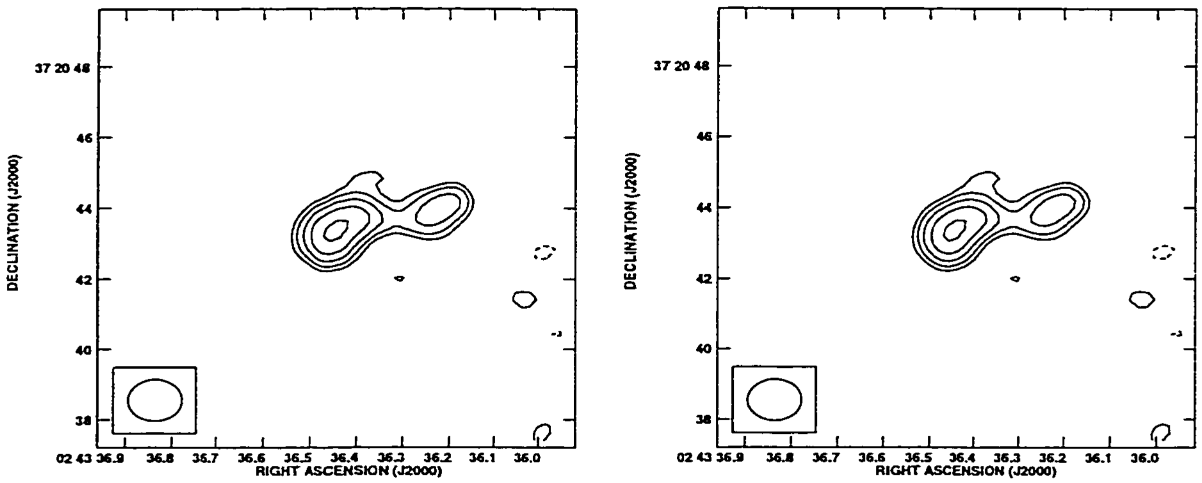

Figure 2.1: *(a.)* (left) Radio contour map at 20 cm (1.5 GHz) of SN 1961V (the strong eastern source) and a neighboring SNR (western source). Contour levels are -0.11, -0.08, -0.06, 0.06, 0.08, 0.11, 0.16, 0.23, and 0.32 mJy beam^{-1}, with a beam size of $1''.26 \times 1''.05$, p.a. = 89°, and rms noise of 0.020 mJy beam^{-1}. Observations taken with the VLA in A configuration 15 November 1984. *(b.)* (right) Radio contour map at 18 cm (1.7 GHz) of the same region. Contour levels are -0.11, -0.08, -0.06, 0.06, 0.08, 0.11, 0.16, 0.23, and 0.32 mJy beam^{-1}, with a beam size of $1''.20 \times 1''.01$, p.a. = 82°, and rms noise of 0.020 mJy beam^{-1}. Observations taken with the VLA in A configuration 14 September 1999.

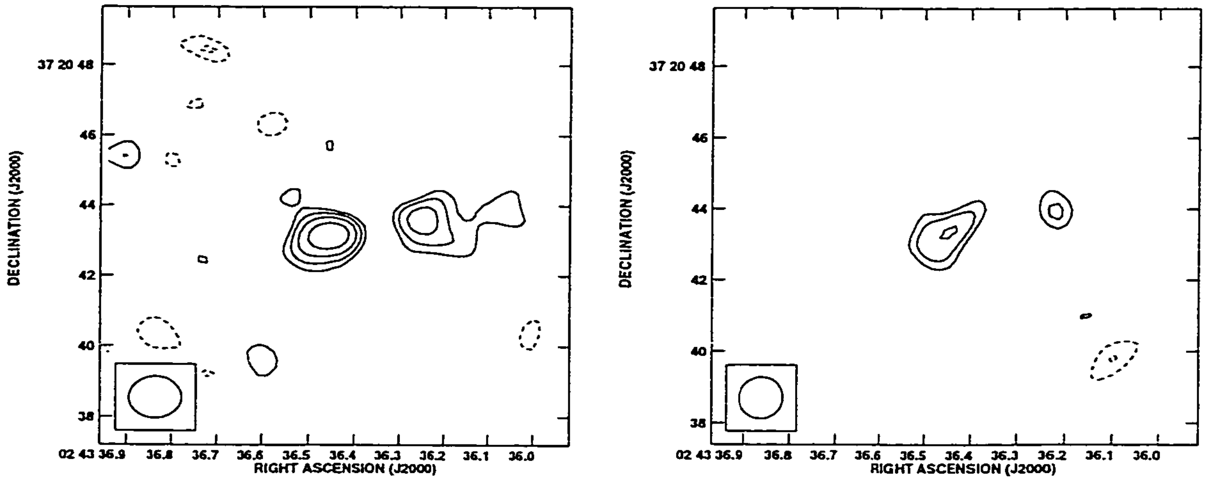

Figure 2.2: *(a.)* (left) Radio contour map at 6 cm (4.9 GHz) of SN 1961V (the strong eastern source) and a neighboring SNR (western source). Contour levels are -0.07, -0.05, -0.03, 0.03, 0.05, 0.07, 0.10, 0.14, and 0.19 mJy beam^{-1}, with a beam size of $1\farcs39 \times 1\farcs17$, p.a. $= -89°$, and rms noise of 0.013 mJy beam^{-1}. Observations taken with the VLA in B configuration 13 August 1986. *(b.)* (right) Radio contour map at 6 cm (4.9 GHz) of the same region. Contour levels are -0.07, -0.05, -0.03, 0.03, 0.05, 0.07, 0.10, 0.14, and 0.19 mJy beam^{-1}, with a beam size of $1\farcs17 \times 1\farcs13$, p.a. $= -35°$, and rms noise of 0.008 mJy beam^{-1}. Observations taken with the VLA in B configuration 21 & 25 January 2000.

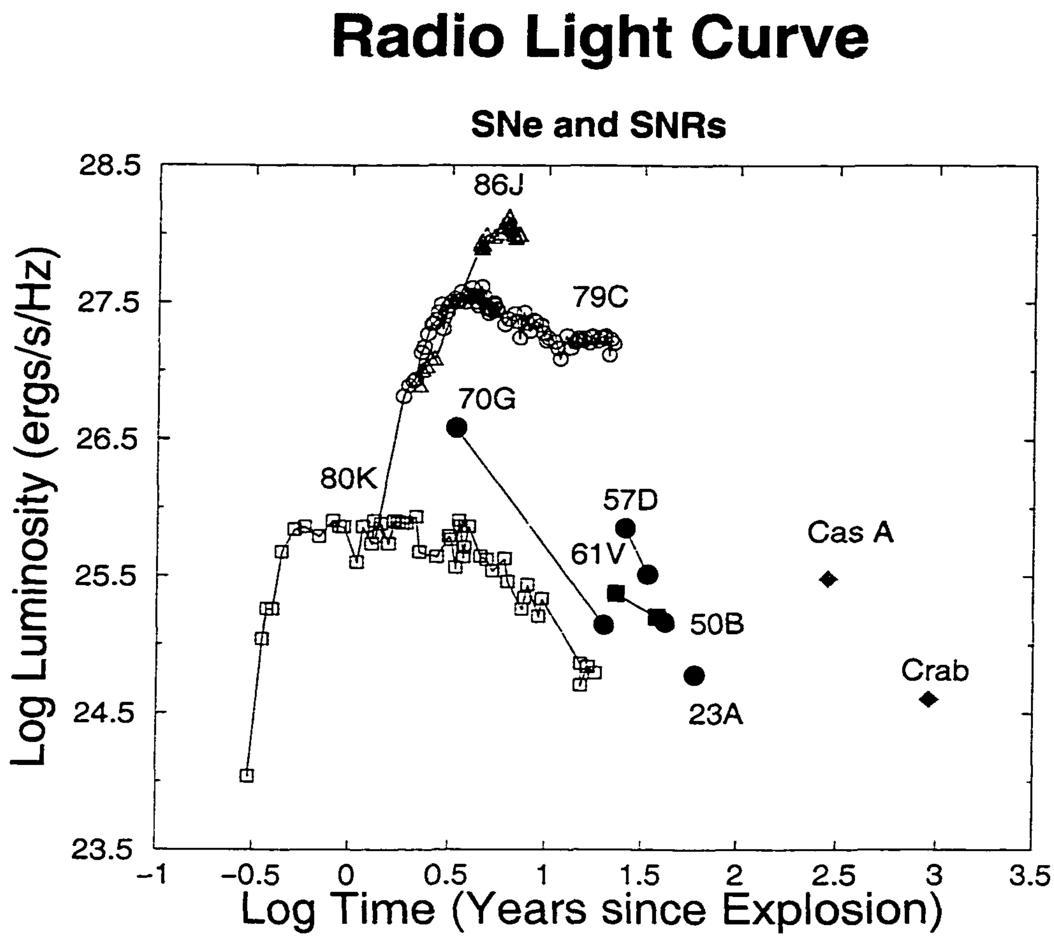

Figure 2.3: Radio light curve for SN 1961V at 20 cm compared to several RSNe and SNRs. Data, fits and distances for SN 1923A, from Eck *et al.* (1998) and Saha *et al.* (1995); for SNe 1950B & 1957D, from Cowan *et al.* (1994) and Saha *et al.* (1995); for SN 1961V, from this Chapter and Silbermann *et al.* (1996); for SN 1970G, from Cowan *et al.* (1991) and Kelson *et al.* (1996); for SN 1979C, from Weiler *et al.* (1986, 1991), Montes *et al.* (2000), and Ferrarese *et al.* (1996); for SN 1980K, from Weiler *et al.* (1986, 1992), Montes *et al.* (1998), and Tully (1988); and for SN 1986J, from Rupen *et al.* (1987), Weiler *et al.* (1990), and Silbermann *et al.* (1996). Luminosities for Cas A and the Crab from Eck *et al.* (1998).

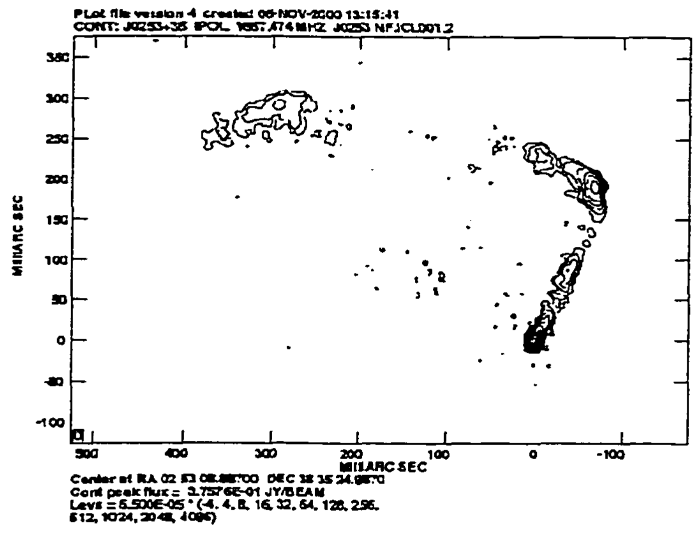

Figure 2.4: VLBI radio contour map at 18 cm (1.7 GHz) of J0253+3835. Contour levels are -0.26, 0.26, 0.52, 1.0, 2.1, 4.2, 8.3, 17, 33, 67, 133, and 266 mJy beam^{-1}, with a beam size of 9.4 milli-arcsec $\times$ 6.9 milli-arcsec, p.a. $= 5°$, and rms noise of 0.065 mJy beam^{-1}. The beam is shown to scale in the lower left of the plot. Observations taken with the VLBA 14 September 1999.

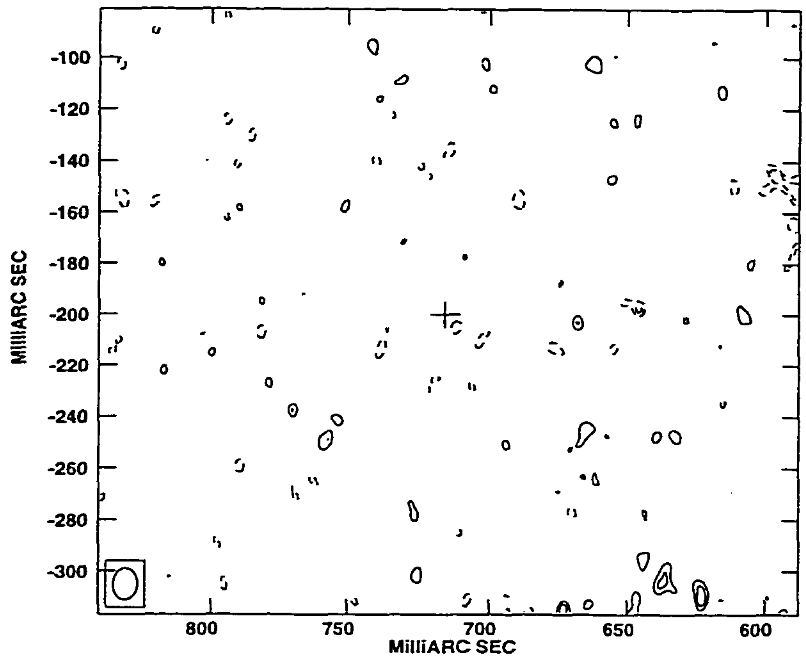

Figure 2.5: VLBI radio contour map at 18 cm (1.7 GHz) of SN 1961V. Contour levels are -0.07, -0.05, -0.03, 0.03, 0.05, 0.07, 0.10, 0.14, and 0.19 mJy beam^{-1}, with a beam size of 11. 5 milli-arcsec $\times$ 7.56 milli-arcsec, p.a. $= 0°$, and rms noise of 0.030 mJy beam^{-1}. The beam is shown to scale in the lower left of the plot. Observations taken with the VLBA 14 September 1999.

Chapter 3

The Evolution of Intermediate-aged Radio Supernovae

3.1 Introduction

Intermediate-age radio supernovae (RSNe) have been defined as having ages from $\sim$ 10–100 years old (Cowan & Branch 1985), spanning the period well after the optical emission fades (usually about 2 years) and before the turn-on of radio emission from the supernova remnant (SNR). Chevalier (1984) proposes that synchrotron radiation is produced in the region of interaction between the ejected supernova shell and the circumstellar shell that originated from the prior mass loss of the progenitor star. In such models the radio emission drops as the expanding shock wave propagates outward through the surrounding and decreasingly dense circumstellar material (CSM). Radio emission from SNRs is normally observed long after the supernova phase. Such factors as the density of the local interstellar medium affect the turn-on time in models such as those of Cowsik & Sarkar (1984) based upon the Gull (1973) piston model. These models typically suggest a minimum of 100 years for the formation and brightening of an SNR. Recent observations of M31, may have detected emission from the site of SN 1885A indicating the turn-on of radio emission from the SNR 1885A (Sjouwerman & Dickel 2001). They report a very faint radio source (28 μJy $\sim$6.1 $\times$ 10^{22} erg s^{-1} Hz^{-1}) within 1.″4 of the position reported by Fesen *et al.* (1996). However, final confirmation of this emission being linked to a forming SNR will require multi-wavelength radio measurements to determine the spectral nature of this source. The intermediate-age time period is, therefore, *critical* in understanding the later stages of stellar evolution. In particular, the circumstellar mass-loss rate for the supernova progenitors is a crucial component in the initiation and duration of radio emission in models, such as those of Chevalier (1984).

To study this transition period from SN to SNR, I and others have attempted to detect radio emission from intermediate-age SNe. While there have been a number of unsuccessful searches, a few supernovae have been detected in the radio more than a decade after explosion [SNe 1923A, 1950B, & 1957D in M83 (Cowan &

Branch 1985; Cowan *et al.* 1994; Eck *et al.* 1998), SN 1961V in NGC 1058 (Cowan *et al.* 1988; Stockdale *et al.* 2001a), SN 1968D in NGC 6946 (Hyman *et al.* 1995), and SN 1978K in NGC 1313 (Ryder *et al.* 1993)]. One of the motivations for these studies has been that individual decades-old supernovae, such as SN 1970G, can undergo abrupt and rapid changes in flux densities on a timescale of only a few years. Such variability was seen in the radio emission from SN 1980K, which abruptly dropped after ten years of slow decline (Weiler *et al.* 1992; Montes *et al.* 1998). Also the radio luminosity from SN 1979C, after declining steadily for years, has flattened and become relatively constant, perhaps as a result of the supernova shock wave hitting a denser region of the CSM (Montes *et al.* 2000). Observations also indicate that SN 1957D, after being relatively constant (~ 3 mJy), suddenly appeared to have faded (in two years) below (< 1 mJy) the level of an associated HII region (Cowan *et al.* 1994a). However, new observations presented in this Chapter may cast doubt on this interpretation.

In this chapter, I report new radio observations of SNe 1970G, 1957D, 1950B, and 1923A, including their current flux densities and spectral indices and examine how their radio emission have varied during the time they have been monitored.

SN 1970G, a Type II supernova (SN) in M101 (Lovas 1970; Kirshner *et al.* 1973), was the first SN to be detected in the radio (Gottesman *et al.* 1972; Allen *et al.* 1976). It then faded from view (Weiler *et al.* 1986), until it was recovered again in 1990 (Cowan, Goss & Sramek 1991; hereafter referred to as CGS). SN 1970G is one of a very rare group of SNe that have been recovered in the radio more than a decade following maximum optical light and is now - 31 years after outburst - the longest monitored such object.

M83, an SABc galaxy, is host to 5 historical supernovae (SNe) of the last 100 years: SN 1923A (Lampland 1936), SN 1945B (Liller 1990), SN 1950B (Haro 1950), SN 1957D (Gates 1958), and SN 1968L (Bennett 1967). The detection of SN 1923A, a Type II SN, makes it the oldest radio supernova (RSN) observed (Eck *et al.* 1998). SNe 1923A, 1950B, 1957D, and 1968L are classified by radio and optical properties as Type II SNe (Barbon *et al.* 1998; Eck *et al.* 1998; Cowan, Roberts, & Branch 1994; Wood & Andrews 1974), while the designation of SN 1945B is uncertain as it was detected by archival studies. This rich sampling of intermediate-age SNe makes M83 the ideal galaxy to study the evolution of SNe, removing any uncertainties involving accurate distance measurements and differences in the host galaxy's evolution (Rosa & Richter 1988; Cowan & Branch 1985; Bartunov, Tsvetkov, & Filimonova 1994).

3.2 Observations

3.2.1 SN 1970G in M101

The new VLA data on SN 1970G were taken from six observing runs. In the first three, SN 1970G was observed for 4.5 total hours on 4 and 6 November and 3 December 2000, at 20 cm (1.425 GHz) using the VLA's most extended (A) configuration, with a maximum baseline of 34 km. During the second group of observing runs, SN 1970G was observed on 10 January 2001 with the VLA in its A configuration and on 5 and 21 February 2001 with VLA in its BnA configuration (maximum baseline of 24 km) at 6cm (4.860 GHz) for a total of 6.5 hours. These observations were done using the standard VLA continuum mode, obtaining a total of 100 MHz bandwidth in each of the two orthogonal circular polarizations. The phase calibrator was J1400+621, and 3C286 was used to set the flux density scale. In all observations the pointing center was $14^h03^m00^s$ and $+54°14'33''$ (J2000), and flux densities for 3C286 were taken from Perley, Butler, & Zijlstra (2001).

Data were Fourier transformed and deconvolved using the CLEAN algorithm as implemented in the AIPS routine IMAGR. The data were weighted using Brigg's robustness parameter of 0, which minimizes the point-spread function while maximizing sensitivity. I have also re-analyzed the CGS observations of the region, using the same data reduction procedures and inputs as were used on the current data. The 6 cm observations were combined using the AIPS routine DBCON, and a final 6 cm image was produced using the AIPS routine CONVL to correct for differences in the beam size and shape since they were taken in different array configurations. To derive the peak flux density and position for SN 1970G, a series of one dimensional plots of flux densities vs. position were made using the AIPS routine SLICE at constant right ascension and then at constant declination. This was necessary due to the relative brightness of the nearby H II region, NGC 5455 [centered $\simeq 5$ sec from SN 1970G], which artificially introduced a modest slope in the flux density baseline from the HII region outward. This artifice resulted in minor reductions in the peak flux density when employing the AIPS routines, IMFIT and JMFIT, for all of the observations.

The position measured for SN 1970G, from the new images and the re-analysis of the 20 cm observations taken in 1990, is $14^h03^m00\overset{s}{.}88 \pm 0\overset{s}{.}01$ and $+54°14'33\overset{''}{.}1 \pm 0\overset{''}{.}2$. Uncertainties in the peak intensities are reported as the rms noise from the observations. At 20 cm, the beam size is $1\overset{''}{.}42 \times 1\overset{''}{.}21$, p.a. $= -39.18°$, and the rms noise is 0.015 mJy beam^{-1}. At 6 cm, the beam size is $1\overset{''}{.}20 \times 1\overset{''}{.}20$, p.a. $=$ 0.00°, and the rms noise is 0.020 mJy beam^{-1}. The results of my analyses are presented in Table 3.1 and Figure 3.1.

3.2.2 SNe 1923A, 1950B, and 1957D in M83

M83 was monitored over the course of four VLA observing runs. In the first two, M83 was observed for 8.7 total hours on 13 and 15 June 1998 at 20cm (1.450 GHz), using the VLA in its BnA configuration (the southern arms in B configuration and the northern arm in A configuration), with a maximum baseline of 24 km. During the second group of observing runs, M83 was observed on 31 October and 1 November 1998 with the VLA in its CnB configuration (maximum baseline of ~11 km) at 6cm (4.860 GHz) for a total of 8.9 hours. These were done using the VLA spectral observing mode 4. For the purposes of this study, we are only interested in the continuum observations of the SNe. So we have only analyzed the only the continuum data taken during these observations, obtaining a total of 100 MHz bandwidth in each of the two orthogonal circular polarizations. The phase calibrator was J1313-333, and 3C286 was used to set the flux density scale. Flux densities for 3C286 were taken from Perley, Butler, & Zijlstra (2000). It should be noted that J1313-333 is a slightly resolved source with the VLA in these configurations. This rules out the direct application of simple gaussian model for this source. In order to correct for this, J1313-333 was self-calibrated using an iterative process to ensure that all of its emission was properly modelled for the 20 cm observations. The problem was not as pronounced at 6 cm, so the standard VLACALIB routine was applied with minimal weighting applied to baselines larger than 50 kilo-wavelengths. This resulted in an acceptable model to be applied to the M83 data. J1313-333 was also used as a phase calibrator in the earlier observations discussed in Cowan *et al.* 1994, although there is no indication of any such resolution problems in those observations. In all observations, the pointing was (B1950) $13^h34^m11^s$ and $-29°36'48''$, centered on the nuclear region of M83.

Data were Fourier transformed and deconvolved using the CLEAN algorithm as implemented in the AIPS routine IMAGR. The data were weighted using a Brigg's robustness parameter of 0, which minimizes the point-spread function while maximizing sensitivity. Uncertainties in the peak intensities are reported as the rms noise from the observations. The measured positions (B1950) from these new maps are listed as follows: for SN 1957D $13^h34^m14\overset{s}{.}36$ and $-29°34'24\overset{''}{.}3$, for SN 1950B $13^h34^m03\overset{s}{.}67$ and $-29°36'39\overset{''}{.}0$, and for SN 1923A $13^h34^m20\overset{s}{.}00$ and $-29°35'44\overset{''}{.}9$. At 20 cm, the beam size is $3\overset{''}{.}29 \times 2\overset{''}{.}71$, p.a. $= 59.0°$, and the rms noise is 0.030 mJy beam^{-1}. At 6 cm, the beam size is $3\overset{''}{.}49 \times 2\overset{''}{.}95$, p.a. $= 66.51°$, and the rms noise is 0.030 mJy beam^{-1}. The results of my analyses (positions and peak flux densities) are presented in Table 3.1 and Figures 3.2, 3.3, 3.4.

3.3 Results

3.3.1 SN 1970G

I have detected a radio source at the position of SN 1970G at 20 cm and 6 cm, coincident, within the error limits, with the CGS position. My measured flux density at 20 cm indicates a reduction in the 20 cm flux density of 11% from 1990 to 2000 (see Table 3.1). Extrapolating from the 3.5 and 20 cm measurements and assuming the spectral index reported by CGS, the 6 cm flux density in 1990 would have been 0.11 mJy, which is virtually identical to the current value of 0.12 ± 0.020 mJy (see Table 3.1). The CGS observations indicated that the flux density of SN 1970G had dropped between 1974 and 1990 with a power-law index ($S \propto t^{\beta}$) of $\beta = -1.95 \pm 0.17$ at 20 cm. Assuming the CGS power-law decline and spectral index from 1990, we would expect a much lower 6cm flux density, $\simeq 0.050$ mJy, and 20 cm flux density, $\simeq 0.090$ mJy than we now measure. The radio light-curve for SN 1970G between 1990 and 2000 has flattened considerably and (based upon the 20 cm flux densities) the power-law index is now $\beta = -0.28 \pm 0.13$ (see Table 3.2). As indicated in Table 3.2 (and shown in Figure 3.1), our new observations indicate that SN 1970G is still a (marginally) non-thermal radio source. The current spectral index, α, of -0.24 ± 0.20 has flattened from the value of -0.56 ± 0.11 reported in 1990 by CGS, although the error bars are rather large.

3.3.2 SN 1957D

I have detected radio emission from the site of SN 1957D at 20 cm and 6 cm, coincident, within the error limits, with the source detected by Cowan *et al.* (1994) which has faded from 1992 to 1998 by 33%, at 20 cm, and by 76%, at 6 cm (see Table 3.2). The 20 cm and 6 cm power-law indices ($S \propto t^{\beta}$) for SN 1957D are $\beta = -2.29 \pm 0.07$ and -6.42 ± 0.09, respectively, indicating a dramatic decline in the flux density. We illustrate the radio evolution of these SNe in Figure 3.4, where we show the radio light curves of several intermediate-age SNe along with a few SNRs, plotting the time since supernova explosion versus the luminosity at 20 cm (i.e.. the monochromatic luminosity).

As shown in Table 1 and Figures 3.2, SN 1957D is now non-thermal with a spectral index of -0.73 ± 0.12. Previous determinations for SN 1957D's spectral index in the early 1990s and mid 1980's yielded very different values of $+0.11 \pm 0.06$ and -0.23 ± 0.04, respectively (Cowan *et al.* 1994). The thermal spectral indices reported by Cowan *et al.* (1994) for SN 1957D were attributed to an intervening HII region whose brightness is comparable to that of the faded SN. A possible explanation for the change of the spectral index could be that the SN shock has overrun a portion of this HII emission region, resulting in a partial decline of the thermal emission. The current non-thermal spectral index and steep decline in measured flux densities of SN 1957D closely model the predictions of Weiler *et al.* (1986, 1990, 2001).

3.3.3 SNe 1923A and 1950B

I have detected radio emission from the sites of SNe 1923A, and 1950B at 20 cm and 6 cm, coincident, within the error limits, of the sources detected by Cowan *et al.* (1994) and Eck *et al.* (1998). My measured flux densities at 20 cm indicate a reduction from 1992 to 1998 for these SNe, SN 1923A by 33% and SN 1950B by 28%. The 6 cm peak flux densities for these two SNe have remained the same, within the error limits (see Table 3.2). The 20 cm power-law indices ($S \propto t^{\beta}$) for SNe 1923A and 1950B between 1992 and 1998 are $\beta = -4.54 \pm 0.22$ and -2.27 ± 0.08, respectively. The 20 cm power-law index for SN 1923A is steeper than the values reported for the younger SNe. The 6 cm power-law index for SN 1950B ($\beta = +0.70 \pm 0.11$) and SN 1923A ($\beta = +4.24 \pm 0.38$) indicate a modest brightening, but no substantial change.

As indicated in Table 3.2 (and shown in Figures 3.2, 3.3, and 3.4), our new observations indicate that SNe 1923A and 1950B are still marginally non-thermal radio sources. Their current spectral indices, (α; $S \propto \nu^{\alpha}$), of -0.24 ± 0.26 and -0.18 ± 0.12, respectively, have flattened from the values of -1.00 ± 0.24 and

-0.57 ± 0.08 reported for each source in 1992 by Cowan *et al.* (1994). The evolution of SNe 1923A and 1950B is consistent with the theoretical models of Weiler *et al.* (1986, 1990, 2001) and Montes *et al.* (1997) in that the 6 cm emission is weaker than the 20 cm emission, the 20 cm flux continues to decay at a rapid rate, and the sources are non-thermal. In the case of these two older SNe, their 6 cm emission is likely already at or below the level of the thermal emission from an intervening HII region along the line-of-sight (Montes *et al.* 1997). The 20 cm emission from these two SNe continues to decline and will likely also fade below the level of this thermal emission as well.

3.3.4 SNe 1945B, 1968L and 1983N

There was no detection of emission from either the Type Ib SN 1983N nor from the Type II SNe 1945B and 1968L. Upper limits for emission at both 6 cm and 20 cm from SNe 1983N and 1945B are 0.90 mJy, at the three sigma noise level. SN 1968L is located within the diffuse emission region at the center of M83. Three sigma upper limits for emission from SN1968L are 4.60 mJy at 6 cm and 6.8 mJy at 20 cm. Turner & Ho (1994) attribute the brightest nuclear source in M83 to SN 1968L. However, after years of monitoring this source by Cowan & Branch (1982), Cowan & Branch (1985), and Cowan *et al.* (1994), the measured flux density of this source has not varied significantly, which would be very atypical behavior for a RSN. Given the age of SN 1945B, the fact that it has not been detected in these and prior observations is unusual with emission having been observed from SNe 1923A, 1950B, and 1957D. The most likely reason for it not being detected is a lack of CSM around the object. It's initial detection made by archival studies of plates taken of M83 by Liller (1990), indicate it was a very faint optical SN as well.

The lack of detectable emission from SN 1993N was expected. As mentioned before, SNe Ib & Ic are not long-term radio sources due to the lack of CSM associated with these events (see discussion in Introduction for radio emission from SNe). SN 1983N was detected as a strong radio source by Sramek, Panagia, & Weiler (1984) and Weiler *et al.* (1986) who were able to measure a steep decline in its radio emission within a year following explosion and Cowan *et al.* 1994 in their 1983 and 1984 searches who detected emission $\sim$2 years after the event, with measured flux densities of 4.4 ± 0.15 mJy (20 cm) and 0.52 ± 0.05 mJy (6 cm). All subsequent searches have detected no emission from this source.

3.4 Discussion

The current and previous values of the spectral indices, luminosities, and decay indices for SNe 1970G, 1957D, 1950B, and 1923A are consistent with values reported for other intermediate-age RSNe at similar ages and wavelengths (See

Table 3.2, Figure 3.5, and Stockdale *et al.* 2001a). Figures 3.6 and 3.7 identify the positions of the historical SNe in M83 in relation to the rest of the galaxy. It is clear, for example, from Figure 3.5 that the radio luminosities of SNe 1970G, 1957D, and 1950B at an age of $\simeq$ 30—40 years is very close to that of the Type II SN 1968D, in NGC 6946, and SN 1961V, in NGC 1058, at the same stage in their evolution (Cowan *et al.* 1994; Hyman *et al.* 1995; Stockdale *et al.* 2001a). This correlation in luminosity also lends credence to the identification of SNe 1950B and 1961V as Type II SNe. In particular, there has been some uncertainty in the optical position of SN 1950B that prevented a conclusive identification of the supernovae with the radio source (Cowan & Branch 1985; Cowan *et al.* 1994a). As discussed in the previous chapter concerning SN 1961V, recent optical observations have caused some debate whether it was a supernova event or a luminous blue variable (LBV) (Goodrich *et al.* 1989). On the other hand, recent radio observations of SNe 1961V strongly suggest a supernova interpretation for this event (Stockdale *et al.* 2001a).

The evolution of the radio flux density of these four SNe is consistent with the current models for radio emission from SNe, which predict a general decline in radio luminosity with age and declining density of CSM. Figure 3.5 illustrates a interesting trend for some of the intermediate-age RSNe, with a general flattening of the radio light curve 10-40 years after the supernova event.

The differences in the behavior of the individual SNe (e.g. the rates at which their radio luminosities fade) could, therefore, be explained in terms of the density of the material encountered by the supernova shock. For example, the shocks associated with some RSNe (e.g. SNe 1979C, 1970G, and 1961V) might be traveling through considerably denser CSM than other similarly-aged RSNe (e.g., SNe 1980K and 1957D). One scenario which might explain this increased density of CSM around some Type II RSNe could be that the progenitors underwent large-scale eruptions, akin to LBVs, prior to the supernova event. This is not to say that we are detecting emission from the ejecta of any LBV outburts, which as mentioned in Chapter 2 are weak radio emitters. But, we may be detecting emission as the SN shock interacts with this dense ejecta. The mass loss rates during an LBV eruption can be 10—100$\times$ larger than the typical supergiant mass-loss rate (Humphreys & Davidson 1994). Determing the exact epoch at which this may have occurred depends on the ejection velocities of the CSM during these events, the rate of expansion of the supernova shock, and the density of the CSM. Unfortunately, these intermediate-age RSNe are too under sampled to make any definitive statements as to the exact nature of such a possible outburst or mass loss.

SN 1950B appears to bridge this differentiation, demonstrating a plateau in its light curve followed by a decline in its emission comparable to that of SN 1957D (see Figure 3.5). Consistent with this interpretation is the very rapid decline and disappearance of the radio emissions of Type Ib RSNe, e.g. SNe 1983N and 1984L, which presumably have lower density CSM than Type II SNe (Weiler *et al.* 1986; Sramek *et al.* 1984; Panagia *et al.* 1986). Clearly, additional radio monitoring of these events, and other RSNe, will be important in understanding the continuing evolution and nature of these relatively rare objects.

Table 3.1: Observations of Intermediate-Age Radio Supernovae.

	SN 1970G	SN 1957D	SN 1950B	SN 1923A
Distance (Mpc)	7.4	4.1	4.1	4.1
Most Recent 20 cm				
Flux density (mJy)	0.16 ± 0.015	0.82 ± 0.03	0.52 ± 0.03	0.20 ± 0.03
Supernova age (yrs)	30.29	40.49	48.24	75.09
Luminosity[a]	1.1×10^{25}	1.6×10^{25}	1.0×10^{25}	3.9×10^{24}
Previous 20 cm				
Flux density (mJy)	0.18 ± 0.017	1.22 ± 0.07	0.72 ± 0.04	0.30 ± 0.05
Supernova age (yrs)	19.74	34.04	41.80	68.67
Luminosity[a]	1.2×10^{25}	2.4×10^{25}	1.4×10^{25}	5.9×10^{24}
Most Recent 6 cm				
Flux Density (mJy)	0.12 ± 0.020	0.34 ± 0.03	0.42 ± 0.03	0.15 ± 0.03
Supernova age (yrs)	30.50	40.87	48.62	75.48
Luminosity[a]	7.9×10^{24}	6.7×10^{24}	8.3×10^{24}	3.0×10^{24}
Previous 6 cm				
Flux density (mJy)	...	1.39 ± 0.04	0.37 ± 0.03	0.093 ± 0.03
Supernova age (yrs)	...	32.82	40.58	67.43
Luminosity[a]	...	2.8×10^{25}	7.4×10^{24}	2.6×10^{24}

[a] Units are (ergs s^{-1} Hz^{-1}).

References — (Cowan *et al.* 1991; Cowan *et al.* 1994a; Eck *et al.* 1998; Kelson *et al.* 1996; Saha *et al.* 1995; Silbermann *et al.* 1996; Stockdale *et al.* 2001b)

Table 3.2: Radio Properties of Intermediate-Age Radio Supernovae.

	SN 1970G	SN 1957D	SN 1950B	SN 1923A
Spectral Index[a]				
Most Recent	-0.24 ± 0.20	-0.73 ± 0.12	-0.18 ± 0.12	-0.24 ± 0.26
Previous	-0.56 ± 0.11[b]	$+0.11 \pm 0.06$	$--0.57 \pm 0.08$	$--1.00 \pm 0.24$
Decay Index[c]				
Most Recent				
20 cm	-0.28 ± 0.13	-2.29 ± 0.07	-2.27 ± 0.08	-4.54 ± 0.22
6 cm	...	-6.42 ± 0.09	$+0.70 \pm 0.11$	$+4.24 \pm 0.38$
Previous				
20 cm	-1.95 ± 0.17	-2.66 ± 0.07	$+0.12 \pm 0.13$	...
6 cm	...	-2.44 ± 0.04	$+0.22 \pm 0.04$	-7.90 ± 0.42

[a] α obtained by $S \propto \nu^{\alpha}$.
[b] taken from 20 cm and 3.5 cm observations
[c] β obtained by $S \propto t^{\beta}$.
References — (Cowan *et al.* 1991; Cowan *et al.* 1994a; Eck *et al.* 1998)

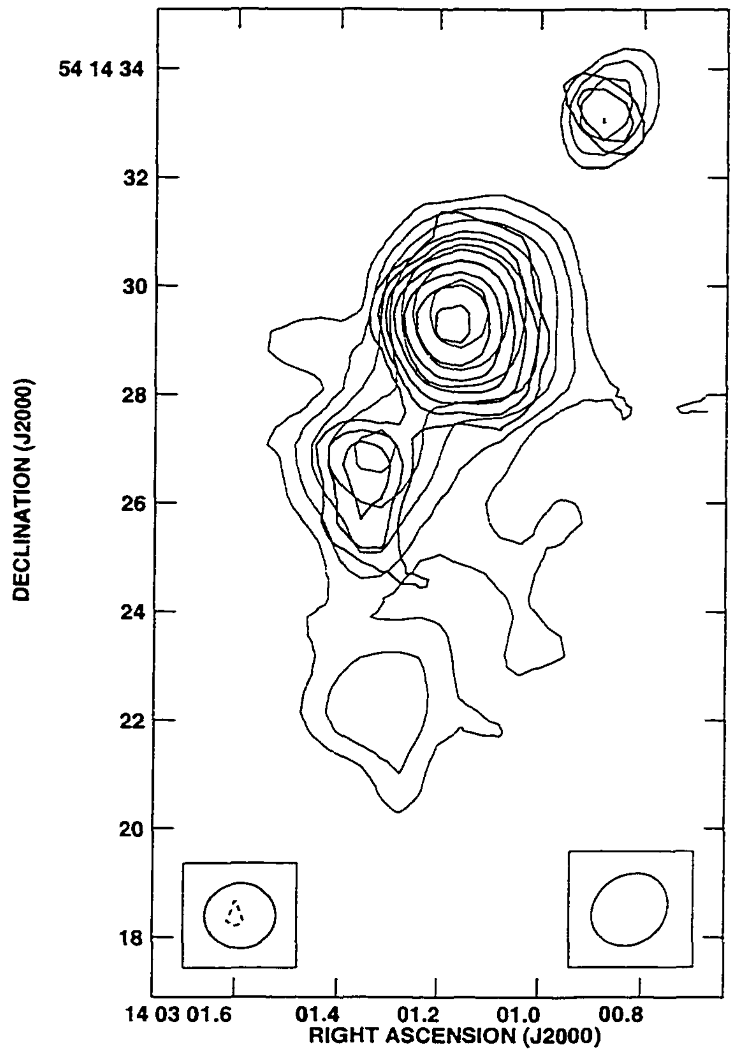

Figure 3.1: Radio contour images at 20 cm (in red) and 6 cm (in blue) of SN 1970G (the source above and to the right of the central H II region, NGC 5455). Contour levels at both wavelengths are -0.060, 0.060, 0.086, 0.12, 0.17, 0.24, 0.34, 0.48, 0.68, and 0.96 mJy beam^{-1}. At 20 cm, the beam size is (shown in lower right) and, at 6 cm, the beam size is (shown in lower left).

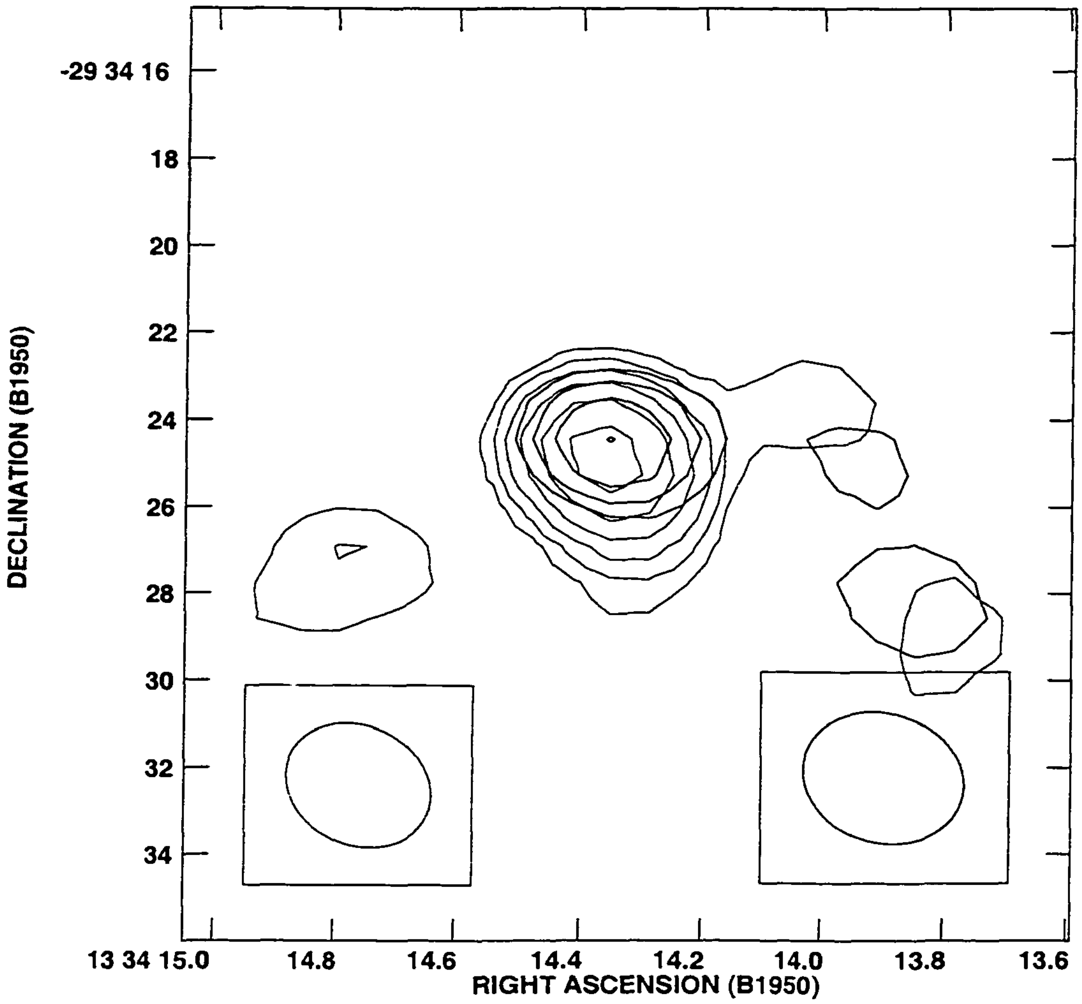

Figure 3.2: Radio contour images at 20 cm (in red) and 6 cm (in blue) of SN 1957D (the central bright source). Contour levels at both wavelengths are -0.12, 0.12, 0.17, 0.24, 0.34, 0.48, 0.68, and 0.96 mJy beam^{-1}. At 20 cm, the beam size is shown in the lower left, and at 6 cm, the beam size is shown in the lower right.

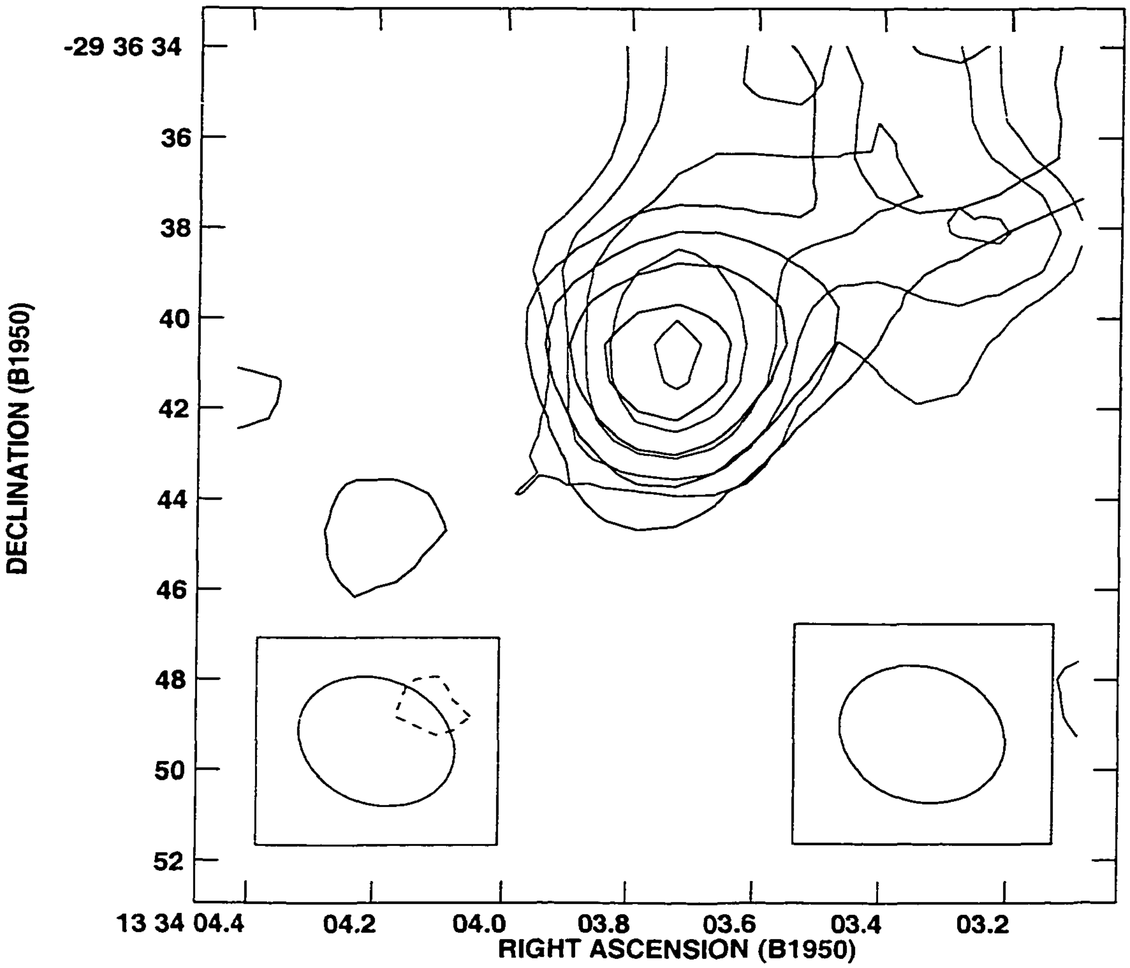

Figure 3.3: Radio contour images at 20 cm (in red) and 6 cm (in blue) of SN 1950B (the central bright source). Contour levels at both wavelengths are -0.12, 0.12, 0.17, 0.24, 0.34, 0.48, 0.68, and 0.96 mJy beam^{-1}. At 20 cm, the beam size is shown in the lower left, and at 6 cm, the beam size is shown in the lower right.

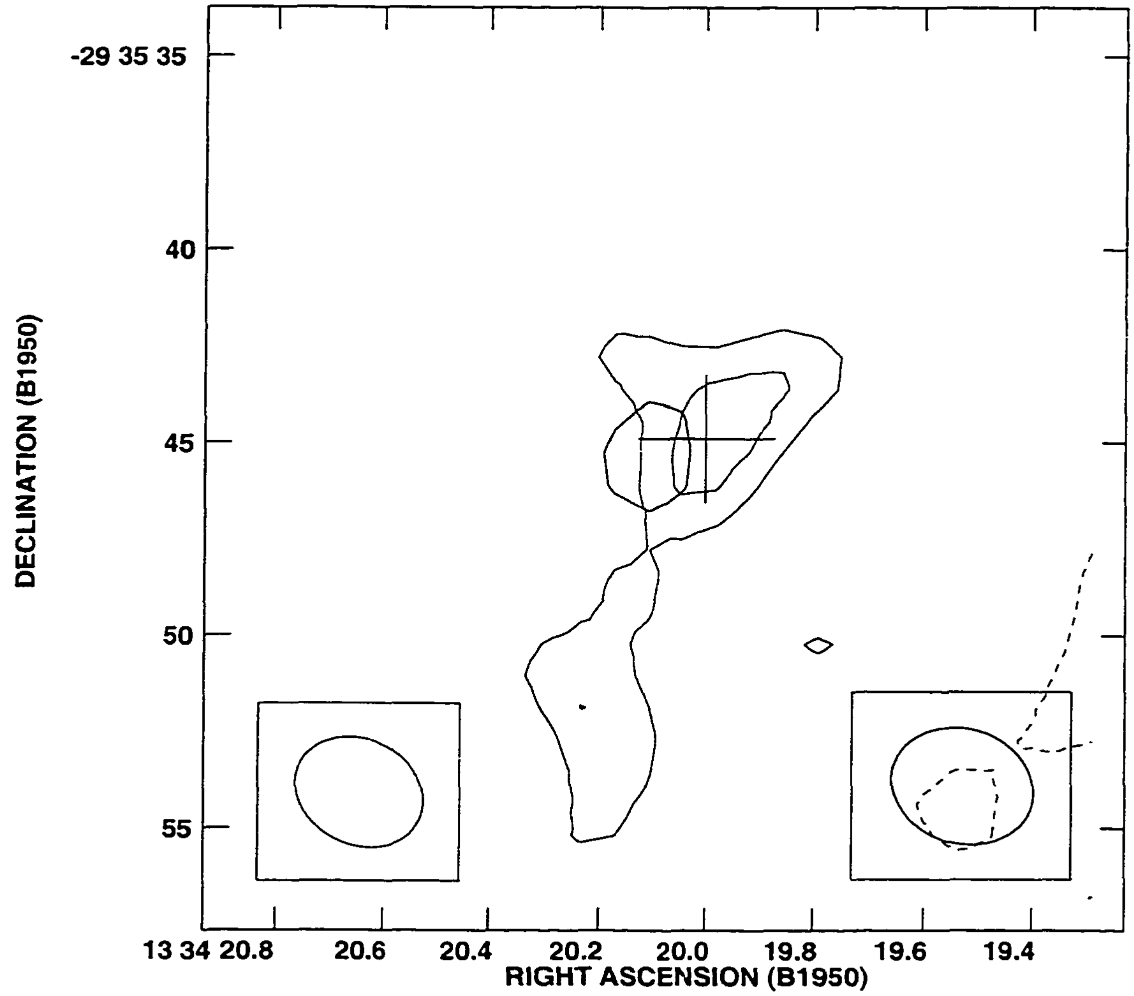

Figure 3.4: Radio contour images at 20 cm (in red) and 6 cm (in blue) of SN 1923A (the source indicated by the cross). Contour levels at both wavelengths are -0.12, 0.12, 0.17, 0.24, 0.34, 0.48, 0.68, and 0.96 mJy beam^{-1}. At 20 cm, the beam size is shown in the lower left, and at 6 cm, the beam size is shown in the lower right.

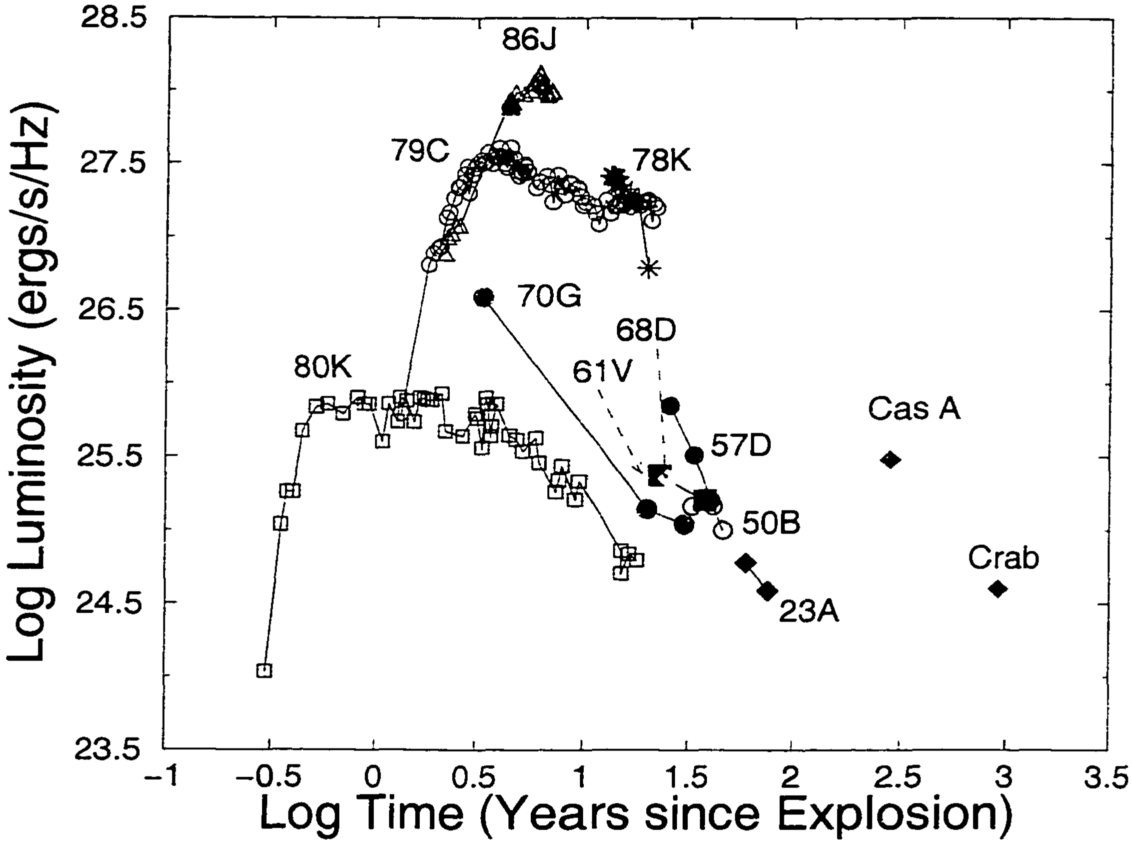

Figure 3.5: 20 cm radio light curve of several RSNe and SNRs. Data, fits and distances for SN 1923A, from this paper, Eck *et al.* (1998) and Saha *et al.* (1995); for SNe 1950B (cyan hoops) & 1957D, from this paper, Cowan *et al.* (1994) and Saha *et al.* (1995); for SN 1961V (blue squares), Stockdale *et al.* (2001a) and Silbermann *et al.* (1996); for SN 1968D (yellow diamond), from Hyman *et al.* (1995) and Tully (1988); SN 1970G (orange circles), from Stockdale *et al.* (2001b), Cowan *et al.* (1991), and Kelson *et al.* (1996); for SN 1978K, from Ryder *et al.* (1993), Schlegel *et al.* (1999), and Tully (1988); for SN 1979C, from Weiler *et al.* (1986, 1991), Montes *et al.* (2000), and Ferrarese *et al.* (1996); for SN 1980K, from Weiler *et al.* (1986, 1992), Montes *et al.* (1998), and Tully (1988); and for SN 1986J, from Rupen *et al.* (1987), Weiler *et al.* (1990), and Silbermann *et al.* (1996). Luminosities for Cas A and the Crab from Eck *et al.* (1998).

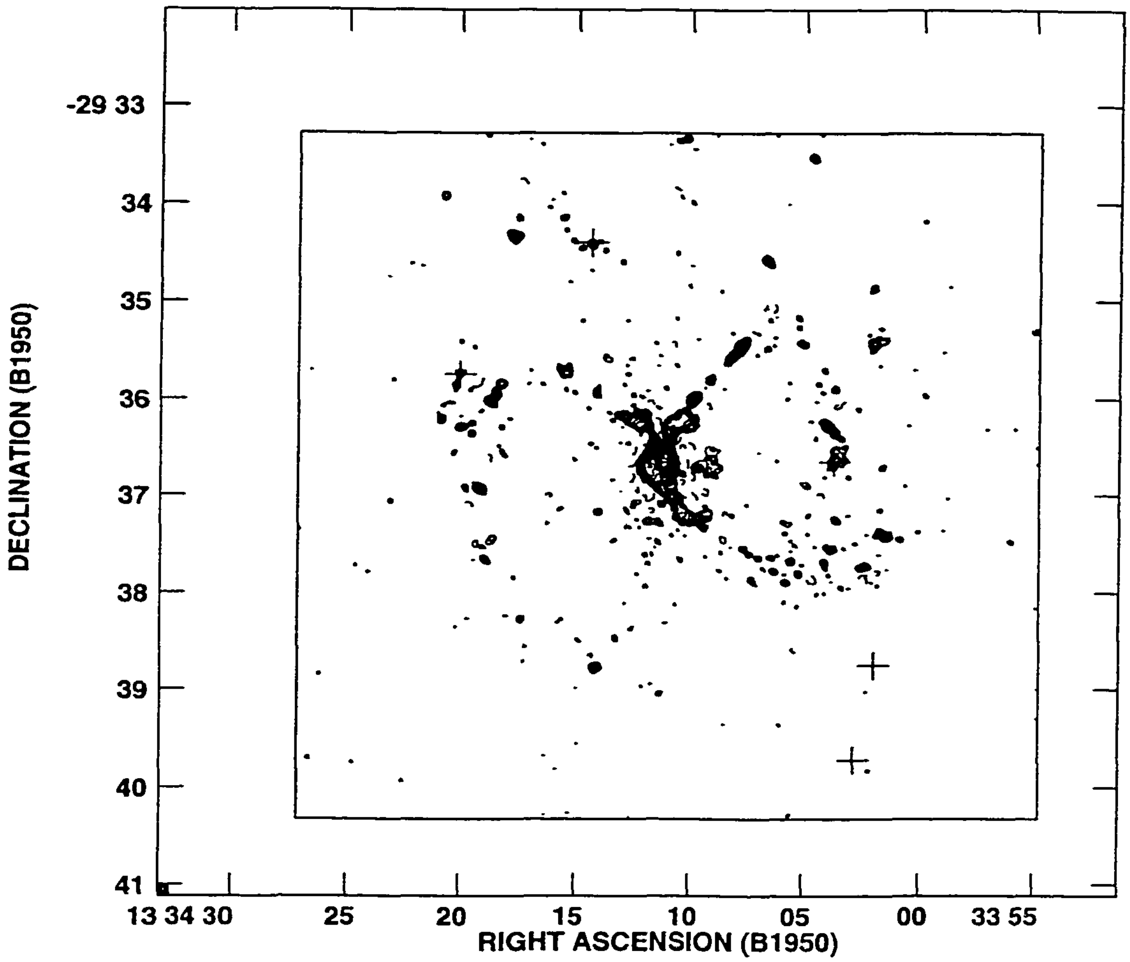

Figure 3.6: Radio contour images at 20 cm of M83, with the historical SNe identified by crosses. Contour levels are -0.12, 0.12, 0.17, 0.24, 0.34, 0.48, 0.68, 0.96, 1.36, 1.92, 2.72, 3.84, 5.44, and 7.68 mJy beam^{-1}. The beam size is shown in the lower left.

M83 20 CM RADIO CONTINUUM

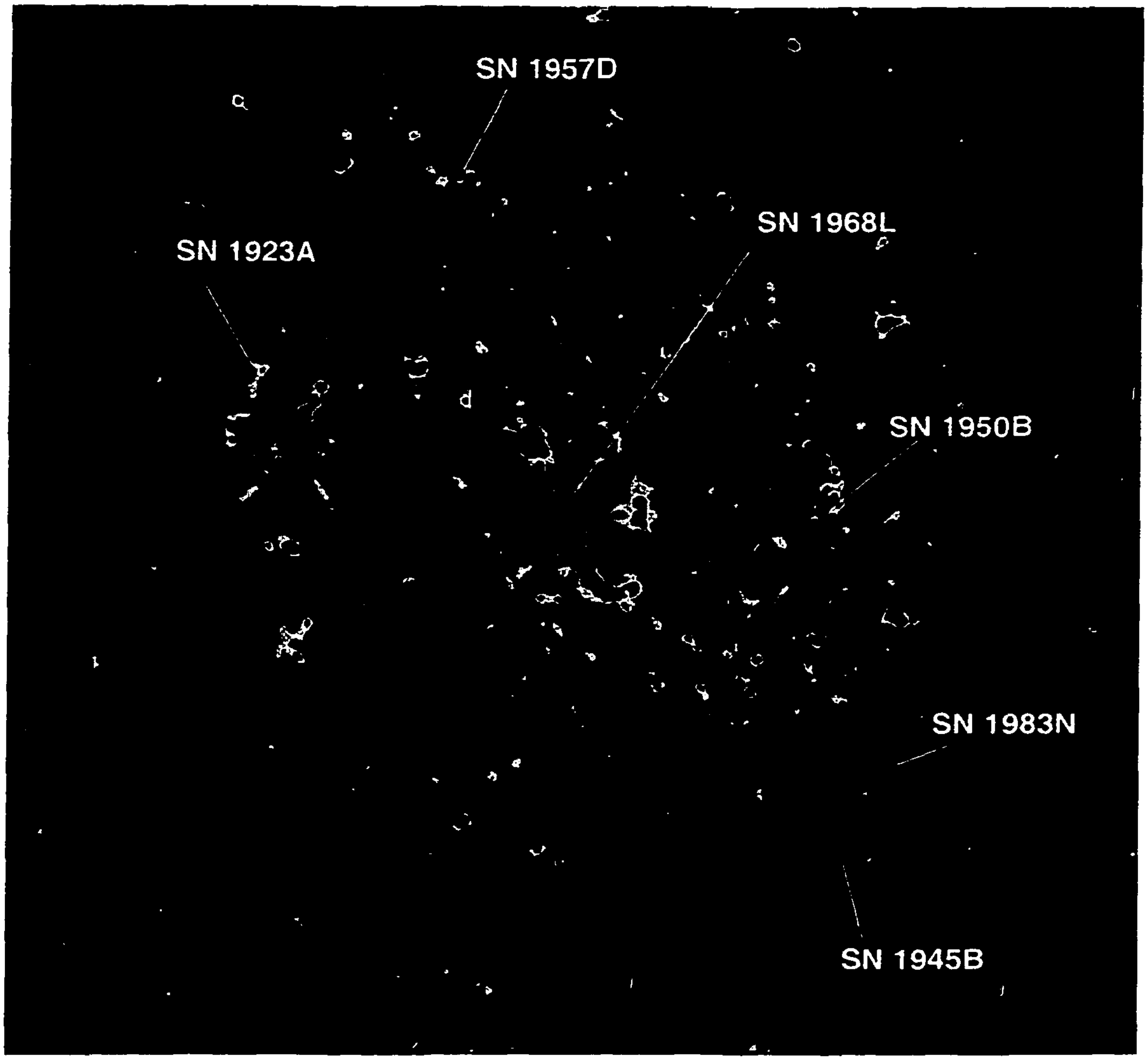

Figure 3.7: Radio false color image of M83, with the positions of the historical SNe shown.

Chapter 4

X-ray Search For Supernovae 1959D & 1961V

4.1 No X-rays from the Supernovae

Only 4 decades-old SNe have been recovered in the X-ray using the Roentgen Satellite (ROSAT) and earlier X-ray missions (SNe 1978K (Ryder *et al.* 1993; Schlegel 1995; Schlegel *et al.* 1999), 1979C (Immler *et al.* 1998a), 1980K (Canizares *et al.* 1982), and 1986J (Houck *et al.* 1998). With *Chandra*, there have been 5 detected X-ray SNe: SNe 1979C (Ray, Petre, & Schlegel 2001), 1987A (Burrows *et al.* 2000), 1998S (Pooley *et al.* 2001), 1999em (Pooley *et al.* 2001), and SN 1999gi (Schlegel 2001). SN 1979C is now the oldest monitored X-ray SN, with emission having been detected for the first time by ROSAT 16 years after the SN explosion in 1995 in the 0.1 — 2.4 keV energy band (Immler *et al.* 1998a). Subsequent observations with *Chandra* in 1999 once again detected soft X-ray emission from SN 1979C but no hard X-ray emission (Ray *et al.* 2001). The source of X-ray emission for these objects is believed to be due to the interaction between a SN shock wave and the SN progenitor's CSM, as discussed in Chapter 1. With the exception of SN 1979C and SN 1987A, both detected recently with *Chandra*, no X-ray SNe have been detected later than a decade following explosion.

4.1.1 Observations, Data Reduction, and Results

In order to probe this hereto unexplored group of intermediate-age SNe in the X-ray, observations were attempted to detect X-ray emission from SN 1961V, in NGC 1058, and from SN 1959D, in NGC 7331. [SN 1961V was also the subject of the radio study mentioned in Chapter 2, and a discussion of the reduction for the SN 1959D data can be found in the following Section.] The reduced image of NGC 7331 is shown in Figure 4.1. SN 1961V, in NGC 1058, an SA(rs)c spiral galaxy, was observed with the ROSAT HRI in February 1996 for 61 ks and later by Schlegel in September 1999 for an additional 43 ks. The HRI is an X-ray photon collector with no spectral resolution, collecting photons with energies ranging from 0.12 keV to 2.4 keV. The first observations were centered on the CHB radio source of SN 1961V at R.A.(2000) = $22^h43^m36\overset{s}{.}0$, Decl.(2000)= $+37°21'00''.0$. The second observations were centered at R.A.(2000) = $22^h43^m36^s.0$, Decl.(2000)= $+37°21'36''.0$. The two images were analyzed with assistance provided by A. Prestwich at the Harvard Center for Astrophysics and Karen Leighly, which I gratefully acknowledge, and are shown in Figure 4.2.

Neither SN 1959D nor SN 1961V were detected, and the 3 sigma upper limits are provided in Table 4.1 along with the X-ray luminosities of those SNe with X-ray spectra available. The later observations on SN 1961V by Schlegel yielded a $\sim 2\sigma$ detection near the position of SN 1961V. While this may be emission from the SN, the transient nature of the source would argue against such an interpretation. The 3 sigma upper-limits for these two SNe were derived from the ROSAT HRI count rate, using a Thermal-Bremsstrahlung Model with a temperature of 2 keV, similar to the models derived from the spectra of the other X-ray SNe presented in Table 4.1, including SN 1979C by Ray *et al.* (2001). The X-ray upper limits are also plotted on Figure 4.3, with light curves of the other X-ray SNe mentioned in Table 4.1. The fact the neither SNe 1959D nor 1961V was detected with the ROSAT HRI, although disappointing, does not come as a complete surprise. Both SNe are radio weak compared to SN 1979C (Cowan *et al.* 1994b; Stockdale *et al.* 2001), and the ROSAT sensitivity was rather poor. Future X-ray observations with instruments such as *Chandra* may be able to detect X-ray emission from these sources, as there have been detections with *Chandra* of very faint X-ray emission from SNe, well below the upper limits established by ROSAT for these two SNe.

4.2 A Nuclear X-ray Source in NGC 7331: Evidence for a Massive Black hole

Deep radio observations of NGC 7331 were first made in an attempt to search for the supernova remnant (SNR) from SN1959D (Cowan, Romanishin, & Branch 1994, hereafter = CRB). Although the SNR was not identified in those observations, an unresolved nuclear source was detected (see Figure 4.4; CRB). Optical observations of the nucleus of NGC 7331 identified an optical LINER spectrum (Keel 1983; Bower 1992). These two discoveries support the possibility that NGC 7331 harbors an MBH. Rubin *et al.* (1965) and Afanasiev, Silchenko, & Zasov (1989) made kinematic studies, measuring rotational motion from [NII] and Hα emission lines. These observations were analyzed by Afanasiev *et al.* (1989) suggested an MBH of $\sim 5 \times 10^8$ $M_\odot$ in NGC 7331. Bower *et al.* (1993), however, suggested that this rotational motion could be explained by models without an MBH and with a constant mass-to-light ratio as a function of radius. Bower *et al.* (1993) were only able to exclude an MBH with a mass greater than $5 - 10 \times 10^8$ $M_\odot$ (CRB), a result which is relatively insensitive to small differences in the assumed distance to the galaxy. The Bower *et al.* (1993) mass limit is also near the upper limit of measured masses for Massive Dark Objects found in

LINER galaxies, which have X-ray and radio properties similar to those found in NGC 7331 (Ho 1998).

In this Chapter, I report on the first deep ROSAT X-ray observations of NGC 7331 and their impact in understanding the nature of its LINER nucleus. In Subsection 2, I discuss the results of the observations and the techniques used to reduce these data. Classically, the possible indicators for an MBH are the detection of an unresolved nuclear source, a non-thermal radio and X-ray spectral index, variability in the nuclear flux over months to years, and an anti-correlation between X-ray and radio variability (Melia 1992). The fact that NGC 7331 possesses an unresolved nuclear source and has a non-thermal radio spectral index was confirmed by CRB. This Chapter identifies a similarly unresolved X-ray source, but can make no statement as to the nature of the X-ray spectra. Confirmation of a non-thermal X-ray spectra and the last two criteria for an MBH require further X-ray and radio observations. While starburst galaxies can also have non-thermal, unresolved sources, there is no evidence for an anti-correlation in X-ray and radio variability in such galaxies. Other indicators of the presence of an MBH in NGC 7331 will be discussed later in Subsection 3 of this Chapter. Also in Subsection 3, I will provide comparisons of our results with current theories and observations of low luminosity active galactic nuclei (LLAGN) powered LINERs and make our conclusions.

4.2.1 Observations and Data Reduction

NGC 7331 is an Sbc spiral galaxy, which was observed with the ROSAT High Resolution Imager (HRI) in December 1995 to study the nuclear source that had been previously observed in the radio with the Very Large Array (VLA) (CRB). The HRI is an X-ray photon collector with no spectral resolution, collecting photons with energies ranging from 0.12 keV to 2.4 keV. The observations were made over a two day period with a total observation time of 30.5 ks. The search was centered on the CRB radio center of NGC 7331 at R.A.(2000) = $22^h37^m4^s.8$, Decl.(2000)= $+34°25'11''.5$.

Raw data reduction was provided by the ROSAT Standard Data Processing Center. Standard ROSAT tests for short term variability are not applicable due to insufficient counts. The data were further reduced using the IRAF routine GAUSS which convolved the data with a circularly symmetric Gaussian function, with the parameter sigma set to one pixel, effectively $0''.5$. The image was smoothed with a Gaussian because of concerns from the Data Processing Center that the standard analysis system was not very reliable in properly identifying sources in complex emission regions. Sources that were initially reported as individual point sources by the Center, are actually part of a more complex X-ray emission region. The data were then evaluated with the NOAO-IRAF routine QPHOT to obtain object counts, count noise, and accurate position measurements. The aperture radius used to determine the count flux from the galaxy was set to 24$''$, and sky background measurements were determined with the specified parameters of an inner annulus of 80$''$ and an outer annulus of 102$''$.

Lacking direct X-ray spectral data, a value for the $log N(H) = 21.3$ (Burstein & Heiles 1978; van Steenberg *et al.* 1988; Stark *et al.* 1992; Smith 1998) and a photon index, Γ ($dF/dE \propto E^{-\Gamma}$), of 1.0 and 2.0 (similar to values for other such objects listed in Table 4.3) for the central sources in NGC 7331 were assumed to determine the unabsorbed X-ray flux. The total column density of hydrogen includes both the Galactic column density (8.61×10^{20} cm^{-2}; Burstein & Heiles 1978) and the column density for the bulge of NGC 7331 (Smith 1998). The ROSAT HRI energy-to-count conversion factors were taken from the ROSAT Users Handbook, assuming a power law spectrum (Zimmerman 1994). The assumption of an X-ray power law spectrum is consistent with both the possible presence of an MBH, as well as for a post starburst galaxy (Fabbiano 1996). The X-ray luminosity for the galaxy was calculated assuming the Cepheid-derived distance to NGC 7331 as 15.1 Mpc (Hughes *et al.* 1998). The detections reported in Table 4.2 all meet at least a 3σ detection threshold. Since little is known about the other detected sources in Table 4.2, a power law spectrum, a photon index of 1.0 and the same line-of-sight, Galactic column density, which was used for NGC 7331, were used to determine their energy flux measurements.

Sources of uncertainty in ROSAT positions include a known attitude solution error, which causes X-ray position offsets of order 6″ (ROSAT Users Guide). Since any correction would require knowing X-ray positions and this is the first high resolution image of the field, it is not possible to accurately correct for this error. Table 4.4 compares the optical, radio, and X-ray positions of the nucleus of NGC 7331. The values for the nuclear positions agree to well within 5″ and are definitely coincident within the acceptable ROSAT error.

4.2.2 Results and Discussion

The observations of the X-ray nuclear source in NGC 7331 support the likelihood of an MBH in its core. In Table 4.3, I compare the luminosity of the nuclear source in NGC 7331 with luminosity values for other LINER galaxies. Also included in this table for comparison are the reported luminosities for two identified starburst galaxies.

An assumed power-law spectrum and photon indices of 1.0 and 2.0 were used to analyze our ROSAT observations of NGC 7331, because these are typical of other observed X-ray LINERs in the energy range from 0.1 keV to 2.4 keV. The X-ray luminosity of NGC 7331 in this bandpass region is within the observed range found in other LINERs and somewhat larger than those luminosities observed in typical starburst galaxies. I note that these LINER X-ray luminosities are near the upper limit of X-ray luminosities typically found in normal spiral galaxies (Fabbiano 1996), and therefore an X-ray luminosity cannot be used solely to identify possible MBHs.

The radio spectrum of a typical LLAGN is predicted to be powered by cylcosynchrotron emissions in the advection dominated accretion flow (ADAF) model used by Mahadevan (1997). The observed spectral index, α, of -0.6 ($S_\nu \propto \nu^{+\alpha}$) for NGC 7331 indicates a non-thermal source powering the radio spectrum between 6 cm and 20 cm and is in agreement with observations of similar sources listed in Table 4.5. The value reported by CRB for the spectral index of NGC 7331 agrees closely with the theoretical value of the spectral index of M31, which was modeled with an MBH by Melia (1992). It should also be noted that this value of α is only slightly greater than the spectral index normally associated with SNRs, -0.8, and this might suggest a post starburst nature (Condon 1996).

Table 4.5 also lists radio fluxes from other LINERs with identified nuclear radio sources. The same value of the spectral index found for NGC 7331 is reported for M51 and M81 by Turner & Ho (1994), and M81 has been confirmed to harbor an LLAGN by Ho *et al.* (1996). While the CRB spectral index alone does not confirm the exact nature of the nuclear source in NGC 7331, it does suggest that NGC 7331 is an LLAGN, given the galaxy's identification as a LINER galaxy and the similarity of its spectral index with other LINER galaxies confirmed to harbor

MBHs.

For a sample of LINER nuclei Table 4.6 lists the ratio of soft X-ray and 6 cm radio fluxes. The X-ray fluxes listed in Table 4.6 are averaged over their stated bandpasses listed in Table 4.3. Among this limited sample there appears to be a range for galaxies, from being relatively radio quiet (or X-ray loud) (log [X-Ray/Radio] $\propto -1.8$) to relatively radio loud (or X-ray quiet) (log [X-Ray/Radio] $\propto -4.6$). It must be noted that this is a small sample and that these observations were taken at various epochs and with different instruments. (Radio observations are from the VLA and the Westerbork Synthesis Radio Telescope and X-ray observations are from ROSAT and ASCA.)

Another predicted indicator of an MBH is the bipolar outflow, which is believed to develop as the result of convective instabilities in the thin disk approximation. This in turn leads to a quasi-spherical accretion flow, characteristic of the advective model (Narayan & Yi 1995). In the case of NGC 7331, these outflows have not been positively identified in any observations to date. If these features do exist, they are likely to extend only a few parsecs. For NGC 3079, a LINER galaxy 16 Mpc away, jets were identified which extended only 1.5 pc from the central engine (Trotter *et al.* 1998). Trotter *et al.* (1998) detected a molecular disk with a binding mass of $\sim 10^6\ M_\odot$. The radio observations of NGC 7331 indicate only a compact nuclear source with a ring of non-thermal sources extending beyond the optical galaxy (CRB). The fact that similar jets have not been detected in NGC 7331 can be attributed to the galaxy being 15.1 Mpc away ($1'' = 73$ pc), which makes resolution of parsec-scale outflows beyond the capability of the CRB observations.

Further evidence supporting the existence of a LINER nucleus in NGC 7331, similar to the one in M31, has been presented by Mediavilla *et al.* (1997) and further confirmed by Heckman (1996). M31 was identified as harboring an MBH of 3×10^7 $M_\odot$ by Kormendy & Richstone (1995). Mediavilla *et al.* (1997) and Ciardullo *et al.* (1988) report that the kinematics of the stars and ionized gas are decoupled in NGC 7331 and M31 respectively. This is in contrast to the conditions found in Seyfert galaxies. Also, Tosaki & Shioya (1997) and Young & Scoville (1982) found no CO emission near the nuclei of NGC 7331 and M31. This is atypical for post starburst galaxies. Their results do support the possibility that this absence of CO emission may be due to the presence of a MBH.

Also identified in the HRI image was a source which is within $9''$ of the optical position of NGC 7335 (Klemola *et al.* 1987). The observed flux was 2.15×10^{-13} erg sec^{-1} cm^{-2} (assuming a power-law spectrum, a photon index of 1.0, and the same line of sight, Galactic column density of hydrogen used in the previous section). If this X-ray source is associated with NGC 7335, this would indicate an X-ray luminosity of 3.1×10^{41} erg s^{-1}, assuming a distance to NGC 7335 of 110

Mpc (z=6315 km/s de Vaucouleurs *et al.* (1991) and a Hubble Constant of 55 km s^{-1} Mpc^{-1}). Few observations have been made of this galaxy, and little is known about it. Based upon this derived X-ray luminosity, however, this galaxy warrants further study to determine if it is also a possible candidate for AGN activity.

There are a number of tests associated with X-ray studies that could more definitively determine the nature of the nucleus of NGC 7331 (see e.g., Fabbiano 1996; Serlemitsos *et al.* 1996; Nandra *et al.* 1997; Ho 1998). Such tests will require deep observations, which could provide resolution of the spectrum at multiple wavelengths and identify any form of variability in the observed flux from NGC 7331.

Table 4.1: Soft X-Ray Supernovae Luminosities & Upper Limits

Source	Age (yrs)	Luminosity[a]	Reference
SN 1978K	1.6	1.5×10^{38}	Schlegel *et al.* 1996
	12.1	6.3×10^{38}	—
	12.8	4.3×10^{38}	—
	12.9	7.0×10^{38}	—
	15.1	5.4×10^{38}	—
	16.0	1.9×10^{38}	—
	16.7	2.5×10^{38}	Schlegel *et al.* 1999
	16.7	2.0×10^{38}	—
	16.9	2.3×10^{38}	—
	17.1	2.2×10^{38}	—
	17.1	2.4×10^{38}	—
	19.4	2.2×10^{38}	—
	19.9	2.1×10^{38}	—
SN 1979C	16.2	6.2×10^{38}	Ray *et al.* 2001
	20.6	1.4×10^{39}	—
SN 1980K	0.1	3.4×10^{38}	Canizares *et al.* 1982
	0.2	5.3×10^{37}	—
	11.6	2.0×10^{37}	Schlegel 1994
SN 1986J	5.0	8.2×10^{39}	Houck *et al.* 1998
	6.9	5.1×10^{39}	—
	8.4	4.1×10^{39}	—
SN 1987A	0.9	3.4×10^{35}	Inoue *et al.* 1991
	4.1	9.5×10^{32}	Beuermann *et al.* 1995
	7.4	1.6×10^{34}	Hasinger *et al.* 1996
	8.3	2.0×10^{34}	—
	12.6	1.5×10^{35}	Burrows *et al.* 2000
SN 1959D	36.7	$< 1.2 \times 10^{38}$	this work
SN 1961V	34.3	$< 1.5 \times 10^{40}$	this work

a. Units are erg s^{-1}

Table 4.2: X-Ray Sources in the Field of NGC 7331

Source	RA (2000)	Decl. (2000)	Counts ($ksec^{-1}$)	Flux[a]
1[b]	$22^h37^m3\overset{s}{.}64$	$+34°24'59\overset{''}{.}27$	$4.17 \pm .4$	$41.3 \pm .63$
2[c]	$22^h37^m1\overset{s}{.}86$	$+34°26'53\overset{''}{.}90$	$1.3 \pm .3$	$2.15 \pm .36$
3	$22^h36^m29\overset{s}{.}38$	$+34°25'56\overset{''}{.}78$	$0.9 \pm .3$	$1.49 \pm .50$
4	$22^h36^m33\overset{s}{.}13$	$+34°30'11\overset{''}{.}49$	$1.9 \pm .4$	$3.16 \pm .66$
5	$22^h37^m28\overset{s}{.}97$	$+34°25'25\overset{''}{.}49$	$1.0 \pm .3$	$1.66 \pm .50$
6	$22^h37^m38\overset{s}{.}15$	$+34°22'27\overset{''}{.}36$	$0.5 \pm .3$	$0.83 \pm .50$
7	$22^h37^m3\overset{s}{.}48$	$+34°9'47\overset{''}{.}85$	$1.4 \pm .7$	2.33 ± 1.16
8	$22^h37^m51\overset{s}{.}93$	$+34°28'29\overset{''}{.}43$	$0.9 \pm .4$	$1.49 \pm .66$
9	$22^h35^m54\overset{s}{.}60$	$+34°13'51\overset{''}{.}34$	$9.2 \pm .9$	15.3 ± 1.5
10	$22^h36^m3\overset{s}{.}43$	$+34°12'14\overset{''}{.}95$	$5.9 \pm .9$	9.80 ± 1.50

a. Units are 10^{13} erg s^{-1} cm^{-2}
b. NGC 7331
c. NGC 7335

Table 4.3: Comparisons of NGC 7331 & Similar X-ray Sources

Source	Type (RC3)	Luminosity 10^{40} erg s^{-1}	Photon Index	Bandpass (keV)	Ref
LINERs					
NGC 7331	SAab	2.7—8.5	1.0—2.0	0.1-2.4	
NGC 4258	SABbc	0.51	3.7	0.1-2.4	1
NGC 4736	R SA(r)ab	0.34	2.3	0.1-2.0	2
NGC 4594	SAa	5.3	1.80	0.5-2.0	3
M51	SAbc	2.5	1.76	0.5-2.0	3
NGC 3079	SBc	4.4	1.76	0.5-2.0	3
M81	SAab	1.2	1.9	0.5-2.0	3
NGC 3642	SA(r)bc	3.9	2.84	0.2-2.2	4
NGC 3147	SA(r)bc	24	1.74	0.5-2.0	3
NGC 4579	SAB(rs)b	28	1.87	0.5-2.0	3
Starburst					
M33	SAcd	0.1248	0.74	0.1-2.4	5
NGC 3628	SAb	< 0.06—1.7	0.27—1.16	0.1-2.0	6

References:
1. Pietsch *et al.* (1994)
2. Cui *et al.* (1997)
3. Serlemitsos *et al.* (1996)
4. Koratkar *et al.* (1995)
5. Long *et al.* (1996)
6. Dahlem *et al.* (1995)

Table 4.4: Nuclear Positions for NGC 7331

Observation	R.A. (2000)	Decl.(2000)	Reference
X-ray	$22^h37^m3\overset{s}{.}64$	$+34°24'59\overset{''}{.}27$	
Radio	$22^h37^m4\overset{s}{.}00$	$+34°24'57\overset{''}{.}07$	CRB (1994)
Optical	$22^h37^m4\overset{s}{.}01$	$+34°24'56\overset{''}{.}07$	Klemola (1994)
Optical	$22^h37^m4\overset{s}{.}04$	$+34°24'56\overset{''}{.}47$	Argyle & Clements (1990)

Table 4.5: Core Radio Flux Comparisons of NGC 7331 & Similar Sources

Source Type	2cm mJy	3.6cm μJy	6cm mJy	20cm mJy	Spectral Index
NGC 7331[1]	...	...	0.121	0.234	−0.6
SAab	...	...	(B array)	(A array)	
NGC 4258[2,3,5]	3.2	...	2.4	< 10	+0.4
	...	...	1.5	2.0	−0.2
SABbc	(C array)	...	(B array)	(A array)	
NGC 4579[2]	...	...	...	40	...
SAB(rs)b	...	...	...	(see ref)	
NGC 4736[2,5]	3.2	...	6.1	27	−0.3
	2.2	...	3.6	...	−0.4
R SA(r)ab	(C array)	...	(B array)	(see ref)	
M31[4]	...	28 & 39	...	...	...
SA(s)b	...	(A array)	...	...	
M51[5]	2.3	...	1.6	...	−0.6
SAbc	(C array)	...	(B array)	...	
M81[5]	45	...	92	...	−0.6
SAbc	(C array)	...	(B array)	...	

References:
1. CRB
2. Hummel (1980) (Westerbork Synthesis Radio Telescope)
3. Vila *et al.* (1990)
4. Crane *et al.* (1992); Crane *et al.* (1993)
5. Turner & Ho (1994)

Table 4.6: Soft X-ray & 6 cm Radio Flux Ratios for Selected LINERs

Source	Radio Flux[a] 10^{-27}	X-ray Flux[a] 10^{-30}	log $[\frac{\text{X-Ray}}{\text{Radio}}]$	Ref
NGC 7331	0.121	1.93 — 5.90	(−1.80) — (−1.31)	1
NGC 4258	2.4	7.4	−2.1	2 & 3
M51	1.6	3.2	−2.7	5 & 6
NGC 4736	3.6	4.1	−2.9	3 & 4
NGC 4736	6.1	4.1	−3.2	3 & 4
NGC 4579	40	5.3	−3.9	3 & 6
M81	92	2.3	−4.6	5 & 6

a. erg s^{-1} cm^{-2} Hz^{-1}

References:
1. CRB
2. Pietsch *et al.* (1994)
3. Hummel (1980)
4. Cui *et al.* (1997)
5. Turner & Ho (1994)
6. Serlemitsos *et al.* (1996)

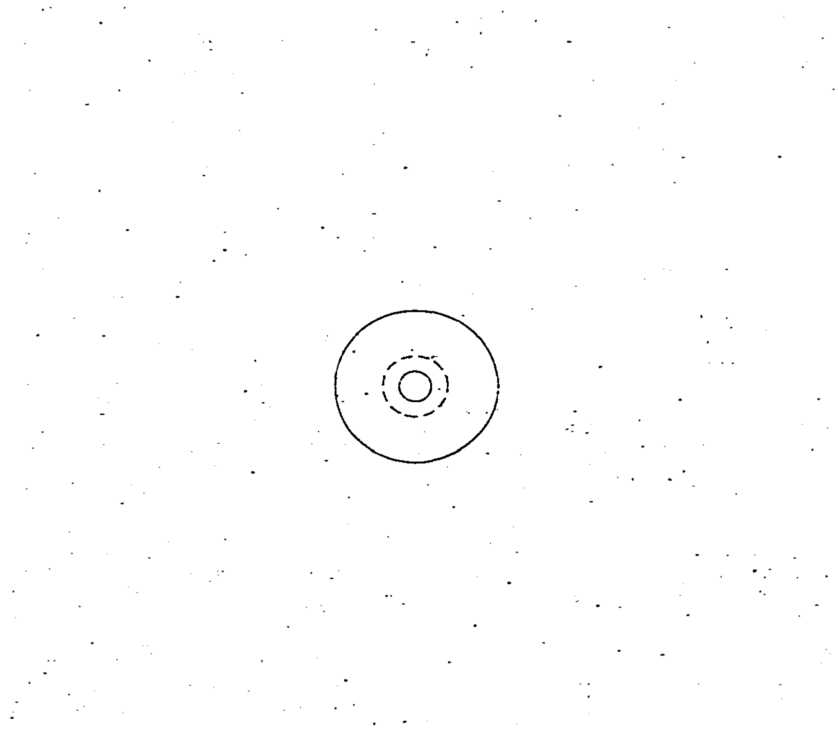

Figure 4.1: A grey-scale X-ray image of SN 1961V and the field. SN 1961V is the circled object in the center, with the annulus used for background counts also indicated.

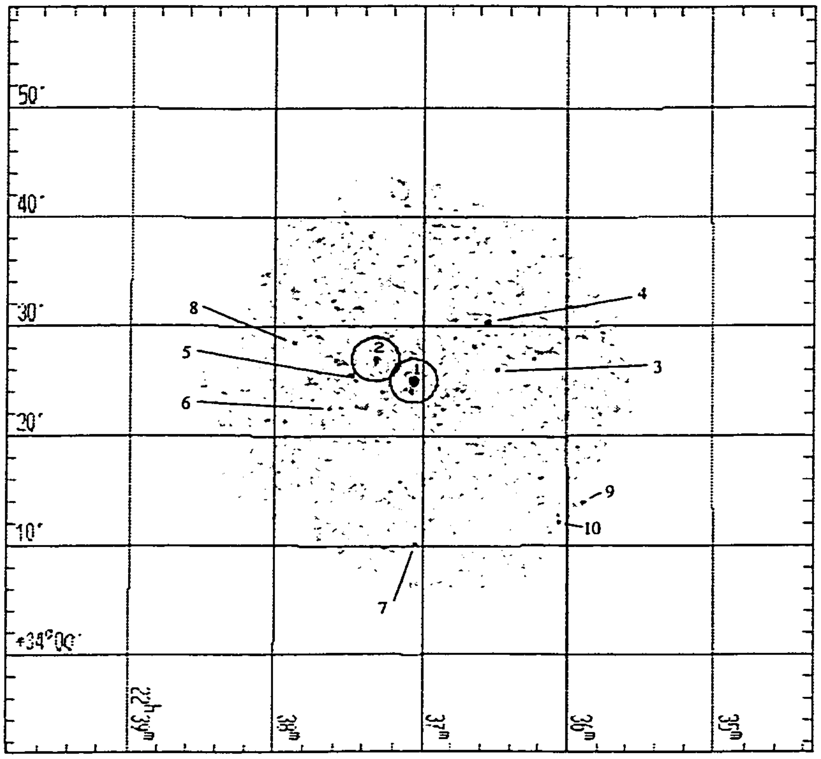

Figure 4.2: A grey scale X-ray image of NGC 7331 and the field. NGC 7331 is the circled object labeled #1 and NGC 7335 is the circled object labeled #2. The X-ray detection of the nuclear source in NGC 7331 is within 5.″0 of prior radio observations of the nucleus given in Table 4.2. The remaining eight unidentified sources listed in Table 4.2 (#3 - #10) are indicated on this figure.

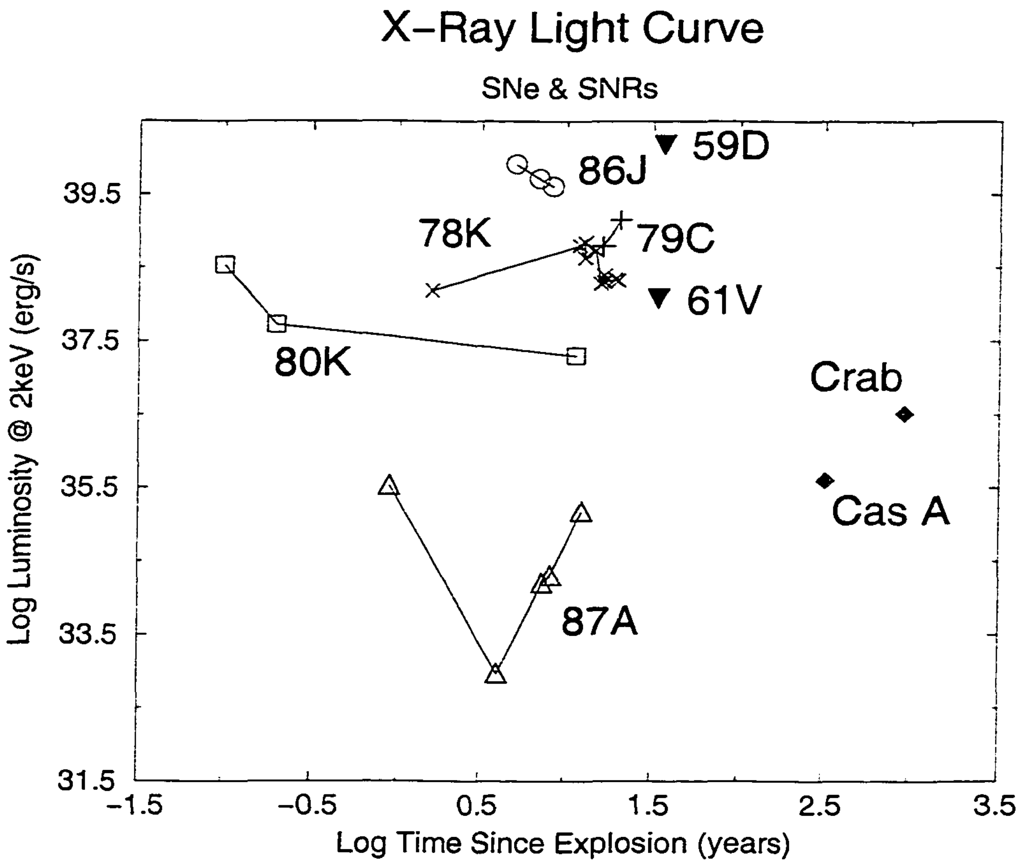

Figure 4.3: Soft X-ray Light Curve of Supernovae & SNRs. References given in Table 4.1.

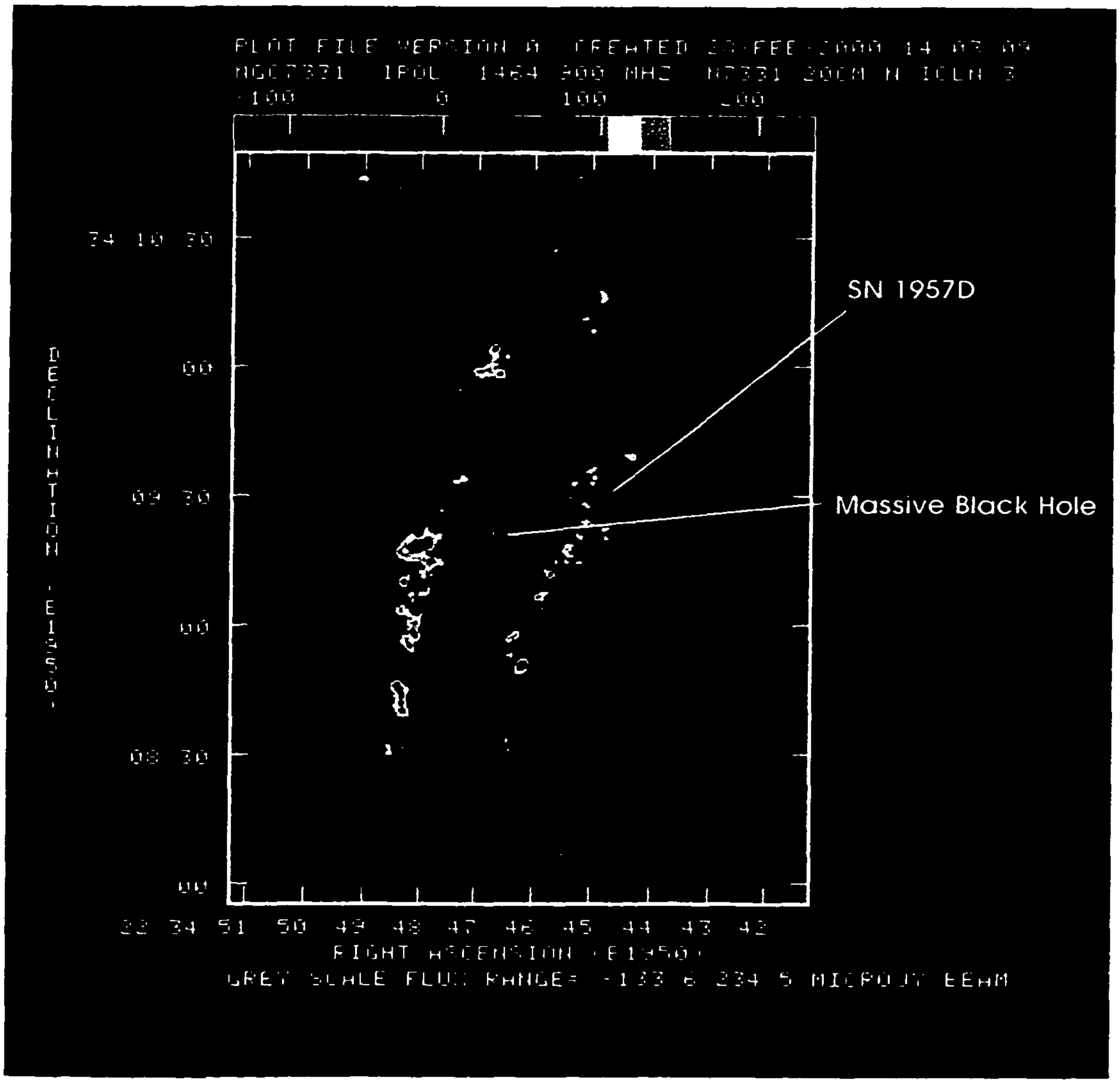

Figure 4.4: Radio Image of NGC 7331 at 20 cm with the location of the nucleus and the site of SN 1959D indicated.

Chapter 5

Conclusions

5.1 Summary of Results

Through this study, I am able to report the radio rediscovery of five intermediate-age SNe and upper limits for the detection of three other RSNe and two X-ray SNe. Further, the VLA observations of SNe 1961V and 1950B appear to clearly identify these sources as Type II SNe. All of the radio properties of these two sources are consistent with those of other established Type II SNe. SN 1961V's radio luminosity has faded at both 20 cm and 6 cm in a manner consistent with similarly-aged SNe. In particular, its rate of decline lies between the decay indices of SNe 1970G and 1957D, both of which are confirmed Type II SNe (Tully 1988). Also, the non-thermal nature of SN 1961V at this late epoch in its evolution is inconsistent with evolutionary models of LBVs, which predict thermal emission as the weak eruption of the LBV dissipates into the CSM of the progenitor star (White 2001). The question of SN 1950B's exact nature was due to a lack of good optical spectra following the SN event. Through radio studies well after the optical peak, I am able to identify SN 1950B and 1961V as Type II SNe.

I am able to conclude that the observed radio and X-ray emission from SNe do appear to be related to one another, as outlined in the theoretical models of Weiler *et al.* (1986, 1990, 1996, 2001). This can be most clearly demonstrated in Figures 5.1 and 5.2, which illustrate the radio and X-ray light curves for these sources. As illustrated by these two light curves, there is an obvious correlation between the X-ray and radio luminosities of supernovae. The most radio luminous are also exceptionally bright in their X-ray emission, as is evident for SNe 1978K, 1979C, and 1986J. The dimmest supernova ever detected in the radio, SN 1987A, is also the weakest X-ray SN observed [It was only detectable due to being $\sim$100$\times$ closer than the next nearest SN (Mitchell *et al.* 2001).] The lack of previous X-ray SNe with measured spectra and luminosities, as compared to the number of RSNe, will soon be remedied by new and pending *Chandra* observations. These new measurements will also help to explain the peculiar differences between the radio and X-ray evolution of these events.

Figure 5.1 also illustrates a potential wrinkle in the Weiler *et al.* (1986, 1990, 1996, 2001) models for the evolution of RSNe. Their models all assume a uniformly ejected CSM with which the SN shock interacts. While this seems to be case for the first ten years, the intermediate-age evolution demonstrates a degree of heterogeny amongst Type II SNe. There appear to be two distinct behavioral patterns. The first is the continual decay predicted by Weiler *et al.* (1986, 1990, 1996, 2001), which can be demonstrated through the linear declines of SNe 1957D, 1980K, and 1981K (this Dissertation; Eck *et al.* 1998; Cowan *et al.* 1994a; Weiler *et al.* 1986,1992; Van Dyk *et al.* 1992). The second group appears to fall off at varying rates, as shown by the light curves for SN 1950B and 1970G (this Dissertation; Cowan *et al.* 1994a,1994b). The reason for this difference is likely due to the nature of the CSM surrounding the SN event and how it was ejected. The different progenitor stars could have undergone a variety of phases prior to the SN explosion, possibly including either a Wolf-Rayet phase and/or an LBV phase. SN 1987A experienced neither and has a very sparse CSM (Ball *et al.* 1995). SN 1979C has also experienced a flattening of its light curve, but this is likely due to the presence of a binary companion (Montes *et al.* 2000). SN 1961V could belong in either of these categories, as its decay index falls between values reported for SNe in each of these categories (see Tables 2.2, 3.1, and 3.2). The emission from SN 1923A appears to follow the Weiler *et al.* (1986) predictions closely as it begins to transition into a SNR. But due to a lack of previously detected emission, these measurements do not rule out the possibility that it too could have experienced a short term flattening of its light curve, as is evident for SN 1950B, which is now decaying at a rate similar to that of SN 1957D.

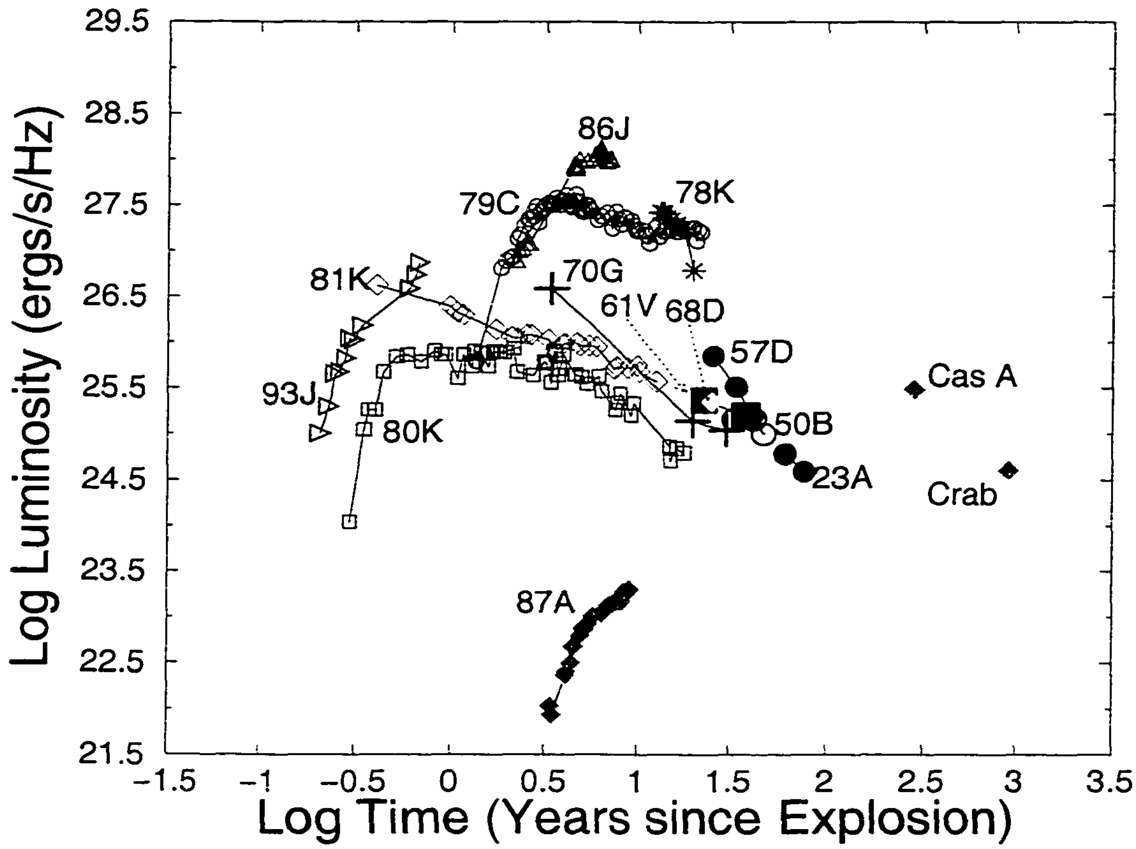

Figure 5.1: 20 cm radio light curve of several RSNe and SNRs. Data, fits and distances for SN 1923A, from this Dissertation, Eck *et al.* (1998) and Saha *et al.* (1995); for SNe 1950B (black hoops) & 1957D, from this Dissertation, Cowan *et al.* (1994) and Saha *et al.* (1995); for SN 1961V (blue squares), Stockdale *et al.* (2001a) and Silbermann *et al.* (1996); for SN 1968D (yellow diamond), from Hyman *et al.* (1995) and Tully (1988); SN 1970G (red crosses), from Stockdale *et al.* (2001b), Cowan *et al.* (1991), and Kelson *et al.* (1996); for SN 1978K, from Ryder *et al.* (1993), Schlegel *et al.* (1999), and Tully (1988); for SN 1979C, from Weiler *et al.* (1986, 1991), Montes *et al.* (2000), and Ferrarese *et al.* (1996); for SN 1980K, from Weiler *et al.* (1986, 1992), Montes *et al.* (1998), and Tully (1988); for SN 1981K from Van Dyk *et al.* (1992) and Freedman *et al.* (2001); for SN 1986J, from Rupen *et al.* (1987), Weiler *et al.* (1990), and Silbermann *et al.* (1996); for SN 1987A from Ball *et al.* (1995) and Mitchell *et al.* 2001; and for SN 1993J from Van Dyk *et al.* (1994) and Freedman *et al.* (2001). Luminosities for Cas A and the Crab from Eck *et al.* (1998).

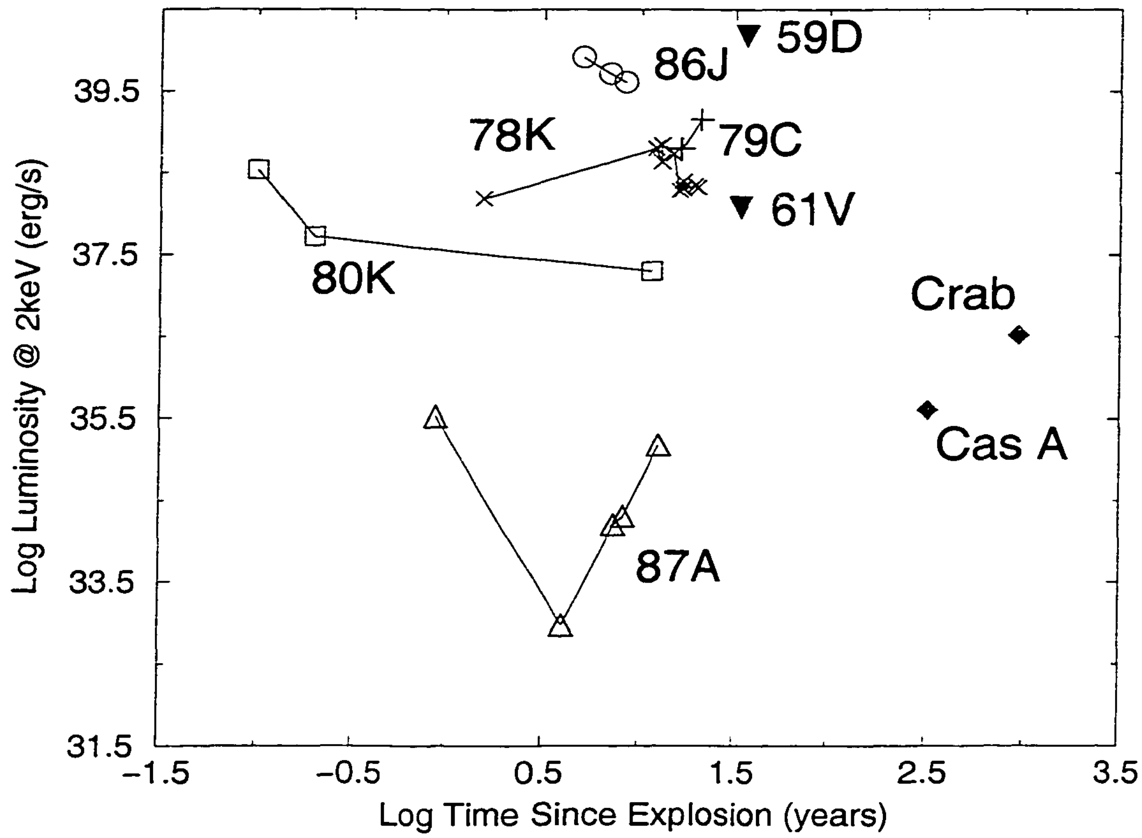

Figure 5.2: Soft X-ray Light Curve of Supernovae & SNRs. References given in Table 4.1.

5.2 Future Plans

I will continue to focus my efforts toward the study of extragalactic SNe, SNRs, and galactic centers, using the VLA, the VLBA, and the *Chandra* X-ray Observatory. With Dr. Kurt Weiler at the Naval Research Laboratory (NRL), I will be studying young SNe before the intermediate-age. As discussed in the Introduction, in this phase the SNe are intrinsically brighter and therefore much easier to detect and study. This work will provide a deeper understanding of high-mass stellar evolution, especially the final stages of the SN progenitor star and the physical processes responsible for the supernova explosion. These short-lived stars comprise an exceptionally small subset of a galaxy's stellar population, but play extremely important roles in heavy element enrichment and in the triggering of star formation within their host galaxies. The combination of X-ray and radio emission from SNe provides an unparalleled opportunity to study the nature of SNe & SNRS and their CSM. Through continual monitoring of these sources, it becomes possible to probe the early mass-loss rates and ejection velocities of the progenitor star, as the SN shock encounters CSM ejected at earlier epochs of the star's life. As is indicated in Figures 5.1 and 5.2, few young SNe have been observed in radio and X-ray frequencies, so the need for further studies is clear. Further, the search for SNe will often provide opportunities to also monitor the nuclei in the host galaxies of these SNe. This will provide an excellent opportunity to detect variability in these sources, a possible sign for MBHs.

Dr. Weiler and his research group at the NRL have pioneered efforts in the radio monitoring of young SNe and in developing new techniques and instrumentation for expanding the frontiers of radio astronomy. At the NRL, I will make new VLA observations of radio SNe, with observing time already allocated to Dr. Weiler and his research group. And, I will have access to their VLA archival data of previously observed sources. I also intend to apply for *Chandra* observations with Dr. Weiler in an attempt to detect X-ray emission from both new and historical SNe.

My work will also include ongoing VLA and *Chandra* observations to detect radio and X-ray emission from SNe and SNRs [of which I am a Co-Investigator]. These two observatories are ideal tools to probe this complex subject, offering complimentary sensitivity and spatial resolution. We will utilize the high sensitivity and spatial resolution of *Chandra* to identify X-ray point sources in a number of nearby (low-inclination) spiral galaxies, chosen to span a range of Hubble types. Our radio observations, particularly spectral index information, will be critical in determining the nature of these sources. We will be able to identify previously undetected SNRs in these galaxies. Multiwavelength comparisons will provide a number of important scientific clues about the nature of SNRs. For example, the observations will provide constraints on the density of the local interstellar medium, which affects the turn-on time and duration of radio emission in theoretical SNR models such as those of Cowsik & Sarkar (1984). Our observations will be important in addressing other important questions such as how are the radio, X-ray and optical emissions related? Are they from the same region, and how do the mechanisms differ in terms of energy efficiencies for particle acceleration at the shock interface, shock energies or even presupernova mass-loss rates, all important parameters in models of radio emission such as those by Chevalier (1984). Additionally, we will be able to determine variability in any known SNRs, as well as perhaps recover known historical supernovae. We also note that the detection of a number of SNRs in any of the spiral galaxies would also demonstrate (or confirm) an unusual star formation history. My observations of M83 and M101 (included in Chapter 3) will be incorportated into this study, along with proposed observations of eight other spiral galaxies. The *Chandra* observations are currently being made, and Figure 5.3 illustrates the recent X-ray observations made of M83. While the results are still preliminary, there are obvious correlations with the X-ray and radio images of M-83 (see Figure 3.7), especially noteworthy are the nuclear region, the spiral arms (with an X-ray source near SN 1950B), and other point sources in the field.

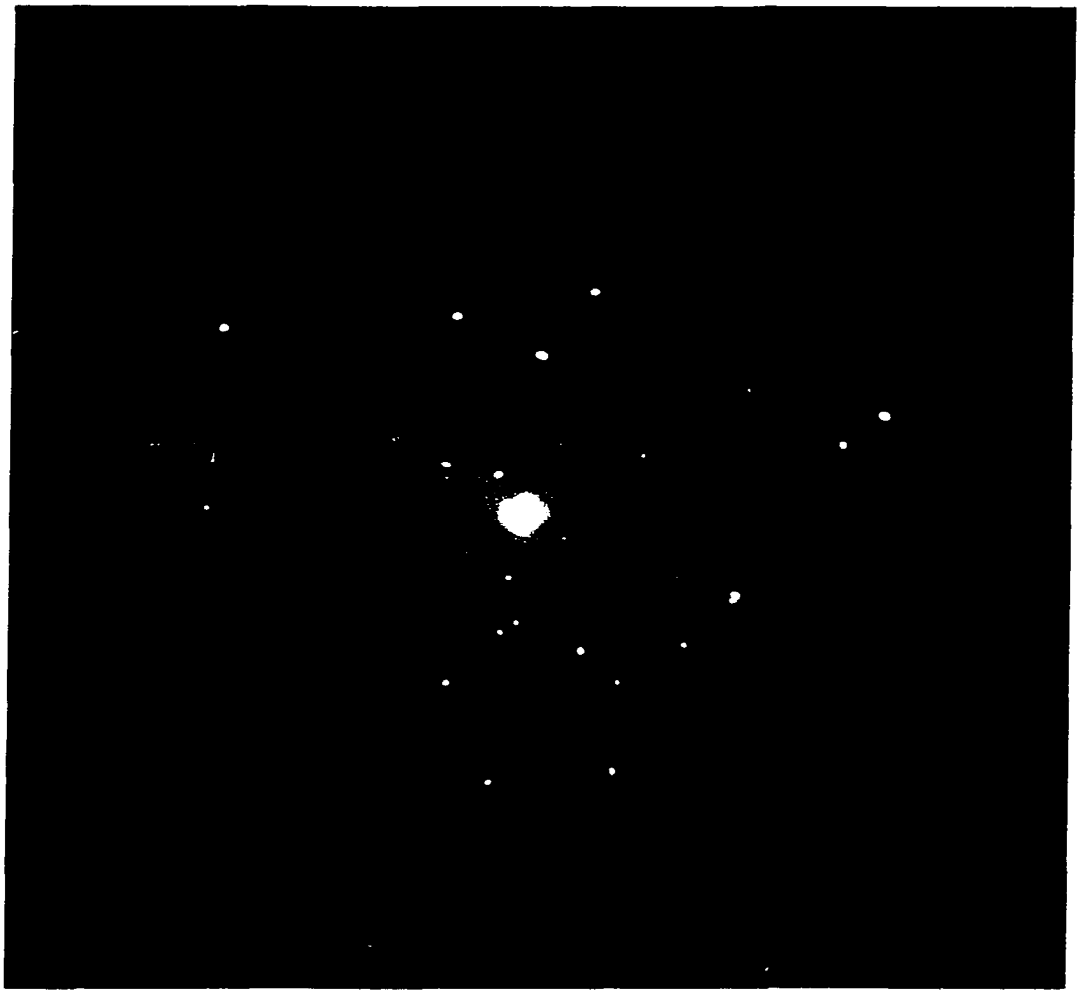

Figure 5.3: *Chandra* X-ray false color image of M83, with bluer emission indicating higher energy photons.

I also look forward to working with Dr. Namir Kassim, a member of the NRL radio astronomy group, to improve the observational capabilities of Low Frequency Radio Astronomy (LFRA). The efforts currently being pursued at the NRL, especially the proposed Low Frequency Array, exhibit a great potential for future scientific exploration. LFRA has been one of the most poorly observed portions of the EM spectrum. LFRA probes the 15 MHz to 150 MHz (or 2-20 meter) region of the radio spectrum, previously limited to short baselines (and subsequent poor resolution) by ionospheric distortions. An innovative answer to this problem was developed by N. E. Kassim and researchers at the NRL involving self-calibration techniques. It has been successfully demonstrated with a joint NRL-NRAO project, installing new Q-band (74 MHz) receivers at the VLA. This advancement in LFRA has been successful in allowing new discoveries in the fields of planetary, solar, Galactic, and extragalactic astronomy. The latest advance in LFRA is the Low Frequency Array (LOFAR), a proposed facility that will allow for high resolution observations through the LFRA frequency band. LOFAR will fill an important role in radio astronomy with the VLA and the proposed Square Kilometer Array (Kassim, Lazio, & Erickson 1999).

The particular aspect of LFRA which intrigues me the most is being able to probe the structure of Galactic SNRs. Observations in this frequency range will allow us to better understand the environment in which SNe occur by observing their interactions between the expanding shock front and the local ISM. They will also provide an unprecedented look into the inner dynamics of SNRs. And, in the case of many SNRs, LFRA will allow us to search for hereto undiscovered stellar corpses such as neutron stars and black holes due the low extinction at these frequencies. Observations could also be made of extragalactic SNRs, which would allow us to determine the relationship between the ISM and high mass stellar evolution in different galaxies. Further, the observations will constrain models concerning the acceleration of cosmic rays, which has been clearly linked to SNRs.

Although my experience in radio astronomy has centered primarily on observations and imaging, I look forward to developing new skills in assisting in the design and development of the instrumentation for the new LOFAR facility. This will undoubtly give me a better understanding of radio interferometry and new insights into its observational capabilities. My new position offers a unique opportunity to engage in making extremely important observations of radio SNe and in designing cutting-edge technology to further study these rare objects.

A long-term prospect for the study of intermediate-age SNe is the eventual completion of the Expanded VLA (EVLA). This project will strongly enhance the VLA's scientific capabilities, especially in the search for very faint radio sources like intermediate-age SNe. The project is split into two phases, improving the current VLA antennae and replacing the correlator and the construction of eight new receiving stations (the New Mexico Array) with maximum baselines of $\sim$300 km linked to the current VLA. The first stage is currenty being implemented and the second has been proposed and is awaiting funding. When completed, the new array will be 5—20 times more sensitive and have a resolution of $0\farcs2$ at 20 cm. Such improvements will allow for a more extensive study of intermediate-age SNe, reducing the necessary observing time for such faint sources from $\sim$10—12 hours to less than 2 hours for a comparable signal to noise ratio. The EVLA will also be more compatible with the VLBA antennae, making combined VLA/VLBA observations (such as my study of SN 1961V) much less complicated. With *Chandra* and the upcoming EVLA, the study of intermediate-age SNe and young SNRs will become much more fruitful as astronomers continue to explore the fascinating transition period between supernova and supernova remnant.

Bibliography

[Afanasiev *et al.* 1989] Afanasiev, V. I., Silchenko, O. K., & Zasov, A. V. 1989, *Astronomy & Astrophysics*, 213, L9

[Allen *et al.* 1976] Allen, R. J., Goss, W. M., Ekers, R. D., & de Bruyn, A. G. 1976, *Astronomy & Astrophysics*, 48, 253

[Anderson *et al.* 1991] Anderson, M., Rudnick, L., Leppick, P., Perley, R., & Braun, R. 1991, *Astrophysical Journal*, 373, 146

[Argyle & Clements 1990] Argyle, R. W. & Clements E. D. 1990, *Observatory*, 110, 93

[Baars *et al.* 1977] Baars, I. W. M., Genzel, R., Pauliny-Toth, I. I. K., & Witzel, A. 1977, *Astronomy & Astrophysics Supplement*, 61, 99

[Barbon *et al.* 1998] Barbon, R., Buond, V., Cappellaro, E., & Turatto, M. 1998, *Astronomy & Astrophysics*, 139, 531

[Barbon *et al.* 1979] Barbon, R., Ciati, F., & Rosino, L. 1998, *Astronomy & Astrophysics*, 72, 287

[Bartunov *et al.* 1994] Bartunov, O. S., Tsvetkov,D, Y., & Filimonova, I. V. 1994, PASP, 106, 1276

[Bennett 1967] Bennett, R. J. M. 1967, IAU Circ. 2085

[Beuermann *et al.* 1994] Beuermann, K., Brandt, S., & Pietsch, W. 1994, *Astronomy & Astrophysics*, 281, L45

[Boffi & Panagia 2001] Boffi, F. R., & Panagia, N. 2001, *Young Supernova Remnants: Eleventh Astrophysics Conf.*, ed. S. S. Holt & U. Hwang (Melville, N. Y.: AIP Press), 69

[Bower 1992] Bower, G. A. 1992, PhD Thesis, Univ. Michigan

[Bower *et al.* 1993] Bower, G. A., Richstone, D. O., Bothum, G. D., & Heckman, T. M. 1993, *Astrophysical Journal*, 402, 76

[Bregman & Pildis 1992] Bregman, J. N. & Pildis, R. A. 1992, *Astrophysical Journal*, 398, L107

[Branch *et al.* 1995] Branch, D., Livio, M., Yungelson, L. R., Boffi, F. R., & Baron, E. 1995, *Publications of the Astronomical Society of the Pacific*, 107, 1019

[Branch & Greenstein 1971] Branch, D., & Greenstein, J. L. 1971, *Astrophysical Journal*, 167, 89

[Burrows *et al.* 2000] Burrows, D. N., Michael, E., Hwang, U., McCray, R., Chevalier, R. A., Petre, R., Garmire, G. P., Holt, S. S., Nousek, J. A. 2000, *Astrophysical Journal*, 543, L149

[Burstein & Heiles 1984] Burstein, D. & Heiles C. 1984, *Astrophysical Journal Supplement*, 54, 33

[Canizares *et al.* 1982] Canizares, C., Kriss, G., & Feigelson, E. 1982, *Astrophysical Journal*, 253, L17

[Chevalier 1982a] Chevalier, R. A. 1982, *Astrophysical Journal*, 258, 790

[Chevalier 1982b] Chevalier, R. A. 1982, *Astrophysical Journal*, 259, 302

[Chevalier 1982c] Chevalier, R. A. 1982, *Astrophysical Journal*, 259, L85

[Chevalier 1984] Chevalier, R. A. 1984, *Astrophysical Journal*, 285, L63

[Chevalier 1990] Chevalier, R. A. 1990, *Supernovae*, ed. A. Petschek (Berlin: Springer-Verlag), 91

[Chevalier & Fransson 1994] Chevalier, R. A., & Fransson, C. 1994, *Astrophysical Journal*, 420, 268

[Chevalier 1998] Chevalier, R. A. 1998, *Astrophysical Journal*, 499, 810

[Ciardullo *et al.* 1988] Ciardullo, R., Rubin, V., Jacoby, G. H., Ford, H. C., & Ford W. K. 1988, *Astronomical Journal* 95, 438

[Colgate & McKee 1969] Colgate & McKee 1969, *Astrophysical Journal*, 157, 623

[Condon 1996] Condon, J. J. 1996, ASP Conf., 103, 132

[Corcoran *et al.* 1998] Corcoran, M. F. *et al.* 1998, *Astrophysical Journal*, 494, 381

[Cowan & Branch 1985] Cowan, J. J. & Branch, D. 1985, *Astrophysical Journal*, 293, 400

[Cowan *et al.* 1991] Cowan J. J., Goss, W. M., & Sramek, R. A. 1991, *Astrophysical Journal*, 379, L49 (CGS)

[Cowan *et al.* 1988] Cowan, J. J., Henry, R. B. C., & Branch, D. 1988, *Astrophysical Journal*, 329, 116 (CHB)

[Cowan *et al.* 1994a] Cowan, J. J., Roberts, D. A., & Branch, D. 1994, *Astrophysical Journal*, 434, 128

[Cowan *et al.* 1994b] Cowan, J.J., Romanishin, W., & Branch D. 1994, *Astrophysical Journal*, 436, L139 (CRB)

[Cowsik & Sarkar 1984] Cowsik, R., & Sarkar, S. 1984, *Monthly Notices of the Royal Astronomical Society*, 207, 745

[Crane *et al.* 1993] Crane, P. C., Cowan, J. J., Dickel, J. R., & Roberts, D. A. 1993, *Astrophysical Journal*, 417, L61

[Crane *et al.* 1992] Crane, P. C., Dickel, J. R., & Cowan, J. J. 1992, *Astrophysical Journal*, 390, L9

[Cui *et al.* 1997] Cui, W., Feldkhun, D., & Braun, R. 1997, *Astrophysical Journal*, 477, 693

[Cumming *et al.* 1996] Cumming, R. J., Lundqvist, P., Smith, L. J., Pettini, M., & King, D. L. 1996, *Monthly Notices of the Royal Astronomical Society*, 283, 1355

[Dahlem *et al.* 1995] Dahlem, M., Heckman, T. M., & Fabbiano, G. 1995, *Astrophysical Journal*, 442, L49

[de Vaucouleurs *et al.* 1991] de Vaucouleurs, G., de Vaucouleurs, A, Corwin, H. G., Buta, R. J., Paturel, G., Fouqué, P. 1991, *Third Reference Catalog of Bright Galaxies*, Springer-Verlag, New York (RC3)

[Dickey & Lockman 1990] Dickey, J. M. & Lockman F. J. 1990, *Annual Review of Astronomy & Astrophysics*, 28, 215

[Doggett & Branch 1985] Doggett, J. B., & Branch, D. 1985, *Astronomical Journal*, 90, 2303

[Dotani *et al.* 1987] Dotani *et al.* 1987, *Nature*, 330, 230

[Eck *et al.* 1998] Eck, C. R., Cowan, J. J., & Branch, D. 1998, *Astrophysical Journal*, 508, 664

[Eck *et al.* 2001] Eck, C. R., Roberts, D. A., Cowan, J. J., & Branch, D. 2001, *Astrophysical Journal*, submitted

[Fabbiano 1996] Fabbiano, G. 1996, ASP Conf, 103, 56

[Fabian & Terlevich 1996] Fabian, A. C., & Terlevich, R. 1996, *Monthly Notices of the Royal Astronomical Society*, 280, L5

[Ferrarese *et al.* 1996] Ferrarese, L. *et al.* 1996, *Astrophysical Journal*, 464, 568

[Fesen 1985] Fesen, R. A. 1985, *Astrophysical Journal*, 297, L29

[Fesen *et al.* 1999] Fesen, R. A., Gerardy, C. L., McLin, K. M., & Hamilton, A. J. S. 1999, *Astrophysical Journal*, 514, 195

[Filippenko 1991a] Filippenko, A. V. 1991a, *Supernovae*, ed. S. E. Woosely (New York: Springer-Verlag), 467

[Filippenko 1991b] Filippenko, A. V. 1991b, *Supernova 1987 and Other Supernovae*, eds. I. J. Danziger & K. Kjar (Garching: European Southern Obs.), 343

[Filippenko 1997] Filippenko, A. V. 1997, *Annual Review of Astronomy & Astrophysics*, 35, 309

[Filippenko *et al.* 1995] Filippenko, A. V., Barth, A. J., Bower, G. C., Ho, L. C., Stringfellow, G. S., Goodrich, R. W., & Porter, A. C. 1995, *Astronomical Journal*, 110, 2261

[Fransson 1994] Fransson, C. 1994, *Circumstellar Media in the Late Stages of Stellar Evolution*, eds. R. E. S. Clegg, I. R. Stevens, & W. P. S. Meikle (Cambridge: Cambridge Univ. Press), 120

[Fransson *et al.* 1996] Fransson, C., Lundqvist, P., & Chevalier, R. A. 1996, *Astrophysical Journal*, 461, 993

[Gates 1958] Gates, H. S. 1958, Harvard Coll. Obs. Announc. Card, 1394

[Goodrich *et al.* 1989] Goodrich, R. W., Stringfellow, G. S., Penrod, G. D., & Filippenko, A. V. 1989, *Astrophysical Journal*, 342, 908

[Gorenstein *et al.* 1994] Gorenstein, P., Hughes, J. P., & Tucker, W. H. 1994, *Astrophysical Journal*, 420, L25

[Gottesman *et al.* 1972] Gottesman, S. T., Broderick, J. J., Brown, R. L., Balick, B., and Palmer, P. 1972, *Astrophysical Journal*, 174, 383

[Gull 1973] Gull, S. F. 1973, *Monthly Notices of the Royal Astronomical Society*, 161, 47

[Haro 1950] Haro, G. 1950, Harvard Coll. Obs. Announc. Card, 1074

[Hasinger *et al.* 1996] Hasinger, G., Aschenbach, B., & Trümper, J. 1996, *Astronomy & Astrophysics*, 312, L9

[Heckman 1996] Heckman, T. 1996, ASP Conf, 103, 241

[Hensler *et al.* 1998] Hensler, G., Dickow, R., Junkes, N., & Gallagher, J. S. 1998, *Astrophysical Journal*, 502, 47

[Ho *et al.* 1996] Ho, L. C., Filippenko, A. V., & Sargent W. L. W. 1996, *Astrophysical Journal*, 462, 18.

[Ho 1998] Ho, L. C. 1998, Observational Evidence for Black Holes in the Universe, in print

[Hoeflich *et al.* 1996] Hoeflich, P., Wheeler, J. C., Hines, D. C., & Tramaell, S. R., 1996, *Astrophysical Journal*, 459, 307

[Houck *et al.* 1998] Houck, J. C., Bregman, J. N., Chevalier, R. A., & Tomisaka, K. 1998, *Astrophysical Journal*, 492, 431

[Hughes *et al.* 1998] Hughes, S. M. G., Han, M., Hoessel, J., Freeman, W. L., Kennicut, R. C., Mould, J. R., Saha, A., Stetson, P. B., Madore, B. F., Silbermann, N. A., Harding, P., Ferrarese, L., Ford, H., Gibson, B. K., Graham, J. A., Hill, R., Huchra, J., Illingworth, G. D., Phelps, R., & Sakai, S. 1998 *Astrophysical Journal*, 501, 32

[Hummel 1980] Hummel, E. 1980, *Astronomy & Astrophysics Supplement*, 41, 151

[Humphreys & Davidson 1994] Humphreys, R. M., & Davidson, K. 1994, *Publications of the Astronomical Society of the Pacific*, 106, 1025

[Hyman *et al.* 1995] Hyman, S. D., van Dyk, S. D., Weiler, K. W., & Sramek, R. A. 1995, *Astrophysical Journal*, 443, L77

[Immler *et al.* 1998a] Immler, S., Pietsch, W., & Aschenbach, B. 1998a, *Astronomy & Astrophysics*, 331, 601

[Immler *et al.* 1998b] Immler, S., Pietsch, W., & Aschenbach, B. 1998b, *Astronomy & Astrophysics*, 336, L1

[Inoue *et al.* 1991] Inoue, H. *et al.* 1991, *Publications of the Astronomical Society of Japan*, 43, 213

[Keel 1983] Keel, W. C. 1983, *Astrophysical Journal*, 269, 466

[Kelson *et al.* 1996] Kelson, D. *et al.* 1996, *Astrophysical Journal*, 463, 26

[Klemola 1994] Klemola 1994, private communication

[Klemola *et al.* 1987] Klemola, A. R., Jones, B. F., & Hanson, R. B. 1987, *Astronomical Journal*, 94, 501

[Koratkar *et al.* 1995] Koratkar, A., Deustus. S. E., Heckman, T., Filippenko, A. V., Ho, L. C., & Rao, M. 1995, *Astrophysical Journal*, 440, 132

[Kormendy & Richstone 1995] Kormendy, J. & Richstone, D. 1995, *Annual Review of Astronomy & Astrophysics*, 33, 581

[Kothes & Reich 2001] Kothes, R., & Reich, W. 2001, *Young Supernova Remnants: Eleventh Astrophysics Conf.*, ed. S. S. Holt & U. Hwang (Melville, N. Y.: AIP Press), 271

[Lacey *et al.* 1997] Lacey, C., Duric, N. & Goss, W. M. 1997, *Astrophysical Journal*, 109, 417

[Lampland 1936] Lampland, C. O. 1936, *Publications of the Astronomical Society of the Pacific*, 48, 286

[Leibundgut 1994] Leibundgut, B. 1994, *Circumstellar Media in the Late Stages of Stellar Evolution*, eds. R. E. S. Clegg, I. R. Stevens, & W. P. S. Meikle (Cambridge: Cambridge Univ. Press), 100

[Lewin *et al.* 1996] Lewin, W. H. G., Zimmerman, H.-U., & Aschenbach, B. 1996, IAU Circ., 6445

[Liller 1990] Liller, W. 1990, IAU Circ., 5091

[Long *et al.* 1996] Long, K. S., Charles, P. A., Blair, W. P., & Gordon, S. M. 1996, *Astrophysical Journal*, 466, 750

[Long *et al.* 1992] Long, K. S., Winkler, P. F., & Blair, W. P. 1992, *Astrophysical Journal*, 395, 632

[Mahadevan 1997] Mahadevan, R. 1997, *Astrophysical Journal*, 477, 585

[Makino *et al.* 1987a] Makino, F. E. *et al.* 1987a, IAU Circ., 4447

[Makino *et al.* 1987b] Makino, F. E. *et al.* 1987b, IAU Circ., 4466

[1] Manchester, R., Gaensler, B., Wheaton, V., Stavely-Smith, L., Tziousmis, A., Kesteven, M., Reynolds, J., & Bizunok, N. 2001, to appear in *Publications of the Astronomical Society of the Pacific*

[Mediavilla *et al.* 1997] Mediavilla, E., Arribas, S., García-Lorenzo, B., & del Brugo, C. 1997, *Astrophysical Journal*, 488, 682

[Melia 1992] Melia. F. 1992, *Astrophysical Journal*, 398, L95

[Minkowski 1941] Minkowski, R. 1941, *Publications of the Astronomical Society of the Pacific*, 53, 246

[Montes *et al.* 1998] Montes, M. J., van Dyk, S. D., Weiler, K. W., Sramek, R. A., & Panagia, N. 1998, *Astrophysical Journal*, 506, 874

[Montes *et al.* 1997] Montes, M. J., Weiler, K. W., & Panagia, N. 1997, *Astrophysical Journal*, 488, 792

[Montes *et al.* 2000] Montes, M. J., Weiler, K. W., van Dyk, S. D., Panagia, N., Lacey, C. K., Sramek, R. A., & Park, R. 2000, *Astrophysical Journal*, 532, 1124

[Nandra *et al.* 1997] Nandra, K., George, I. M., Mushotzky, R. F., Turner, T. J., & Yaqoob, T. 1997, *Astrophysical Journal*, 477, 602

[Narayan & Yi 1995a] Narayan, R. & Yi, I. 1995, *Astrophysical Journal*, 444, 231

[Nomoto *et al.* 1994] Nomoto, K., Yamaoka, H, Pols, O. R., van der Heuvel, E., Iwamoto, K., Kumagai, S., & Shigeyama, T. 1993 *Nature*, 371, 227

[Nota *et al.* 1995] Nota, A., Livio, M., Clampin, M., & Schulte-Ladbeck, R. 1995, *Astrophysical Journal*, 448, 788

[Palumbo 1988] Palumbo, G. G. C., *et al.* 1988, *Accurate Positions of Zwicky Galaxies*. October 1988 Special Version.

[Panagia *et al.* 1986] Panagia, N., Sramek, R. A., & Weiler, K. W. 1986, *Astrophysical Journal*, 300, L55

[Pearly *et al.* 2001] Perley, R., Butler, B.J., & Zijlstra, A. 2001, in preparation

[Pietsch *et al.* 1994] Pietsch, W., Volger, A., Jain, A., & Klein, U. 1994, *Astronomy & Astrophysics*, 284, 386

[Podsiadlowski *et al.* 1993] Podsiadlowski, Ph., Hsu, J., Joss, P., & Ross, R. 1993 *Nature*, 364, 509

[Pooley *et al.* 2001] Pooley, D. *et al.* 2001, astro-ph/0103196

[Retallack 1983] Retallack, D. S. 1983, *Monthly Notices of the Royal Astronomical Society*, 204, 669

[Ray *et al.* 2001] Ray, A., Petre, R., & Schlegel, E. M. 2001, astro-ph/0104447

[Rosa & Richter 1988] Rosa, M., & Richter, O.-G. 1988, *Astronomy & Astrophysics*, 192, 57

[Rubin *et al.* 1965] Rubin, V. C., Burbidge, E. M., Burbidge, G. R., & Crampin, D. J. 1965, *Astrophysical Journal*, 141, 759

[Rupen *et al.* 1987] Rupen, M. P., van Gorkom, J. H., Knapp, G. R., & Gunn, J. E. 1987, *Astronomical Journal*, 94, 61

[Scharf *et al.* 1997] Scharf, C. A., Jones, J. R., Ebeling, H., Perlman, E., Malkan, M., & Wegner, G. 1997, *Astrophysical Journal*, 477, 79

[Ryder *et al.* 1993] Ryder, S., Staveley-Smith, L., Dopita, M., Petre, R., Colbert, E., Malin, D., & Schlegel, E. 1993, *Astrophysical Journal*, 416, 167

[Saha *et al.* 1995] Saha, A., Sandage, A., Labhardt, L., Schwengler, H., Tammann, G. A., Panagia, N., & Macchetto, F. D. 1995, *Astrophysical Journal*, 438, 8

[Serlemitsos *et al.* 1996] Serlemitsos, P., Ptak, A., & Yaqoob, T. 1996, ASP Conf. 103, 70

[Schlegel 1990] Schlegel, E. M. 1990, *Monthly Notices of the Royal Astronomical Society*, 244, 269

[Schlegel 1995] Schlegel, E. M. 1995, *Reports on Progess in Physics*, 58, 1375

[Schlegel 2001] Schlegel, E. M. 2001, in preparation

[Schlegel *et al.* 1996] Schlegel, E. M., Petre, R., & Colbert, E. 1996, *Astrophysical Journal*, 456, 187

[Schlegel *et al.* 2000] Schlegel, E. M., Petre, R., Colbert, E. J. M., & Miller, S. 2000, *Astronomical Journal*, 120, 2373

[Schlegel *et al.* 1999] Schlegel, E. M., Ryder, S., Staveley-Smith, L., Petre, R., Colbert, E., Dopita, M., & Campbell-Wilson, D. 1999, *Astronomical Journal*, 118, 2689

[Schlegel 1999] Schlegel, E. M. 1999, *Astrophysical Journal*, 527 L85

[Schlegel *et al.* 2001] Schlegel, E. M. 2001, *Young Supernova Remnants: Eleventh Astrophysics Conf.*, ed. S. S. Holt & U. Hwang (Melville, N. Y.: AIP Press), 69

[Schwarz & Pringle 1996] Schwarz, D. H., & Pringle, J. E. 1996, *Monthly Notices of the Royal Astronomical Society*, 282, 1018

[Silbermann *et al.* 1996] Silbermann, N. A. *et al.* 1996, *Astrophysical Journal*, 470, 1

[Sjouwerman & Dickel 2001] Sjouwerman, L. O., & Dickel, J. R. 2001, *Young Supernova Remnants: Eleventh Astrophysics Conf.*, ed. S. S. Holt & U. Hwang (Melville, N. Y.: AIP Press), 433

[Skinner *et al.* 1998] Skinner, C. J., Becker, R. H., White, R. L., Exter, K. M., Barlow, M. J., & Davis, R. J. 1998, *Monthly Notices of the Royal Astronomical Society*, 296, 669

[Smith 1998] Smith, B. J. 1998, *Astrophysical Journal*, 500, 181

[Sutherland 1990] Sutherland, P. 1990, *Supernovae*, ed. S. E. Woosely (New York: Springer-Verlag), 112

[Sramek *et al.* 1984] Sramek, R. A., Panagia, N., & Weiler, K. W. 1984, *Astrophysical Journal* 285, L59

[Stark *et al.* 1992] Stark, A. A., Gammie, C. F., Wilson, R. W., Bally, J., Linke, R. A., Heiles, C., & Hurwitz, M. 1992, *Astrophysical Journal Supplement*, 79, 77

[Stockdale *et al.* 2001a] Stockdale, C. J., Rupen, M. P., Cowan, J. J., Chu, Y.-H., & Jones, S. S. 2001, *Astronomical Journal*, in press

[Stockdale *et al.* 2001b] Stockdale, C. J., Goss, W. M., Cowan, J. J., & Sramek, R. A. 2001, *Astrophysical Journal*, in press

[Takase & Miyauchi-Isobe 1984] Takase, B., & Miyauchi-Isobe, N. 194 *Annals of the Tokyo Ast. Obs.*, 19, 595

[Tosaki & Shioya 1997] Tosaki, T. & Shioya, Y. 1997, *Astrophysical Journal*, 484, 664

[Trimble 2001] Trimble, V. 2001, *Young Supernova Remnants: Eleventh Astrophysics Conf.*, ed. S. S. Holt & U. Hwang (Melville, N. Y.: AIP Press), 3

[Trotter *et al.* 1998] Trotter, A. S., Greenhill, L., J., Moran, J. M., Reid, M. J., Irwin, J. A. & Lo, K. 1998, *Astrophysical Journal*, 495, 740

[Tully 1980] Tully, R. B. 1980, *Astrophysical Journal*, 237, 390

[Tully 1988] Tully, R. B. 1988, *Nearby Galaxies Catalog*, (Cambridge: Cambridge Univ. Press)

[Turner & Ho 1994] Turner, J. L., & Ho, P. T. P. 1994, *Astrophysical Journal*, 421, 122

[Van Den Bergh 1995] Van Den Bergh, S. 1995, *Astronomical Journal*, 110, 613

[van Dyk *et al.* 1993a] van Dyk, S. D., Sramek, R. A., Weiler, K. W., & Panagia, N. 1993, *Astrophysical Journal*, 409, 162

[van Dyk *et al.* 1993b] van Dyk, S. D., Sramek, R. A., Weiler, K. W., & Panagia, N. 1993, *Astrophysical Journal*, 419, L69

[van Dyk *et al.* 1994] van Dyk, S. D., Weiler, K. W., Sramek, R. A., Rupen, M., & Panagia, N. 1994, *Astrophysical Journal*, 432, L115

[van Gorkom *et al.* 1986] van Gorkom, J. H., Rupen, M. P., Knapp, G. R., Gunn, J. E., Neugebauer, G., & Matthews, K. 1986, IAU Circ. No. 4248

[van Steenberg & Shull 1988] van Steenberg, M. E. & Shull, J. M. 1988, *A Decade of UV Astronomy with the IUE Satellite*, Vol. 2 (Noordwijk, The Netherlands: ESTEC), 219

[Vila *et al.* 1990] Vila, M. B., Pedlar, A., Davies, R. D., Hummel, E., & Axon, D. J. 1990, *Monthly Notices of the Royal Astronomical Society*, 242, 379

[Weiler *et al.* 2001] Weiler, K. W., Panagia, N., Montes, M. J., van Dyk, S. D., Sramek, R. A., & Lacey, C. K. 2001, *Young Supernova Remnants: Eleventh Astrophysics Conf.*, ed. S. S. Holt & U. Hwang (Melville, N. Y.: AIP Press), 237

[Weiler *et al.* 1990] Weiler, K. W., Panagia, N., & Sramek, R. A. 1990, *Astrophysical Journal*, 364, 611

[Weiler & Sramek 1988] Weiler, K. W., & Sramek, R. A. 1988, *Annual Review of Astronomy and Astrophysics*, 26, 295

[Weiler *et al.* 1986] Weiler, K. W., Sramek, R. A., Panagia, N., van der Hulst, J. M., & Salvati, M. 1986, *Astrophysical Journal*, 301, 790

[Weiler *et al.* 1992] Weiler, K. W., van Dyk, S. D., Panagia, N., & Sramek, R. A. 1992, *Astrophysical Journal*, 398, 248

[Weiler *et al.* 1991] Weiler, K. W., van Dyk, S. D., Panagia, N., Sramek, R. A., & Discenna, J. L. 1991, *Astrophysical Journal*, 380, 161

[Woods & Andrew 1974] Woods, R., & Andrew, P. J. 1974, *Monthly Notices of the Royal Astronomical Society*, 167, 13

[Ye *et al.* 1991] Ye, T., Turtle, A. J., & Kennicutt, R. C., Jr. 1991, *Monthly Notices of the Royal Astronomical Society*, 249, 722

[Young & Scoville 1982] Young, J. S., & Scoville, N. 1982, *Astrophysical Journal*, 260, L41

[Zimmerman 1993a] Zimmerman, H. U. *et al.* 1993a, IAU Circ., 5748

[Zimmerman 1993b] Zimmerman, H. U. *et al.* 1993b, IAU Circ., 5750

[Zimmerman 1993c] Zimmerman, H. U. *et al.* 1993c, IAU Circ., 5766

[Zimmerman 1993d] Zimmerman, H. U. *et al.* 1993d, IAU Circ., 5899

[Zimmerman 1994] Zimmerman, H. U., ed. 1994, EXSAS User's Guide (Garching: MPE)

Appendix A

Radio Astronomy With the VLA

A.1 What is the Very Large Array?

This appendix contains a description of the VLA (theoretical and instrumentational) and a general description of the steps involved in reducing continuum radio data with the VLA.

The Very Large Array is an aperture synthesis radio telescope with a resolving power similar to most ground-based optical telescopes. The VLA is able to observe the entire northern sky and has a limited capability to observed some southern objects (Dec. $> -30°$). For sources below this declination, observations have limited resolution. The VLA consists of 27 individual antennae (diameter = 25 m) in a large "Y" pattern (9 antennae per arm). They are linked together electronically and, in the VLA largest configuration, have a resolving power equivalent to a a telescope with a diameter of 36 km and sensitivity of an antennae with a diameter of 130 m.

The principles by which the 27 single antennae of the VLA are able to act as one large receiver are interferometry and aperture synthesis. A pair of antennae with cross-correlated signals observing the same source is called an interferometer. The resulting signal is equivalent to the interference pattern of a two-slit optical interferometer. With the 27 antennae of the VLA, there are 351 pairs of interferometers with different baselines (distances between antennae). The cross-correlation of the signals from each baseline pair provides information about the intensities of each source in the beams of the antennae and their positions in the sky relative to the pointing of the baseline pairs. In order to make sense of this information, it becomes essential to accurately measure the time delays and location of each antenna (Hjellming 1992). The distribution of radio emission in an antenna beam can be considered as the superposition of many components of varying size, position, and orientation. One can describe the relation between intensity distributions and individual components in terms of a Fourier integral relationship, where each baseline pair measures a single Fourier component of the apparent angular distribution of sources in the antenna beam. Many such components are needed to reconstruct an spatially-accurate image of the sources. These are "provided" by the Earth's rotation, as the geometric configuration between the antennae on the Earth and the source in the sky are constantly changing, *i.e.* aperture synthesis (Hjellming 1992).

The VLA has four main configurations: A (baselines: max.$\sim$36.4 km; min. $\sim$0.68 km), B (baselines: max. $\sim$11.4 km; min. $\sim$0.21 km), C (baselines: max. $\sim$3.4 km; min. $\sim$0.035), and D (baseline: max. $\sim$1.03 km; min. $\sim$0.035 km). The antennae are moved by a large loader on railroad tracks to specific concrete pads for each configuration. Each configuration is specifically designed to provide optimal resolution at different wavelengths, (beginning with the A config.) 20 cm, 6 cm, 2 cm, and 1.3 cm. Each array configurtion provides comparable resolution with its primary observing wavelength due to the relationship between the observed wavelength and the distances between each baseline pair of antennae. Because radio emission from intermediate-age SNe is brightest at longer wavelengths (*i.e.* 6 and 20 cm), the SNe discussed in this dissertation were observed in the A and B configurations to optimize spatial resolution and sensitivity.

Because the geometry of each array is very well known, it is possible to determine the precise time delay ($\sim$0.5 pico-seconds for 1.5 cm) between signals received at each antenna in a baseline pair as a function of the pointing direction for the array. This delay be can be as large as 125 μs for the longest baselines in the A configuration (Hjellming 1992). Figure A.1 illustrates the basic concept of the delay time as function of the geometry between a baseline pair of antennae.

Because the required timing accuracy of 0.5 ps is too difficult to achieve, the raw radio frequency (RF) signals are mixed with a local oscillator signal and then converted into intermediate frequencies (IFs) which convey the phase and amplitude information from the raw signal. The signal from the "closer" antenna is then delayed by the appropriate time factor to insure proper phase coherence, and now the information from each baseline pair can be cross-correlated (multiplied and filtered). Because of the range in time delays for each baseline pair and the number of baselines in the VLA, it is extremely complicated (although by no means impossible) to convert the incoming signals into measurements of the amplitude and phase of the incoming wavefront. Hjellming (1992) provides a detailed discussion of the processes involved in converting the raw data into a more useful format. The VLA antennae also have two feeds of orthogonal polarizations for each frequency which are normally circular (right and left) but can also be converted to linear polarization with the insertion of linear polarizers. Most observations only use right-right (R-R) and left-left (L-L) polarizations, but it is useful to request cross polarization be applied to observations if interested in whether the emission is polarized and to what extent. The observations discussed in the dissertation do not include such measurements, as the sources were all very faint and do not produce sufficient emission for useful polarization studies. Typical VLA continuum observations are centered on two IFs separated by 100 MHz about the central

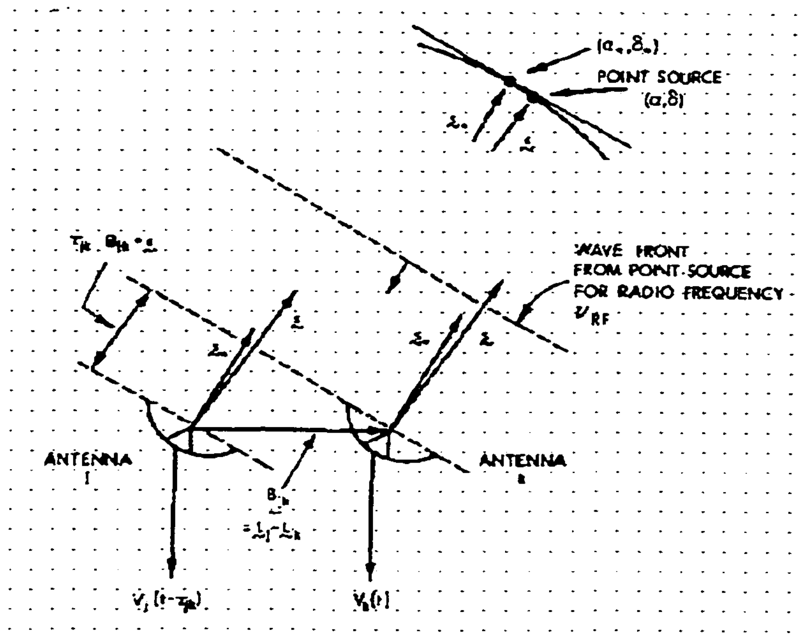

Figure A.1: Schematic of a basic two dish radio interferometer. Figure from Hjellming (1992).

wavelength with bandpasses of 50 MHz, with R-R and L-L polarizations for each IF.

A.2 Calibrating and Flagging VLA Data Sets

Prior to making observations with the VLA, it is necessary to select a primary flux calibrator and secondary phase calibrator to accurately determine the positions and flux densities of the observed sources. To ensure that these calibrations are accurate, it is important to accurately model the chosen calibrators. It is therefore useful to select sources which are unresolved, as the can be most simply modeled as point sources. In the event that the calibrator is resolved, it is necessary to self-calibrate. This possibility, along with the need to minimize the time spent observing the calibrators to get a high signal-to-noise, are the key reasons that calibrators should be fairly luminous radio sources (~1 Jy). The primary flux calibrator, usually either 3C48 or 3C286, is used to set the flux density scale for the observations. Both of these sources have been extensively studied and their emission at the observable VLA frequencies are well understood. It is typical to observe the primary flux calibrator at the beginning of a typical VLA "run" and, for longer observations, at the end of the observing run. The secondary phase calibrator is usually observed for 2 to 4 minutes at 20 to 30 minute intervals during the observing runs at 20 and 6 cm. Phase calibrators should be selected according to their suitability at the observed wavelength and array configuration. Phase calibrators should also be within ~1 degree of the primary source so that the phase solutions derived from them will accurately reflect the "viewing" for the source and that minimal time will be spent slewing the array between the source and the phase calibrator. Since the flux densities of these calibrators usually vary with time, it is necessary to bootstrap their flux densities using the primary flux calibrator. This is accomplished using the Astronomical Image Processing System

(AIPS) routines SETJY and GETJY. SETJY is used to set the flux density scale for the primary flux calibrator and GETJY "bootstraps" the flux density of the phase calibrator. SETJY is run before any other calibrations are made. Following this step, the AIPS routine VLACALIB is used to apply the initial gain calibration. VLACALIB should be run for each calibrator, with special care to set the NRAO recommended limits for maximum baseline lengths for each calibrator to ensure a point source model will accurately describe the modeled data. It may also be necessary to restrict the number of antennae per arm depending upon the individual calibrator, array configuration, and observed wavelength.

After initial gain calibrations, it is important to "flag" the data for each calibrator and source for anomalous amplitude variations, which can be caused by a number of things including cosmic rays, instrumentational glitches, weather, and radio frequency interference (RFI). Flagging by phase variations is generally not necessary for the calibrators and is not recommended for the source, since faint sources may have large phase discrepancies prior to calibration. Flagging can be with a variety of AIPS routines, the most commonly used is TVFLG. TVFLG writes the locations of bad data to a flag table (without actually deleting them) so that later when calibrating and imaging the sources, these data are not selected. TVFLG can be used to flag data in a variety of ways. It is important to note that each IF and each polarization should be carefully checked to ensure the integrity of the data set. This is usually the most time intensive part of the reduction process. Once the data has been flagged, then GETJY is run to set the flux density scale of the flux calibrator. VLACALIB should now be re-run if extensive flagging was made to the calibrators, keeping in the baseline length restrictions for each calibrator. Final calibrations are then applied using the AIPS routine CLCAL, which produce a CL table with calibration and model information. CLCAL is generally run on the primary flux calibrator with self-calibration. Then, it is run with the phase calibrator, applying the model from the flux calibrator to the gain solutions of the phase calibrator. Finally, the source data is calibrated with the model produced for the the phase calibrator. If all has gone well, it is now possible to produce an image of the source. It is useful at this point to use the AIPS routine SPLIT, to SPLIT the calibrated source data from the rest of the data set, as the smaller data set makes imaging faster. It is also essential to do this if the observations have been taken on separate observing runs, as was the case for most of the data in this dissertation. The source data needs to be SPILT off from the multi-source data set and then combined into one set using the AIPS routine DBCON.

A.3 Imaging VLA data

To actually produce an image, all of the Fourier components are transformed together using the Cooley-Tukey Fast Fourier Transform (FFT), which takes a mere fraction of the computing time required when using a direct Fourier transform (Hjellming 1992). This can be accomplished using the AIPS routine IMAGR. IMAGR can be used to image a field as well as applying calibrations for multi-source or self-calibrated single-source data sets. Also for wide-field imaging, IMAGR can accomplish data imaging in 512 simultaneous fields, which allows for three dimensional mapping, as each field is centered on a different tangent plane (such was case for the M83 observations discussed in Chapter 3).

IMAGR has number of user adjustable adverbs which must be carefully chosen to ensure an accurate image is produced with reasonable positions and flux densities, one the most important of which is CELLSIZE. This allows you set the the dimension of each pixel in terms of angular size. The recommended scheme which I have used is to set the cell size so that 3 to 4 pixels cover the beam. Making the cell size too large, may cause some data to be omitted (IMAGR will inform you when this is case). Making the cell size too small will change the beam size, even if no additional data samples are included. Linked to this, is the image size, determined by the adverb IMSIZE. IMSIZE allows you to set the size of your field by pixels, and should always be in powers of two. If the field is too large, as was the case for the 20 cm map of M83, it may be necessary to set a number of fields to image in order to allow for 3-D corrections. Running the task, SETFC, will provide you with recommended cell size, image size, and other pertinent information to accomplish this. You must also set the adverb DO3DIMAG to TRUE. This will require a lot of computing power and disk space and only need be done in rare instances where wide-field imaging is required.

The next most important details in producing a radio image are the weighting schemes. They are applied to the u-v data when they are being Fourier transformed into an accurate representation of the source. With most interferometers, including the VLA and VLBA, there a large number of short baseline pairs and fewer long baseline pairs. With Natural weighting, each baseline is weighted equally, producing a central beam with a core-halo source with a broad halo produced by the shorter baselines. There are also large sidelobes caused by the large gaps in the u-v coverage at longer baselines. This results better imaging of fine structure, as there are many more shorter baselines. Uniform weighting attempts to maximize spatial resolution by weighting each data cell equally, resulting in higher weighting for longer baselines and effectively filling in gaps in the u-v coverage. The "increased" coverage results in some-what ($\sim$1—2$\times$) higher noise levels and provides better imaging of large-scale structure. It has recently become possible to combine the two weighting schemes using the Brigg's robustness parameter which tempers the uniform weights. By varying the parameter from -5 (uniform weighting) to $+5$ (natural weighting) one can attempt to maximize the spatial resolution while minimizing the noise levels for the image. The ROBUST parameter is especially important for faint radio sources (*e.g.*, intermediate-age RSNe).

The last step for imaging radio observations is Cleaning. All AIPS Clean tasks implement a Clean deconvolution devised for array processors by Clark (1980). The IMAGR routines uses this Clean deconvolution with enhancements by Cotton and Schwab (Griesen 2001). The basic Clean routine applies the following steps (Clark 1980):

1. locate the maximum in the image;
2. generate a "Clean component", a δ-function at this location, and of an intensity which is some fraction of the maximum of the image (the "gain");
3. calculate the convolution of this component with the instrumental point source response (PSR) function;
4. subtract this instrumental PSR function from the map;
5. repeat steps 1-4 until the remaining map is satisfactorily small; and
6. generate and restore the clean components, convolved, not with an instrumental PSR function, but with an aesthetically pleasing function (usually a

Gaussian).

For VLA observations, this process is divided into minor and major cycles. Major cycles begin by constructing a histogram of map values and a plot of of the maximum sidelobe in the PSR outside a Clean cell. It is then possible to choose a beam patch size and a map limiting flux value (S_{lim}) such that the largest map point with a flux density less than the limiting value is the same fraction of the map peak as the largest beam value outside the the beam patch. And, both map points above the limiting value and the beam patch will fit the available main memory. A minor iteration cycle consists of Cleaning the brightest parts of the residual image with a "beam patch" of relative size. More precise Cleaning is achieved at the ends of major iteration cycles when the Fourier Transform of the Clean components is computed, subtracted from the visibility data, and a new residual dirty image computed. Major cycles can be run until the the maximum point in the map is smaller than S_{lim}. As this is far from an exact science, many more conservative approaches are discussed in Clark (1980). Over-Cleaning, which results in flux densities lower than they actually are, is caused by running too many major iterations, so it is important to be cautious in Cleaning. Once your image is sufficiently Cleaned, you are now ready to do real science!

Appendix B

Radio Images

This appendix is a compilation of images that were made but not included in the body of this dissertation. Some of these images were previous observations of sources discussed in Chapter 3 and whose flux densities can be found in Table 3.1; Cowan, Roberts, & Branch (1994); and CGS. The remainder of these images are of observations discussed in this dissertation with different weighting schemes, ranging from completely natural to completely uniform weighting. [For a detailed discussion of weighting schemes, see Appendix A.]

Figures B.1 — B.8 are images of SN 1961V and the nearby SNR at both epochs and wavelengths with the Brigg's robustness parameter set to 0 (weighted evenly between natural and uniform) and +1 (slightly natural). Figures 2.1 and 2.2 are similar images with the parameter set to -1 (slightly uniform). Figures B9 and B10 are uniformly weighted images of SN 1970G and the neighboring HII region at 20 cm and 3.5 cm from the CGS observations in 1990. Figures B.11 — B.14 are uniformly weighted images of M83 (with the historical SNe indicated by crosses) made from prior observations originally presented in Cowan *et al.* (1994a) and Cowan & Branch (1985). Figures B.15 and B.16 are uniformly and naturally weighted images, respectively, of the most recent 6 cm observations of M83, discussed in Chapter 4. Figure B.17 is a 20 cm image of the phase calibrator used for the recent M83 observations, J1313-333, with the Brigg's robustness parameter set to 0.

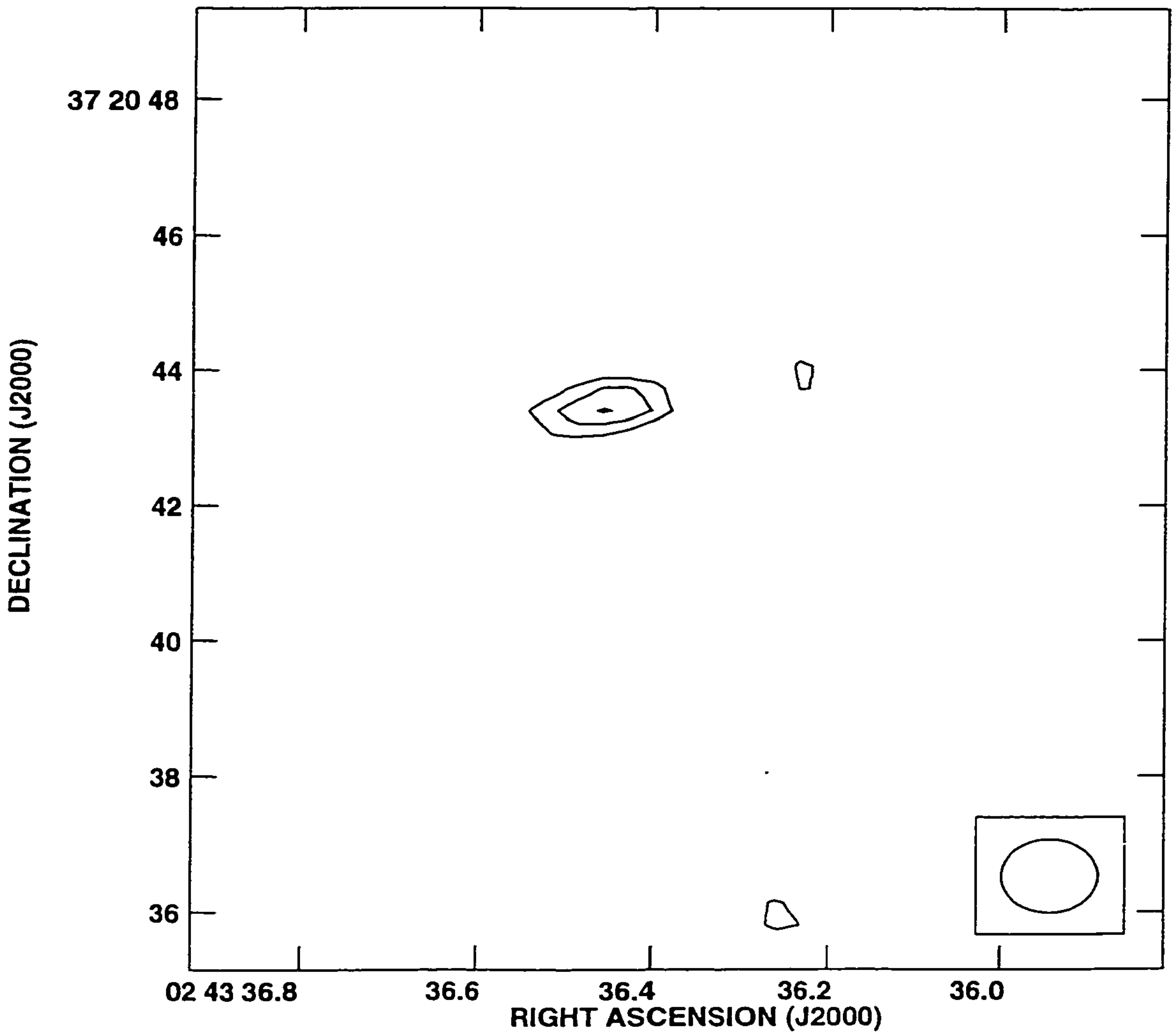

Figure B.1: Radio contour image of SN 1961V at 18 cm with the Brigg's robustness parameter set to 0 (Sept. 1999). Contour levels are -0.12, -0.09, 0.09, 0.12, 0.15, and 0.18. The beam size is shown in the lower right.

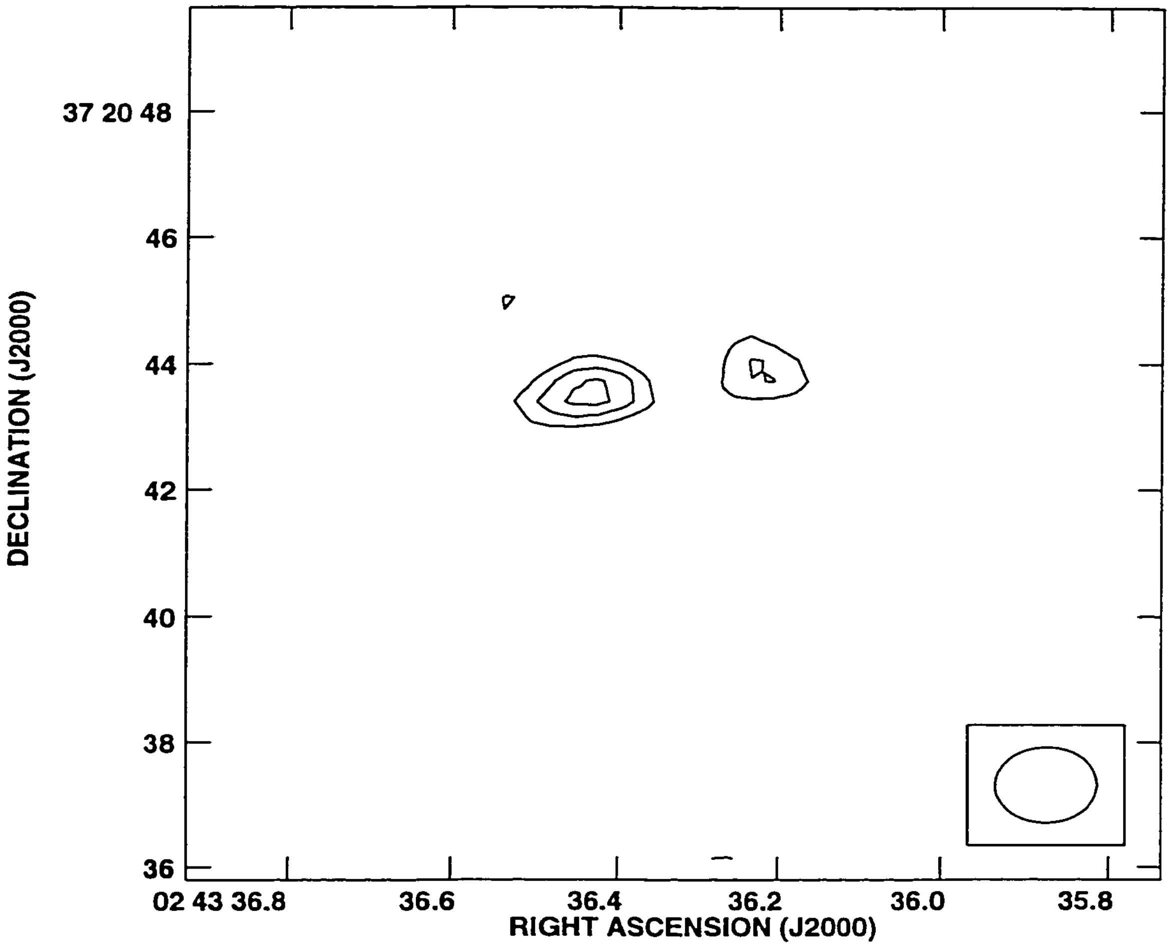

Figure B.2: Radio contour image of SN 1961V at 18 cm with the Brigg's robustness parameter set to +1 (Sept. 1999). Contour levels are -0.12, -0.09, 0.09, 0.12, 0.15, and 0.18. The beam size is shown in the lower right.

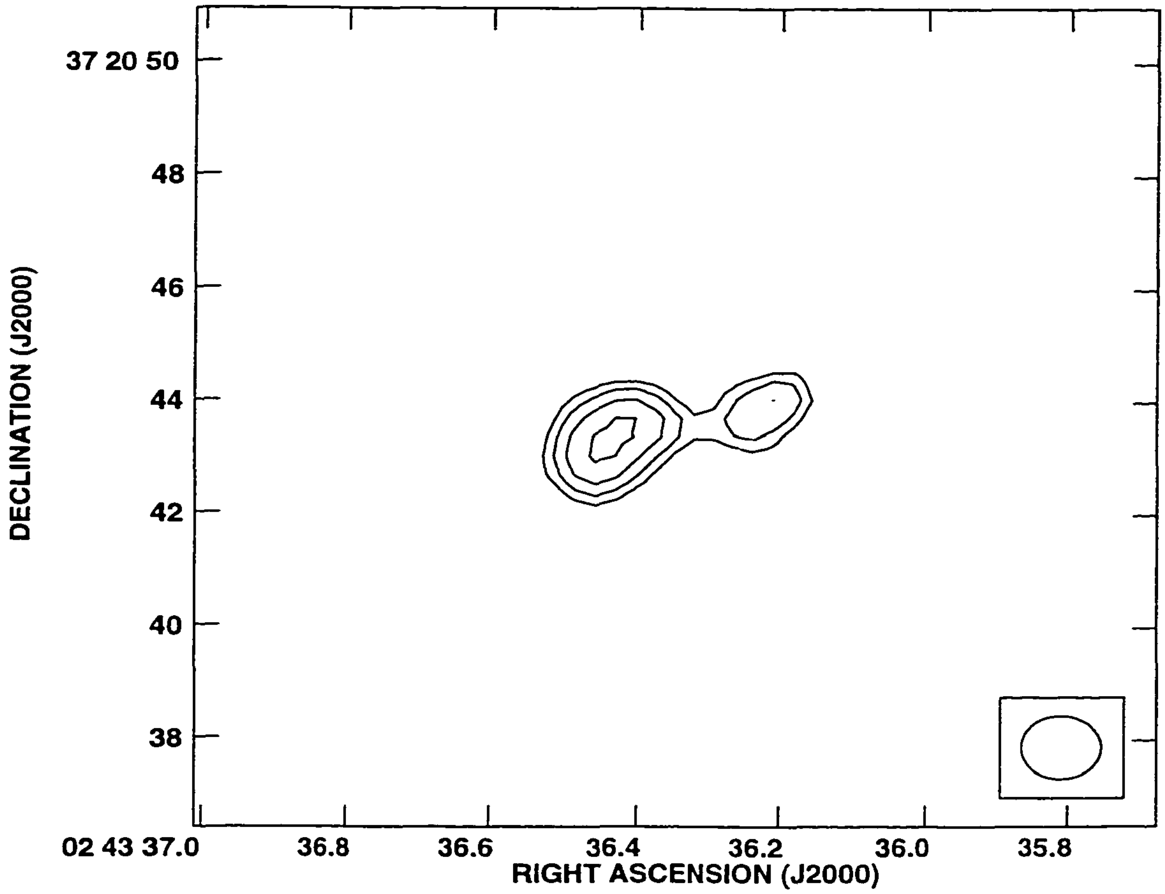

Figure B.3: Radio contour image of SN 1961V at 20 cm with the Brigg's robustness parameter set to 0 (Nov. 1984). Contour levels are -0.10, -0.07, 0.07, 0.10, 0.14, 0.20, 0.28, 0.40, 0.57, and 0.80. The beam size is shown in the lower right.

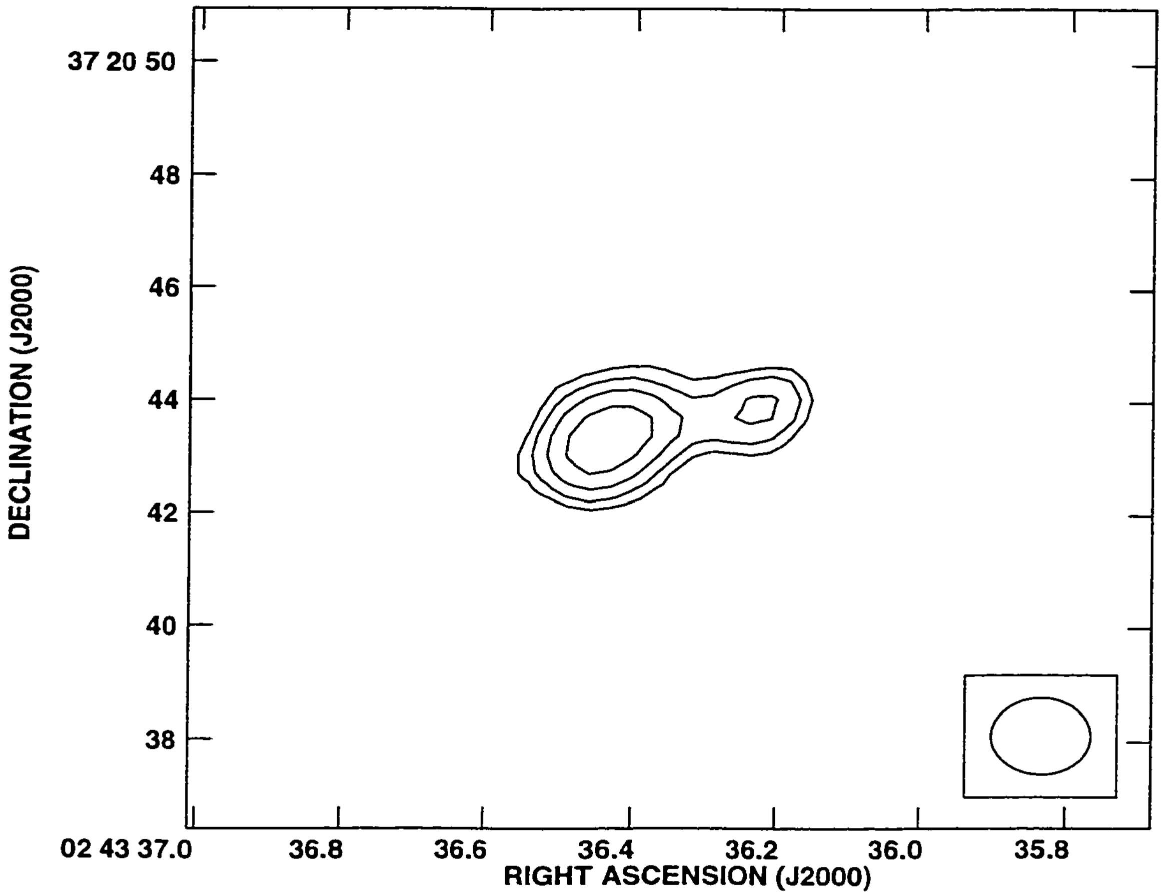

Figure B.4: Radio contour image of SN 1961V at 20 cm with the Brigg's robustness parameter set to +1 (Nov. 1984). Contour levels are -0.10, -0.07, 0.07, 0.10, 0.14, 0.20, 0.28, 0.40, 0.57, and 0.80. The beam size is shown in the lower right.

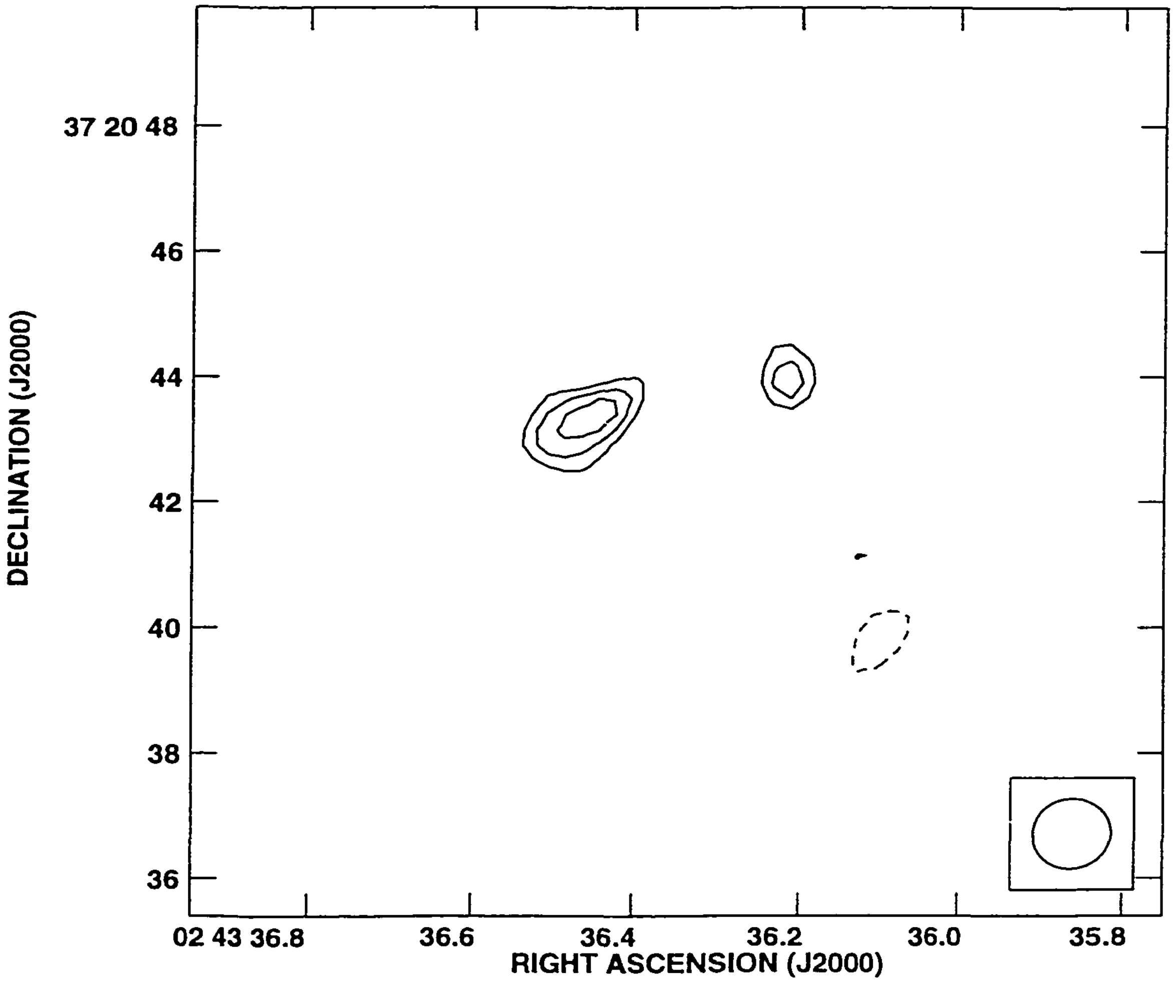

Figure B.5: Radio contour image of SN 1961V at 6 cm with the Brigg's robustness parameter set to 0 (Jan. 2000). Contour levels are -0.048, -0.036, 0.036, 0.048, 0.060, and 0.072. The beam size is shown in the lower right.

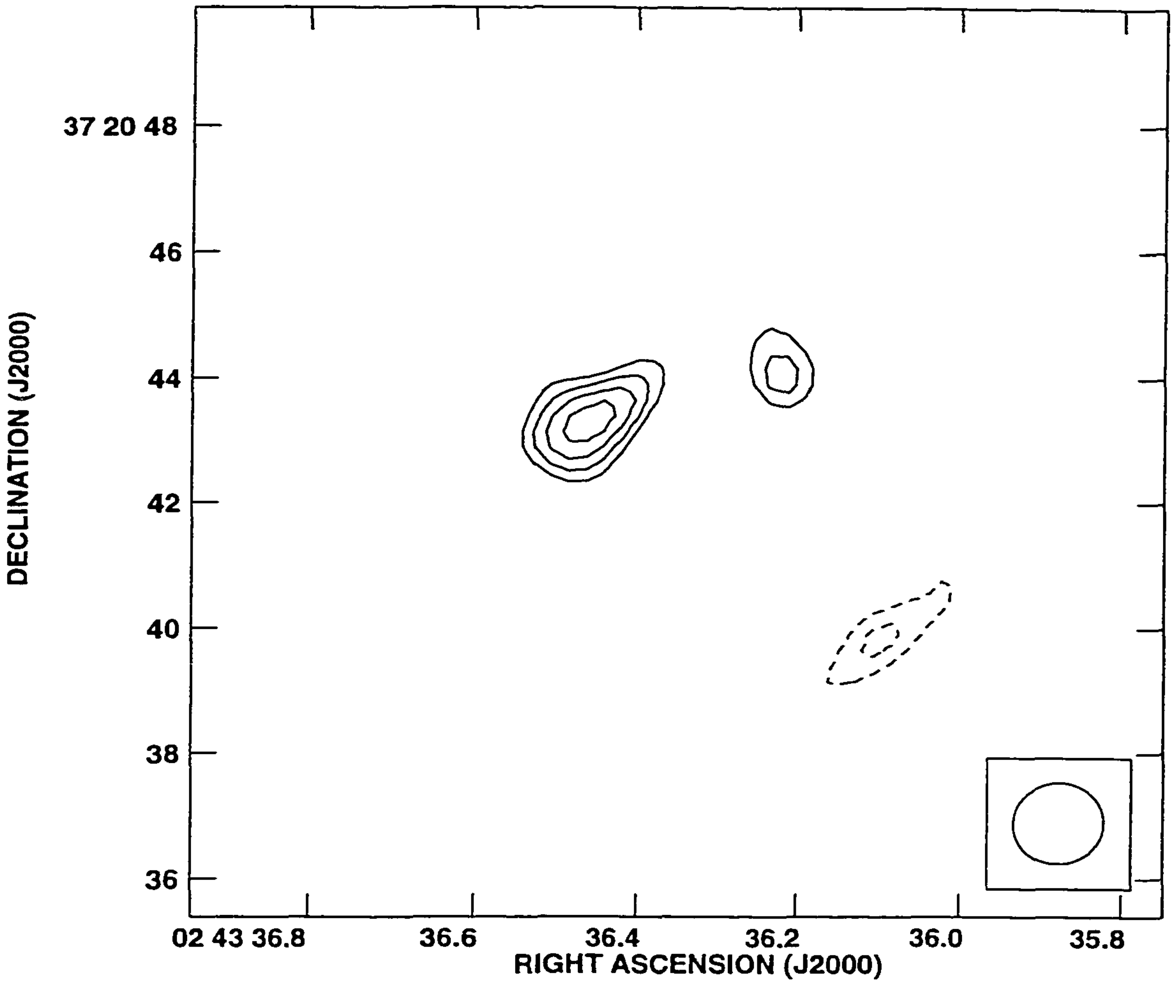

Figure B.6: Radio contour image of SN 1961V at 6 cm with the Brigg's robustness parameter set to +1 (Jan. 2000). Contour levels are -0.048, -0.036, 0.036, 0.048, 0.060, and 0.072. The beam size is shown in the lower right.

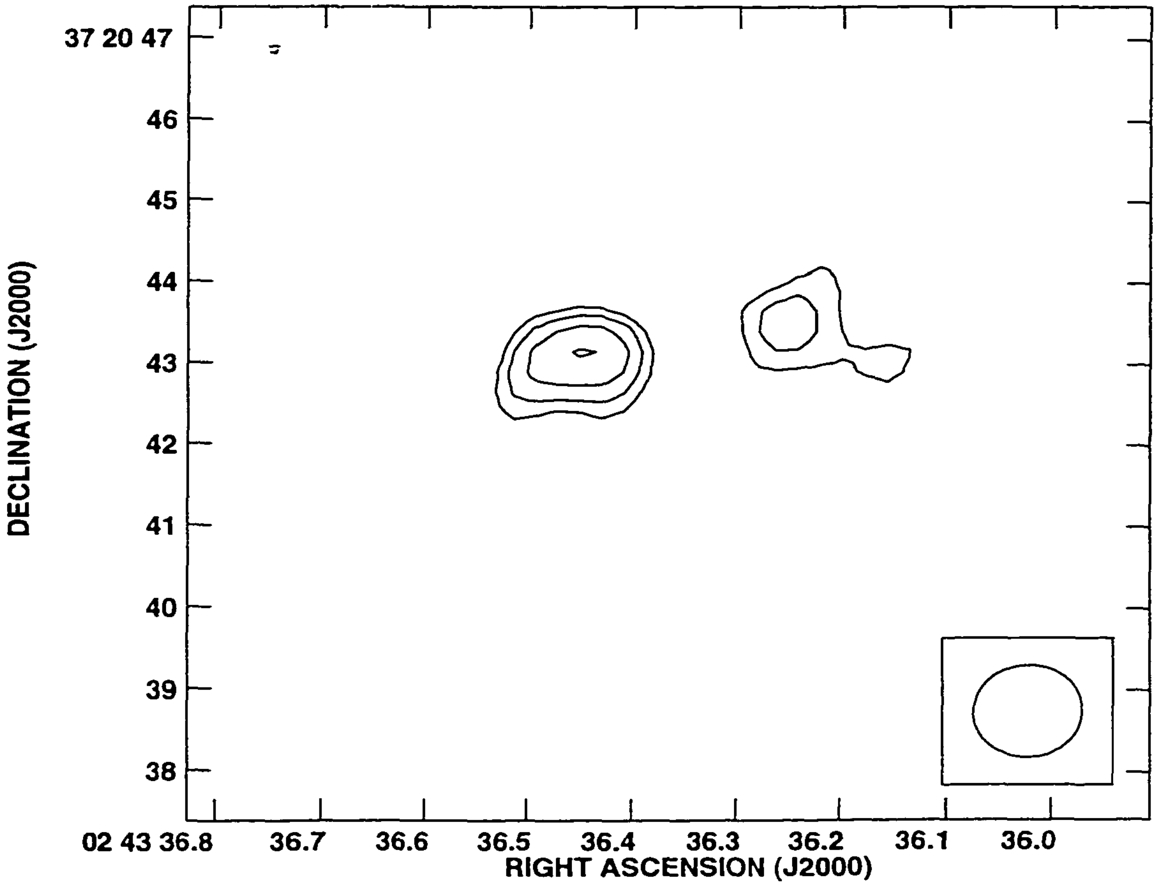

Figure B.7: Radio contour image of SN 1961V at 6 cm with the Brigg's robustness parameter set to 0 (Aug. 1986). Contour levels are -0.060, -0.042, 0.042, 0.060, 0.085, 0.12, 0.17 and 0.24. The beam size is shown in the lower right.

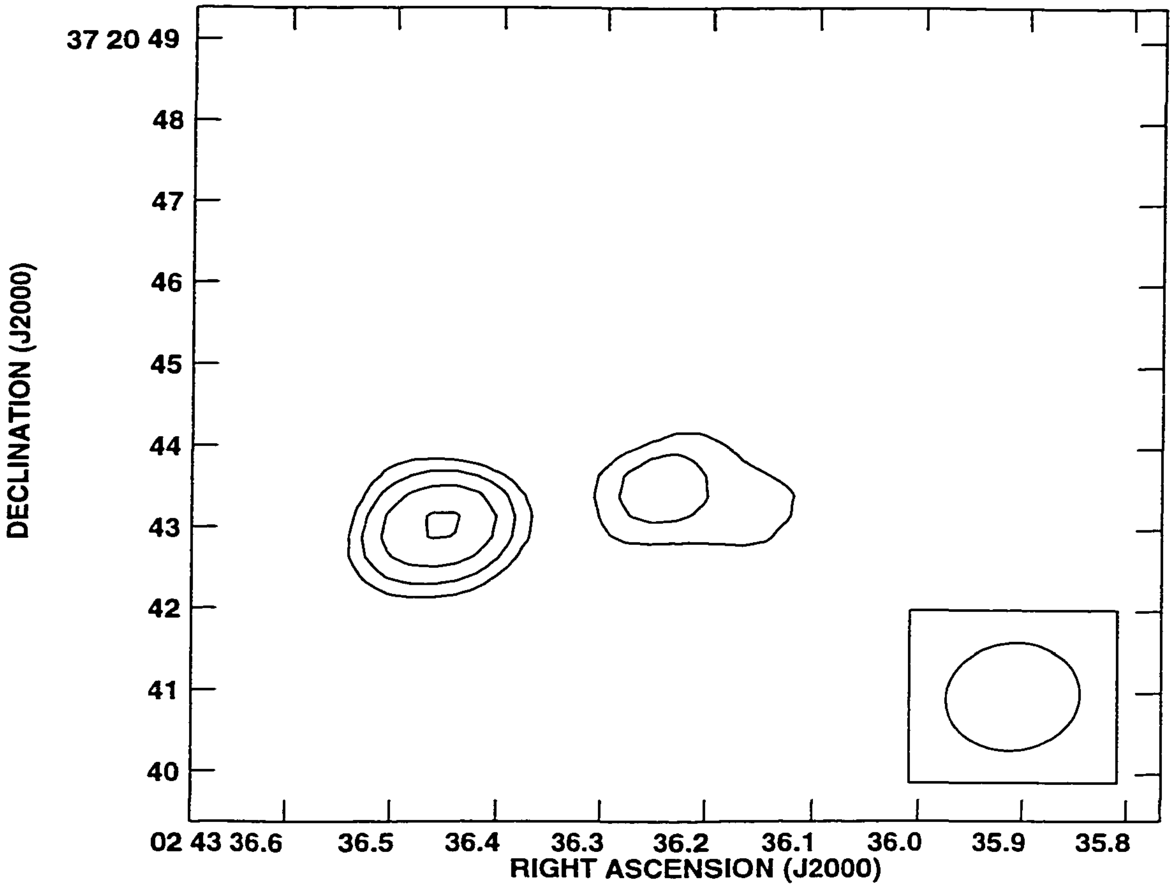

Figure B.8: Radio contour image of SN 1961V at 6 cm with the Brigg's robustness parameter set to +1 (Aug. 1986). Contour levels are -0.060, -0.042, 0.042, 0.060, 0.085, 0.12, 0.17 and 0.24. The beam size is shown in the lower right.

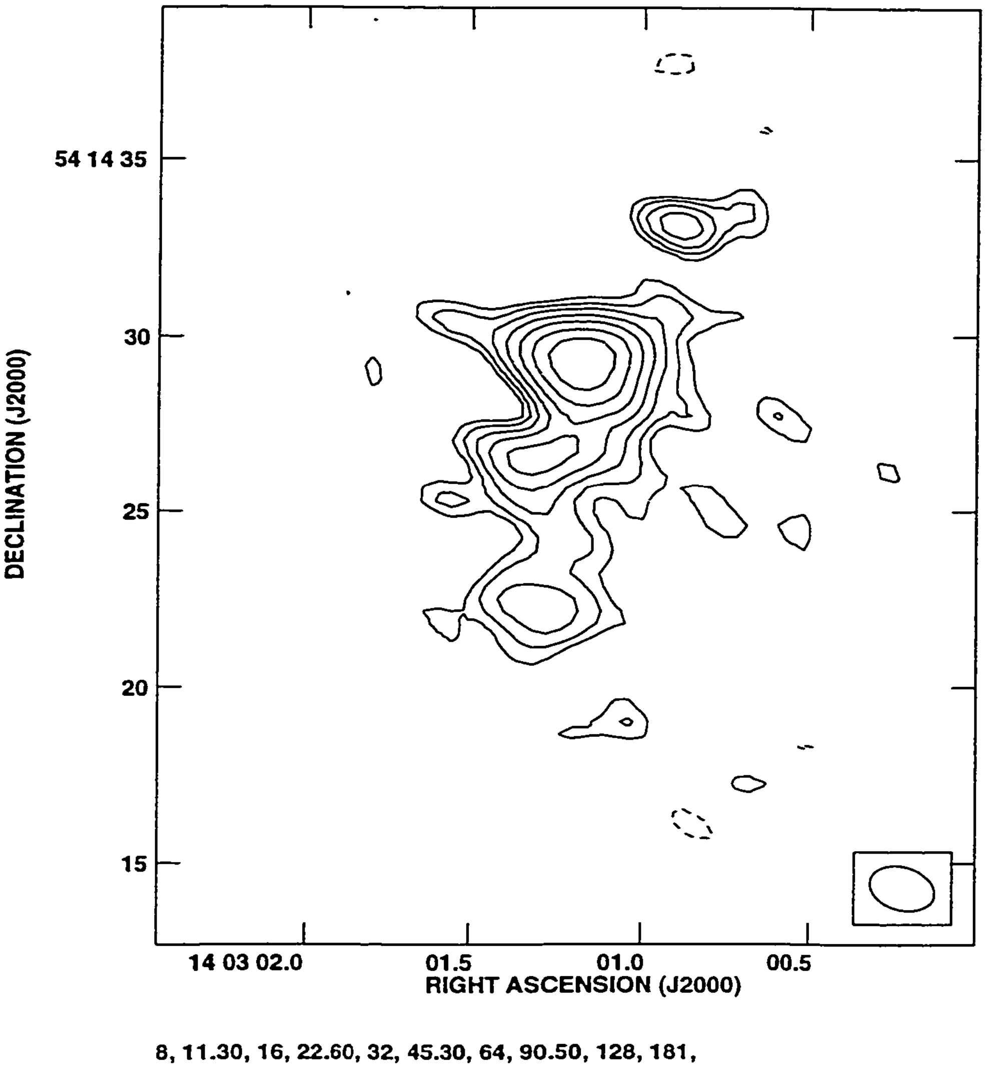

Figure B.9: Radio contour image at 20 cm of SN 1970G in Apr. 1990, with the Brigg's robustness parameter set to 0 (the source above and to the right of the central H II region, NGC 5455). Contour levels are -0.068, -0.048, 0.048, 0.068, 0.096, 0.14, 0.19, 0.27, 0.38, and 0.54. The beam size is shown in the lower right.

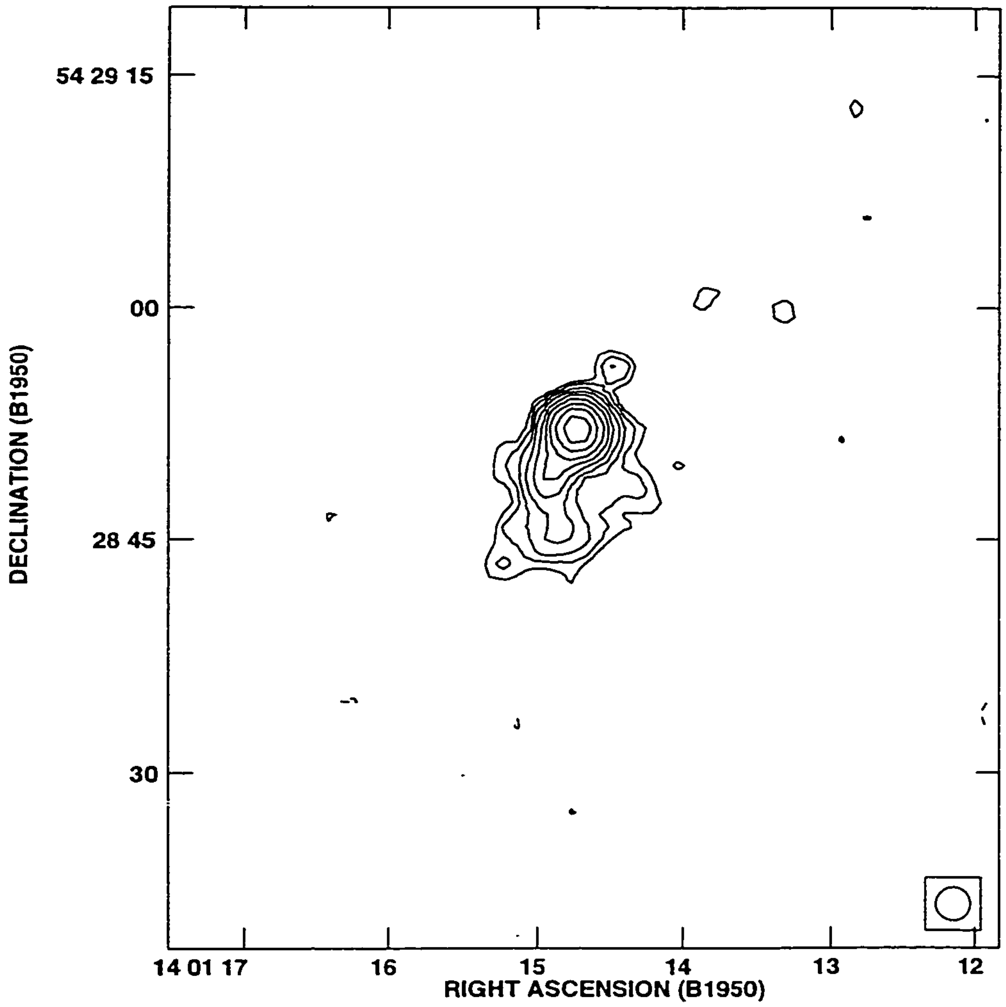

Figure B.10: Radio contour image at 3.5 cm (uniformly weighted) of SN 1970G in Nov. 1990 (the source above and to the right of the central H II region, NGC 5455). Contour levels are -0.052, -0.037, 0.037, 0.052, 0.074, 0.10, 0.15, 0.21, 0.29, 0.42, 0.59, and 0.83. The beam size is shown in the lower right.

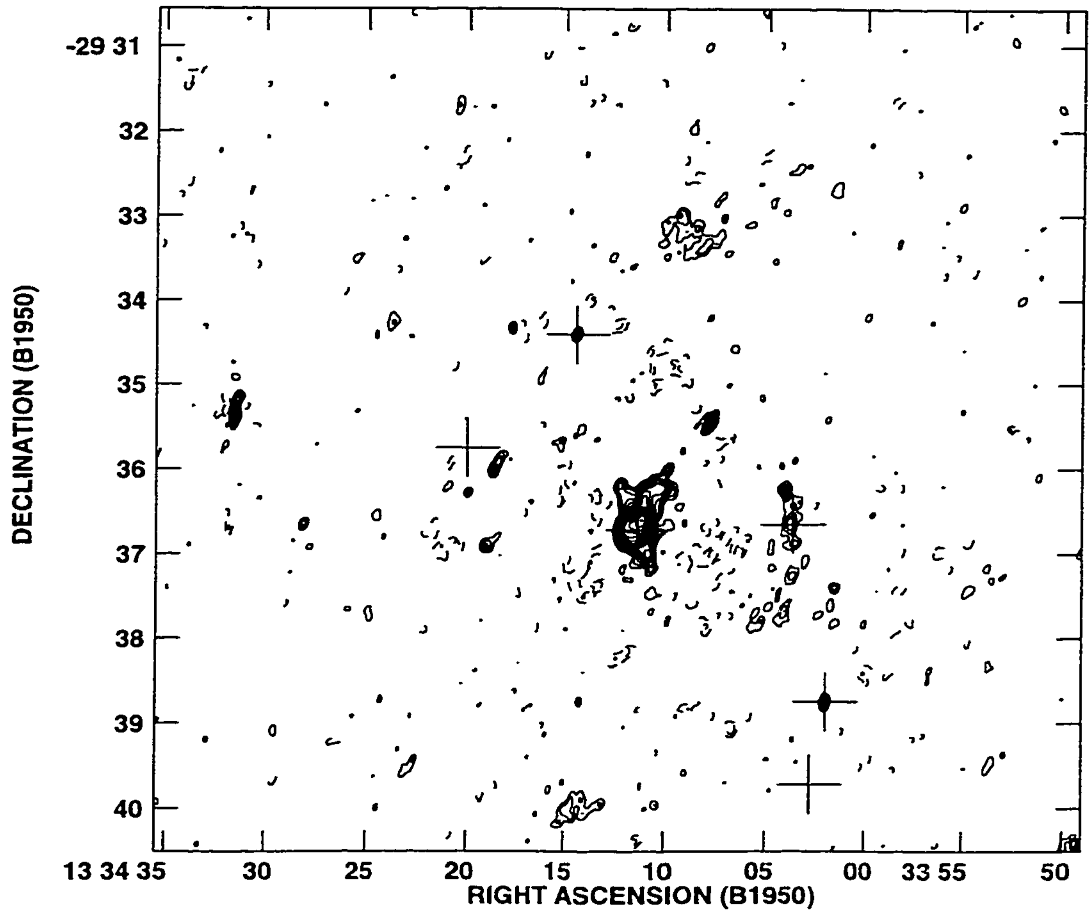

Figure B.11: Radio contour image at 20 cm of M83 made Dec. 1983, (uniformly weighted, with the historical SNe identified by crosses). Contour levels are -0.44, -0.31, 0.31, 0.44, 0.62, 0.88, 1.24, 1.8, 2.5, 3.5, 5.0, 7.0, 10, 14, 20, and 28 mJy beam^{-1}. The beam size is shown in the lower right.

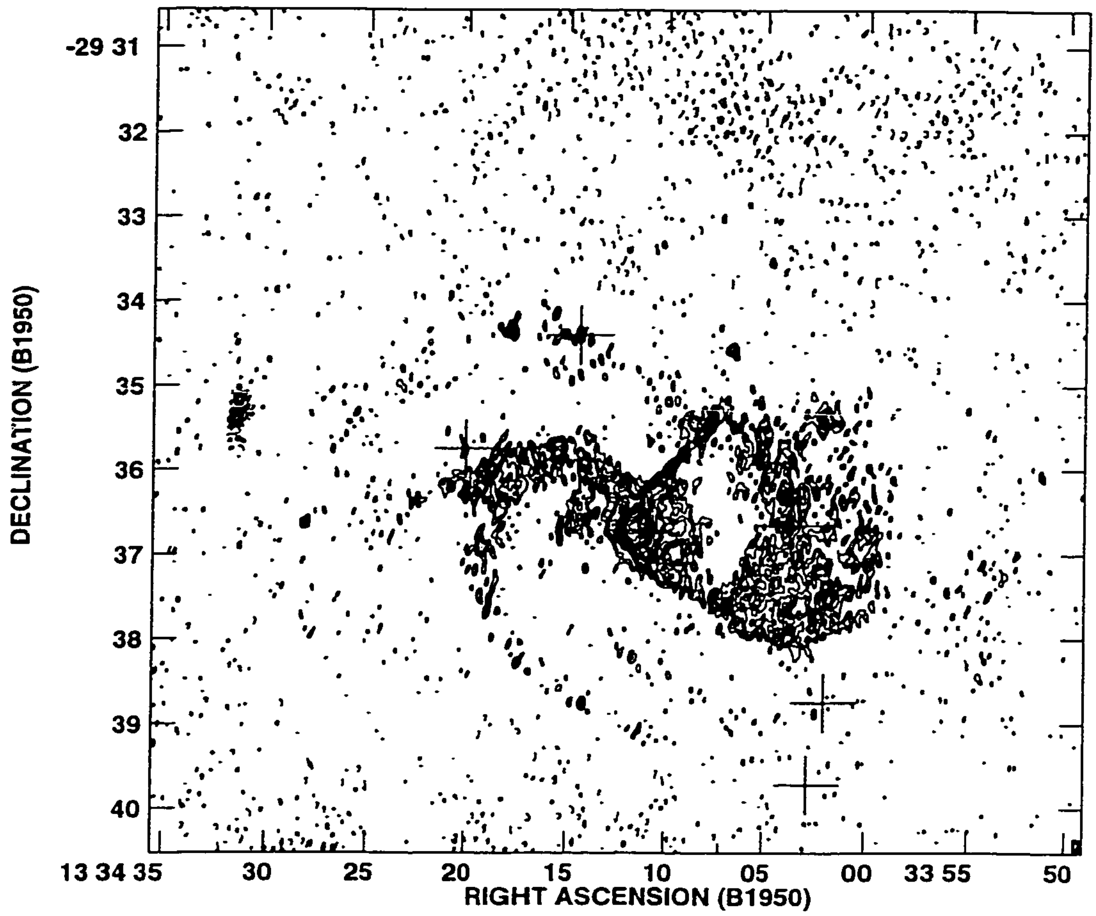

Figure B.12: Radio contour image at 20 cm of M83 made Dec. 1983, (uniformly weighted, with the historical SNe identified by crosses). Contour levels are -0.32, -0.22, 0.22, 0.32, 0.44, 0.63, 0.90, 1.3, 1.8, 2.5, 3.6, 5.1, 7.2, 10, 14, 20, and 29 mJy beam^{-1}. The beam size is shown in the lower right.

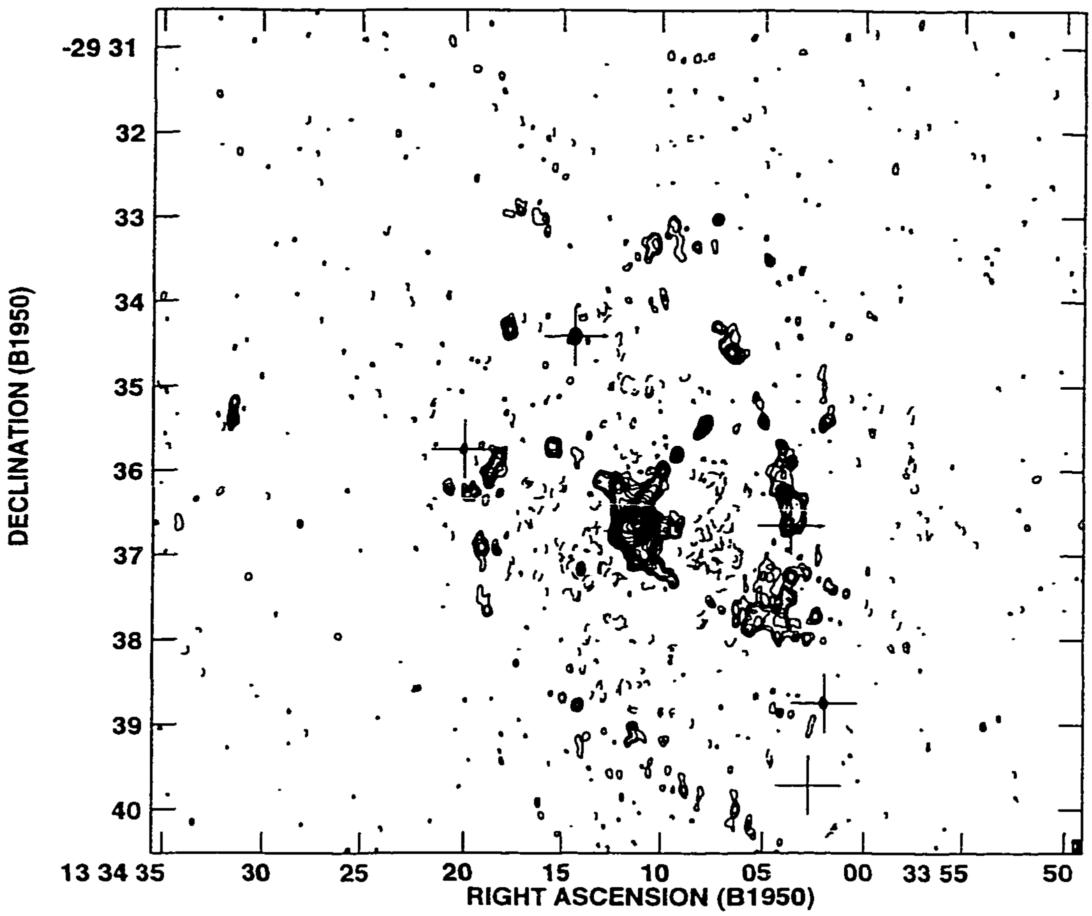

Figure B.13: Radio contour image at 6 cm of M83 made Mar. 1984, (uniformly weighted, with the historical SNe identified by crosses). Contour levels are -0.12, -0.085, 0.085, 0.12, 0.17, 0.24, 0.34, 0.48, 0.68, 0.96, 1.4, 1.9, 2.7, 3.8, 5.4, 7.7, 11, and 15 mJy beam^{-1}. The beam size is shown in the lower right.

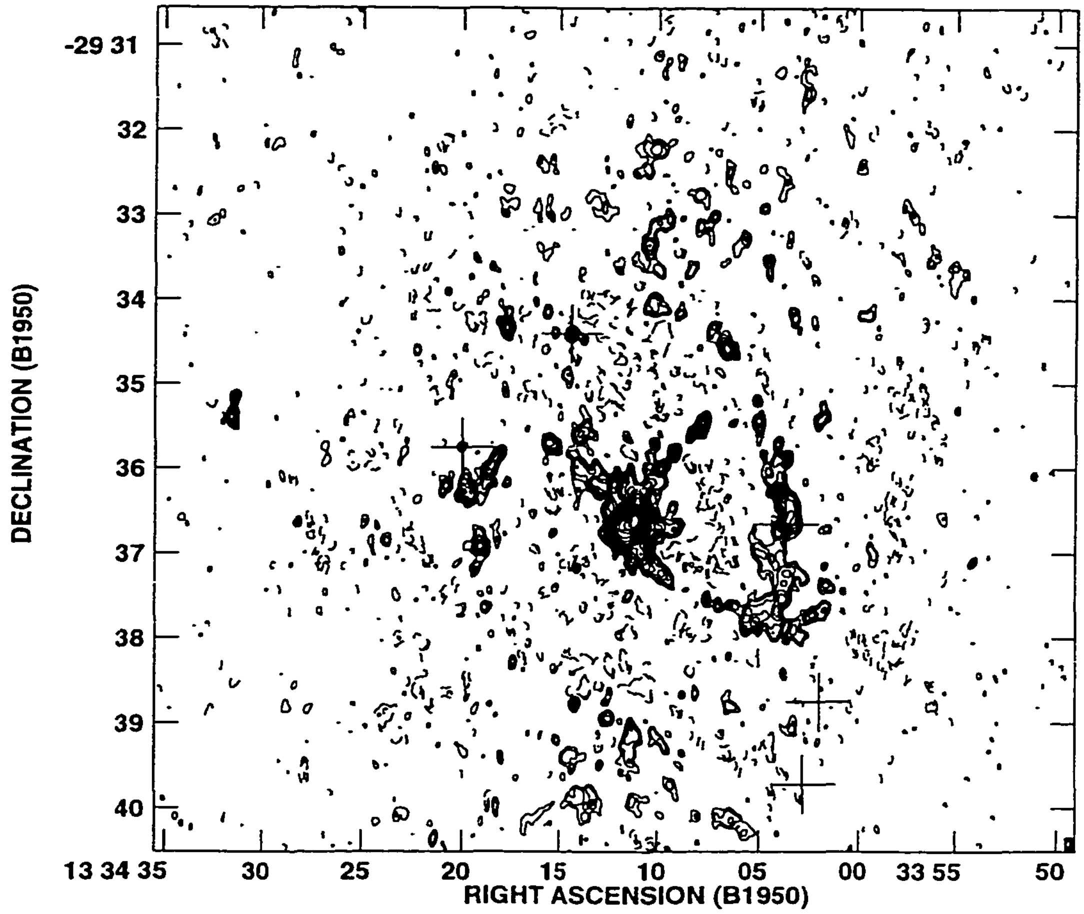

Figure B.14: Radio contour image at 20 cm of M83 made Oct. 1990, (uniformly weighted, with the historical SNe identified by crosses). Contour levels are -0.84, -0.059, 0.084, 0.12, 0.17, 0.24, 0.34, 0.48, 0.67, 0.95, 1.3, 1.9, 2.7, 3.8, 5.4, 7.6, 11, and 15 mJy beam^{-1}. The beam size is shown in the lower right.

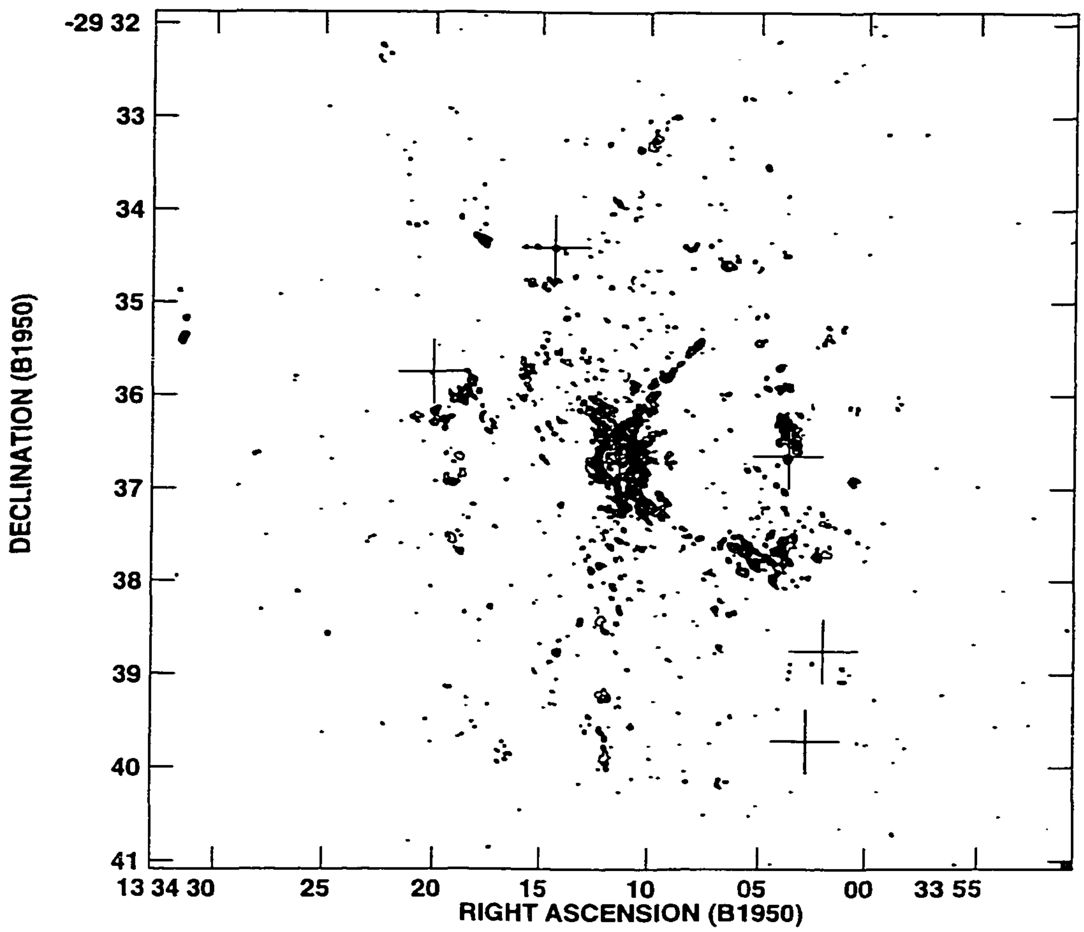

Figure B.15: Radio contour image at 6 cm of M83 made Nov. 1998, (uniformly weighted, with the historical SNe identified by crosses). Contour levels are -0.12, 0.12, 0.17, 0.24, 0.34, 0.48, 0.68, 0.96, 1.4, 1.9, 2.7, 3.8, 5.4, 7.7, and 11 mJy beam^{-1}. The beam size is shown in the lower right.

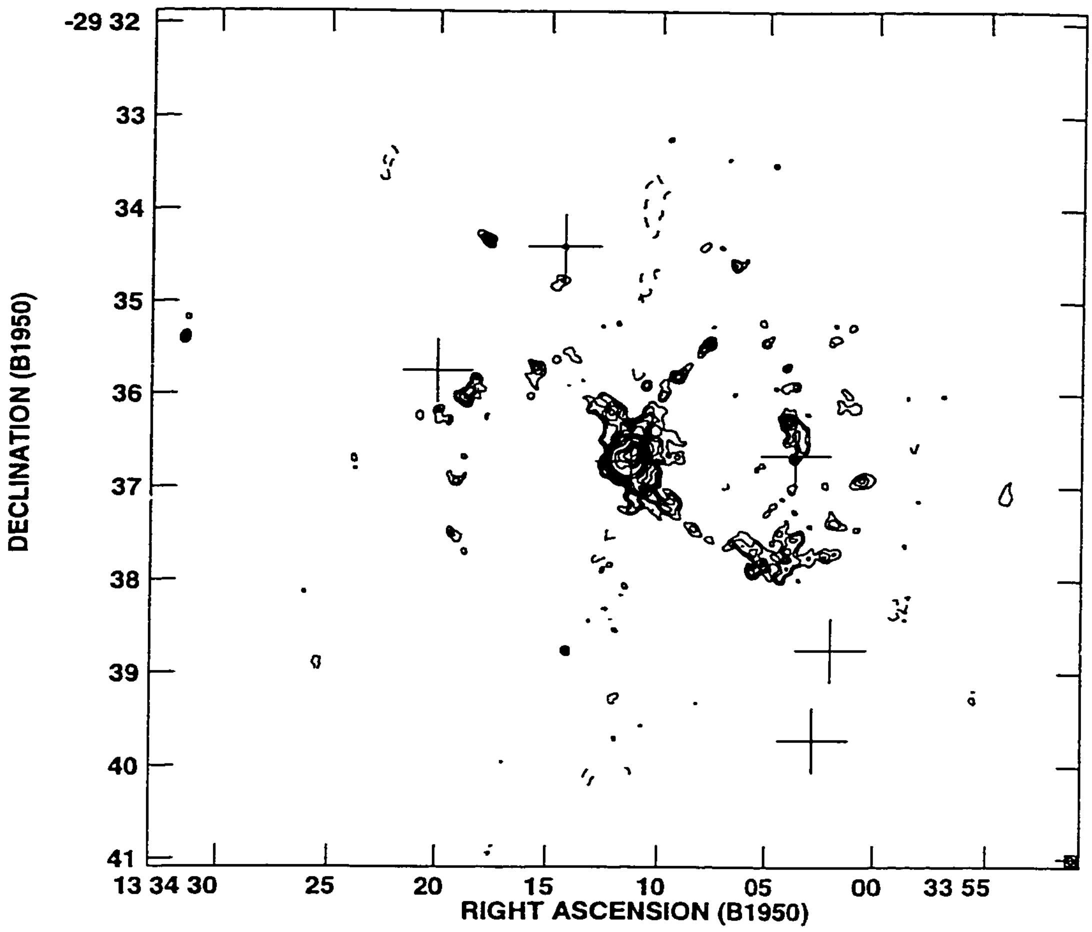

Figure B.16: Radio contour image at 6 cm of M83 made Nov. 1998, (naturely weighted, with the historical SNe identified by crosses). Contour levels are -0.24, 0.24, 0.34, 0.48, 0.68, 0.96, 1.4, 1.9, 2.7, 3.8, 5.4, 7.7, 11, 15, and 22 mJy beam^{-1}. The beam size is shown in the lower right.

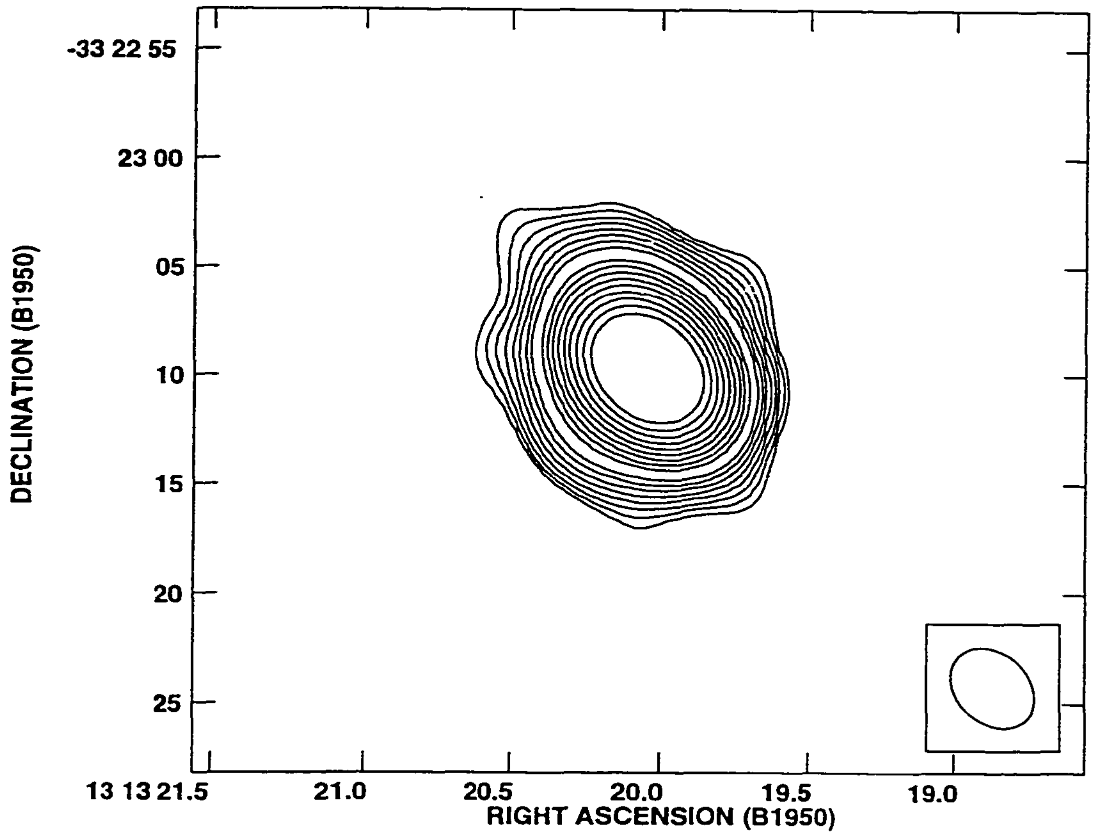

Figure B.17: Radio contour image at 20 cm of J1313-333 made Jun. 1998, with the Brigg's robustness parameter set to 0. Contour levels are logarithmic, with a base of 2, the base contour level of 0.26 mJy, an integrated flux density of 1.32 Jy, and a peak flux density of 1.24 Jy/beam. The beam size is shown in the lower right.